NASA Contractor Report 4078

A Combined Stochastic Feedforward and Feedback Control Design Methodology With Application to Autoland Design

Nesim Halyo

CONTRACT NAS1-16158
JULY 1987

NASA

NASA Contractor Report 4078

A Combined Stochastic Feedforward and Feedback Control Design Methodology With Application to Autoland Design

Nesim Halyo
Information & Control Systems, Incorporated
Hampton, Virginia

Prepared for
Langley Research Center
under Contract NAS1-16158

National Aeronautics
and Space Administration

**Scientific and Technical
Information Office**

1987

FOREWORD

The work described in this report was performed by Information & Control Systems, Incorporated (ICS) under Contract NAS1-16158. The work was sponsored by the National Aeronautics and Space Administration, Langley Research Center, Guidance & Control Division, Aircraft Controls Branch. Mr. R. M. Hueschen served as the NASA Technical Representative monitoring this contract.

PRECEDING PAGE BLANK NOT FILMED

PAGE ii INTENTIONALLY BLANK

TABLE OF CONTENTS

	page
FOREWORD	iii
LIST OF TABLES	vii
LIST OF FIGURES	viii
I. INTRODUCTION	1
II. STOCHASTIC FEEDFORWARD/OUTPUT FEEDBACK CONTROL DESIGN	4
A. FEEDFORWARD CONTROL - A STOCHASTIC FORMULATION	4
COMMAND MODEL	5
FEEDFORWARD CONTROL OPTIMIZATION	6
CASE 1. $u_k = -K_z z_k$	10
CASE 2. $u_k = -K_\zeta(\zeta_k + v_k)$	14
AN ALGORITHM FOR K_z	16
CONSTANT COMMAND $\phi_z = I$	20
A SIMPLE EXAMPLE	21
B. A STOCHASTIC FEEDFORWARD/OUTPUT FEEDBACK DESIGN METHODOLOGY	24
ERROR FORMULATION	27
DYNAMIC COMPENSATION AND INTEGRAL FEEDBACK	29
FEEDBACK DESIGN MODEL	31
FEEDFORWARD CONTROL MODEL	33
C. IMPLEMENTATION	36
EIGENVALUES OF IMPLEMENTATION	39
III. DESIGN OF DIGITAL AUTOMATIC LANDING SYSTEM	45
A. LATERAL CONTROL LAW DESIGN	45
LATERAL DESIGN MODEL	45
LATERAL COMMAND DESIGN MODEL	51
B. LONGITUDINAL CONTROL LAW DESIGN	56
LONGITUDINAL PLANT DESIGN MODEL	56
LONGITUDINAL COMMAND DESIGN MODEL	61

PRECEDING PAGE BLANK NOT FILMED

PAGE iv INTENTIONALLY BLANK

TABLE OF CONTENTS (CONCLUDED)

	page
IV. ANALYSIS AND NONLINEAR SIMULATION	67
A. CLOSED-LOOP SYSTEM ANALYSIS	67
B. NONLINEAR SIMULATION	69
V. CONCLUSIONS AND RECOMMENDATIONS	77
REFERENCES	81

LIST OF TABLES

page

TABLE 1. LATERAL CONTROL STRUCTURE 83

TABLE 2. LATERAL FEEDFORWARD DESIGN MODEL 84

TABLE 3. LATERAL FEEDFORWARD AND FEEDBACK CONTROL GAINS 85

TABLE 4. LATERAL EQUIVALENT s-DOMAIN EIGENVALUES 86

TABLE 5. LATERAL SINGULAR VALUES 87

TABLE 6. LONGITUDINAL/VERTICAL CONTROL STRUCTURE 88

TABLE 7. LONGITUDINAL/VERTICAL FEEDFORWARD DESIGN MODEL 89

TABLE 8. LONGITUDINAL/VERTICAL FEEDFORWARD AND FEEDBACK CONTROL GAINS 90

TABLE 9. LONGITUDINAL EQUIVALENT s-DOMAIN EIGENVALUES 91

LIST OF FIGURES

page

FIGURE 1. FUNCTIONAL CLOSED-LOOP BLOCK DIAGRAM 92

FIGURE 2. LATERAL PATH GEOMETRY 93

FIGURE 3. LONGITUDINAL/VERTICAL PATH GEOMETRY 94

FIGURE 4a. EIGENVALUE AND SINGULAR VALUE ANALYSIS OF CONTROL DESIGN .. 95

FIGURE 4b. EIGENVALUE AND SINGULAR VALUE ANALYSIS OF CONTROL DESIGN .. 96

FIGURE 4c. BODE PLOT OF CONTROL DESIGN 97

FIGURE 4d. BODE PLOT OF CONTROL DESIGN 98

FIGURE 5a. NONLINEAR SIMULATION: GS = -3^{o}, U_o = 125 KTS, $\psi_I = -32^{o}$, WT = 85,000 LBS 99

FIGURE 5b. NONLINEAR SIMULATION: GS = -3^{o}, U_o = 125 KTS, $\psi_I = -32^{o}$, WT = 85,000 LBS 100

FIGURE 6a. NONLINEAR SIMULATION: GS = -3^{o}, U_o = 135 KTS, $\psi_I = -32^{o}$, WT = 95,000 LBS, c.g. = .19 101

FIGURE 6b. NONLINEAR SIMULATION: GS = -3^{o}, U_o = 135 KTS, $\psi_I = -32^{o}$, WT = 95,000 LBS, c.g. = .19 102

FIGURE 7a. NONLINEAR SIMULATION: GS = -4^{o}, U_o = 125 KTS, $\psi_I = -32^{o}$, WT = 85,000 LBS 103

FIGURE 7b. NONLINEAR SIMULATION: GS = -4^{o}, U_o = 125 KTS, $\psi_I = -32^{o}$, WT = 85,000 LBS 104

FIGURE 8a. NONLINEAR SIMULATION: GS = -4.5^{o}, U_o = 125 KTS, $\psi_I = -47^{o}$, WT = 85,000 LBS 105

FIGURE 8b. NONLINEAR SIMULATION: GS = -4.5^{o}, U_o = 125 KTS, $\psi_I = -47^{o}$, WT = 85,000 LBS 106

FIGURE 9a. NONLINEAR SIMULATION: GS = -3^{o}, U_o = 125 KTS, $\psi_I = -47^{o}$, WT = 85,000 LBS 107

FIGURE 9b. NONLINEAR SIMULATION: GS = -3^{o}, U_o = 125 KTS, $\psi_I = -47^{o}$, WT = 85,000 LBS 108

FIGURE 10a. NONLINEAR SIMULATION: GS = -3^{o}, U_o = 125 KTS, $\psi_I = -32^{o}$, WT = 95,000 LBS, c.g. = .19, YDDMAX = 5 109

FIGURE 10b. NONLINEAR SIMULATION: GS = -3^{o}, U_o = 125 KTS, $\psi_I = -32^{o}$, WT = 95,000 LBS, c.g. = .19, YDDMAX = 5 110

FIGURE 11a. NONLINEAR SIMULATION: GS = -3^{o}, U_o = 125 KTS, $\psi_I = -32^{o}$, WT = 90,000 LBS 111

FIGURE 11b. NONLINEAR SIMULATION: GS = -3^{o}, U_o = 125 KTS, $\psi_I = -32^{o}$, WT = 90,000 LBS 112

FIGURE 12a. NONLINEAR SIMULATION: GS = -3^{o}, U_o = 125 KTS, $\psi_I = -32^{o}$, WT = 95,000 LBS, c.g. = .19 113

FIGURE 12b. NONLINEAR SIMULATION: GS = -3^{o}, U_o = 125 KTS, $\psi_I = -32^{o}$, WT = 95,000 LBS, c.g. = .19 114

LIST OF FIGURES (CONCLUDED)

page

FIGURE 13a. NONLINEAR SIMULATION: GS = -3°, U_o = 125 KTS, ψ_I = -32°, WT = 95,000 LBS, c.g. = .19, GUSTON = .T 115

FIGURE 13b. NONLINEAR SIMULATION: GS = -3°, U_o = 125 KTS, ψ_I = -32°, WT = 95,000 LBS, c.g. = .19, GUSTON = .T 116

FIGURE 14a. NONLINEAR SIMULATION: GS = -3°, U_o = 125 KTS, ψ_I = -32°, WS = 10 KTS, WD = 122°, WT = 85,000 LBS 117

FIGURE 14b. NONLINEAR SIMULATION: GS = -3°, U_o = 125 KTS, ψ_I = -32°, WS = 10 KTS, WD = 122°, WT = 85,000 LBS 118

FIGURE 15a. NONLINEAR SIMULATION: GS = -3°, U_o = 125 KTS, ψ_I = -32°, WT = 95,000 LBS, c.g. = .19, NOISES 119

FIGURE 15b. NONLINEAR SIMULATION: GS = -3°, U_o = 125 KTS, ψ_I = -32°, WT = 95,000 LBS, c.g. = .19, NOISES 120

FIGURE 16a. NONLINEAR SIMULATION: GS = -3°, U_o = 125 KTS, ψ_I = -32°, WT = 95,000 LBS, c.g. = .19, GUSTON = .T, NOISES 121

FIGURE 16b. NONLINEAR SIMULATION: GS = -3°, U_o = 125 KTS, ψ_I = -32°, WT = 95,000 LBS, c.g. = .19, GUSTON = .T, NOISES 122

I. INTRODUCTION

The Advanced Transport Operating Systems (ATOPS) program conducted by the Langley Research Center of the National Aeronautics and Space Administration is a research and development program aimed at developing capabilities for increased terminal area capacity, safe and accurate flight in adverse weather conditions including shear winds, the avoidance of wake vortices and reduced fuel consumption. Advances in modern control design techniques and increased capabilities of digital flight computers coupled with accurate guidance information from the Microwave Landing System (MLS) make the achievement of some of these goals feasible. The development of the stochastic feedforward/feedback control design methodology and its application to the design of a digital automatic landing system for a small transport jet aircraft was performed within the context of the ATOPS program.

The main objective of a control system may be described as to enable the plant to track a desired trajectory, usually selected out of a given class of trajectories, as closely as possible in the presence of random and deterministic disturbances and despite uncertainties about the plant. Thus, a control system generally has a feedforward controller which tries to track a desired trajectory, and a feedback controller which tries to maintain the plant state near the desired trajectory in the presence of disturbances and system uncertainties. It is essential that the feedback law produce a closed-loop system which is stable about the desired trajectory so that small disturbances can be accommodated while maintaining the plant state near the desired trajectory once the feedforward control law has brought the plant state to the desired trajectory.

The part of a control law which uses only the desired or commanded trajectory explicitly will be referred to as the feedforward control law. On the other hand, the part of a control law which explicitly uses only measurements of the plant state will be referred to

as the feedback control law. Even though in some cases involving nonlinear control laws the distinction between the feedforward and feedback control laws may become somewhat ambiguous, in linear control laws, the distinction is rather straight-forward.

The design of the feedback controller has received considerable attention in the modern control literature in the last two decades; e.g., see [1] - [5], and the references therein. On the other hand, the design of the feedforward controller has received relatively little attention [6] - [10]. In this study, a combined stochastic feedforward and feedback control design methodology is developed and is applied to the design of a digital automatic landing system for the ATOPS Research Vehicle, a Boeing 737-100 aircraft.

The feedforward control problem is formulated as a stochastic optimization problem and is imbedded into a stochastic output feedback problem [11], [12] where the plant contains unstable and uncontrollable modes. As the standard output feedback algorithm requires an initial gain which stabilizes the plant, a new algorithm is developed to obtain the feedforward control gains. The necessary conditions are shown to result in coupled linear matrix equations, implying that when a solution exists, it is indeed the globally optimal control gain.

The formulation of the feedforward problem in a stochastic, rather than the standard deterministic, setting is significant in two ways. First, the class of desired trajectories from which the actually commanded path is selected can be effectively described as a random process generated by a dynamical system driven by a white noise process. The second, and more important, implication of a stochastic optimization formulation is the tacit understanding that "perfect tracking" is often not possible due to various reasons including uncertainties about, or variations in, the plant parameters, the presence of plant nonlinearities and unmatched initial conditions. Thus, questions about the robustness and sensitivity of the feedforward controller arise naturally in this context.

A combined stochastic feedforward/feedback control methodology is developed where the main objectives of the feedforward and feedback control laws are clearly seen. Fur-

thermore, the inclusion of error integral feedback, dynamic compensation, rate command control structure, etc. is an integral element of the methodology. Another advantage of the methodology is the flexibility that a variety of feedback control design techniques with arbitrary structures may be employed to obtain the feedback controller; these include stochastic output feedback, multi-configuration control, decentralized control [13] or frequency and classical control methods.

Finally, a specific incremental implementation is recommended for the combined feedforward/feedback controller. Some advantages of this digital implementation are the simplicity of implementation, the fact that trim values are not needed and that problems such as integrator wind-up can be largely avoided. The closed-loop eigenvalues using this implementation are shown to contain the designed closed-loop eigenvalues which would result if an incremental implementation were not used.

A digital automatic landing system for the ATOPS Research Vehicle (a Boeing 737-100) is designed using the stochastic feedforward controller and stochastic output feedback. The system control modes include localizer and glideslope capture, localizer and glideslope track, crab, decrab and flare. Using the recommended incremental implementation, the control laws are simulated on a digital computer and interfaced with a nonlinear digital simulation of the aircraft and its systems.

II. STOCHASTIC FEEDFORWARD/OUTPUT FEEDBACK CONTROL DESIGN

A control system generally contains a feedforward and a feedback control subsystem. The feedforward controller tries to track a desired input (or commanded) trajectory, while the feedback controller tries to maintain the plant state near the desired trajectory despite the presence of disturbances, random noises and system uncertainties usually by using error feedback. In the modern control literature, the design of the feedback controller has received considerable attention, while the design of the feedforward controller and its relationship to the feedback controls has received relatively little attention. On the other hand, classical control techniques have treated the design of both feedback and feedforward controllers jointly.

In this section, we will formulate the design of a feedforward controller as a stochastic optimization problem. We will present the solution to this problem for two important special cases. Then we will present a control design methodology which combines the feedforward and feedback control designs and addresses various questions which arise in practical control law design.

A. Feedforward Control – A Stochastic Formulation

In general terms, the objective of a control law is to enable the plant to track a "desired or commanded trajectory" as closely as possible, in the presence of disturbances and despite uncertainties about the plant.

In this study, for purposes of discussing terminology, the part of a control law which uses only the desired trajectory, or the command state, explicitly will be referred to as the feedforward control law. On the other hand, the portion of the control law which explicitly uses measurements of the plant state will be referred to as the feedback control law. Even

though in some cases it is difficult to separate the feedforward and feedback controllers, in most linear control laws, the distinction is relatively straight-forward.

Command Model.

Consider the desired trajectory or command model

$$z_{k+1} = \phi_z z_k + \varsigma_k, \tag{1}$$

where z_k is a n_z-component command state vector; the order, n_z, of the command model is arbitrary, and can be higher or lower than the order of the plant to be controlled. Note that not all the components of the command state, z_k, need correspond to actual physical quantities such as plant states or measured sensor outputs. Let H_z be a $n_o \times n_z$ matrix. We assume that only the vector $H_z z_k$ will be directly commanded as the desired trajectory. For example, in an altitude control law, only the altitude may be commanded as the desired trajectory; however, the command state vector may be defined with two components (i.e., $n_z = 2$) possibly corresponding to commanded altitude and sink rate.

From Eq. (1), it is clear that for an arbitrary command state history $\{z_k,\ k \geq 0\}$, it is always possible to determine the "forcing function" (or vector) $\{\varsigma_k,\ k \geq 0\}$ such that the command model Eq. (1) holds. This can simply be achieved by solving for ς_k. If the command state history $\{z_k,\ k \geq 0\}$ is fixed or completely known a 'priori', then a control sequence which makes the plant track this trajectory can be obtained provided that the trajectory is realizable [5]. However, this control sequence would be a fixed, open loop control sequence corresponding only to that specific trajectory, rather than being a feedforward control law.

In most applications, we are interested in designing a feedforward control law which can track any one trajectory selected from a given class of command trajectories, say $z(\mathcal{L})$. One method of specifying a class of trajectories is to specify a dynamical model driven by a random process with given statistics.

For example, consider the command model in Eq. (1), where the sequence $\{\varsigma_k, k \geq 0\}$ is specified as a vector random sequence with white noise statistics. The class of command trajectories thus specified would be the family of command state histories $\{z_k, k \geq 0\}$ which can be generated by any realization of the random sequence $\{\varsigma_k, k \geq 0\}$. On the other hand, $\{\varsigma_k, k \geq 0\}$ may be specified as a random sequence with colored noise statistics. If ς_k itself can be obtained as the output of a discrete dynamical system driven by white noise, then the command state may be augmented to obtain a new system of higher order driven by white noise but still having the form of Eq. (1).

It is clear that a large family of command trajectory classes can be expressed by the model given in Eq. (1) by appropriate selection of the system order n_z, transition matrix ϕ_z, and the covariance of $\{\varsigma_k, k \geq 0\}$. In the remainder of this study, we will assume that the random sequence $\{\varsigma_k, k \geq 0\}$ in Eq. (1) has white noise statistics, unless specified otherwise.

Feedforward Control Optimization.

Consider a linear plant model of the form

$$x_{k+1} = \phi_x x_k + \Gamma_u u_k + \Gamma_z z_k + \Gamma_\varsigma \varsigma_k + w_k, \tag{2}$$

where x_k is the n-component plant state vector, u_k the r-component control vector, w_k the plant noise process, ϕ_x the plant state transition matrix and Γ_u the control effectiveness matrix. The vectors z_k and ς_k are the command state vector and the command forcing vector, respectively.

It should be noted that when the matrices Γ_z and Γ_ς are selected to be zero, the plant state x_k does not depend on the command trajectory, which is the usual case. However, it is often desirable to include in the plant model, states which describe the error, or the deviation from the command value. To accommodate design models of this type, it is of interest to include the command trajectory terms at this point in the formulation.

Let H_x be a $n_o \times n$ matrix. The objective is to obtain a feedforward control law so that the plant variables $H_x\, x_k$ continuously track the commanded variables $H_x\, z_k$ as closely as possible when $\{z_k,\, k \geq 0\}$ belongs to a given class of command trajectories, $\mathcal{L}$.

By its nature, a feedforward control law is intended not to modify the stability, noise attenuation and robustness properties that are already present in the plant model. These properties are generally obtained by appropriate design of the feedback control law. For the purpose of designing the feedforward control law, we will assume that the plant model already incorporates the feedback control law. Thus, in this section, Eq. (2) represents the closed-loop plant model where the feedback control law has satisfactorily achieved the desired closed-loop objectives. In particular, we will assume that the closed-loop system is stable; i.e., all the eigenvalues of the state transition matrix ϕ_x lie inside the unit circle.

We will consider feedforward control laws of the form

$$u_k = -K_z\, z_k - K_\varsigma\, \varsigma_k, \tag{3}$$

where K_z and K_ς are control gains to be selected in order to track the command trajectory as closely as possible. It is important to note that Eq. (3) is one of the simpler control structures that can be selected. More complex feedforward structures should be investigated to extend the results obtained in this study.

In order to obtain a set of feedforward gains K_z, and K_ς, it is desirable to select a criterion or objective function which describes the goals to be achieved, and then optimize this criterion. Since our goal is to track $H_z\, z_k$, an obvious selection would be

$$J = \lim_{N\to\infty} \frac{1}{2(N+1)} E \sum_{k=0}^{N} (H_x\, x_k - H_z\, z_k)^T (H_x\, x_k - H_z\, z_k) \tag{4}$$

While more general yet quadratic objective functions can be selected, some properties of this expression may be noted. Since only the tracking error is penalized, if a control can achieve perfect tracking then it will optimize the criterion. Thus, the optimal control will

result in perfect tracking when that is possible with the form of control selected in Eq. (3). Otherwise, the optimal solution will minimize a quadratic function of the tracking error. It should be noted that, in this context, perfect tracking implies that almost all command trajectories in the class $\mathcal{L}$ can be tracked by the plant using the feedforward control law in Eq. (3).

While the lack of control weighting allows perfect tracking, when possible, it may also result in more control activity than desired. To accommodate such cases, it is always possible to include a non-zero control weighting term. However, this inevitably results in less than perfect tracking; in such cases, it may be a better policy to change (e.g., to smooth) the commanded trajectory so that tracking it does not require as high a level of control activity.

In the following, we will use the objective or cost function

$$J = \lim_{N\to\infty} \frac{1}{2(N+1)} E \sum_{k=0}^{N} \begin{pmatrix} x_k \\ z_k \end{pmatrix}^T \begin{pmatrix} Q_{11} & Q_{12} \\ Q_{21} & Q_{22} \end{pmatrix} \begin{pmatrix} x_k \\ z_k \end{pmatrix} \tag{5}$$

which does not explicitly contain a control weighting term. The case given in Eq. (4) is obtained when

$$Q_{11} = H_x^T H_x, \qquad Q_{12} = -H_x^T H_z, \tag{6a}$$

$$Q_{21} = -H_z^T H_x, \qquad Q_{22} = H_z^T H_z. \tag{6b}$$

The stochastic feedforward optimization problem can now be posed as: Given the plant model in Eq. (2) and the command model in Eq. (1), find a feedforward control law of the form of Eq. (3) which minimizes the cost function J in Eq. (5).

When the plant model is augmented by the command model, the feedforward control optimization problem posed is seen to be a stochastic output feedback optimization prob-

lem [6] - [8], where the "feedback" vector contains only the command variables z_k and ς_k.* Thus, it would appear that the stochastic feedforward problem can be embedded in the stochastic output feedback problem. In fact, when the command model transition matrix, ϕ_z, is stable, the output feedback algorithm can be directly used to determine the optimal feedforward gains K_z, K_ς.

However, most realistic command models require the use of unstable, in particular marginally (un)stable, systems. For example, the command model for the usual case of a constant command would have an eigenvalue of unity.

$$z_{k+1} = z_k + 0\,\varsigma_k, \qquad z_o = const. \tag{7}$$

Therefore, for the stochastic feedforward problem, the assumption that the command system is stable is not a realistic hypothesis, and is of limited use. Since the command model is not controllable, it is not stabilizable except when it is already stable. Thus, it is not realistic to assume that the augmented system is output stabilizable. Since the output feedback algorithm [9], [12], requires a stabilizing gain, it cannot be used to obtain the optimal feedforward gain. The fact that, in most cases of interest, the command model is not output stabilizable produces the major difficulty in determining the optimal feedforward gains.

In overcoming this problem to obtain an optimal feedforward control law, we will consider two cases. However, first we restate the necessary conditions for the optimal stochastic infinite-time output feedback problem [4], [9].

$$P(K) = \phi^T(K)\,P(K)\,\phi(K) + C^T K^T R K C + Q \quad , \tag{8}$$

$$S(K) = \phi(K)\,S\,\phi^T(K) + \Gamma K \hat{V} K^T \Gamma^T + \hat{W} \quad , \tag{9}$$

*Note that ς_k can also be included in the augmented state and, hence, in the "feedback" vectors, as is shown in Case 2 which is discussed later.

$$\hat{P}(K)\,K\,\hat{S}(K) = \Gamma^T\,P(K)\,\phi\,S(K)\,C^T \quad , \tag{10}$$

$$\phi(K) = \phi - \Gamma\,K\,C \quad , \tag{11}$$

$$\hat{P}(K) = \Gamma^T\,P(K)\,\Gamma + R \quad , \quad \hat{S}(K) = C\,S(K)\,C^T + \hat{V} \quad , \tag{12}$$

where $P(K)$ and $S(K)$ represent the discrete cost and state covariance matrices, respectively, when the gain K is used. Q and R are the discrete state and control weighting matrices, respectively; $\hat{W}$ and $\hat{V}$ are the plant and measurement noise covariance matrices, respectively; C is the output gain matrix, as described in [12], and K is in the stability set S.

CASE 1. $u_k = -K_z\,z_k$.

The augmented system for this problem can be expressed as

$$\begin{pmatrix} x_{k+1} \\ z_{k+1} \end{pmatrix} = \begin{pmatrix} \phi_x & \Gamma_z \\ 0 & \phi_z \end{pmatrix} \begin{pmatrix} x_k \\ z_k \end{pmatrix} + \begin{pmatrix} \Gamma \\ 0 \end{pmatrix} u_k + \begin{pmatrix} w_k + \Gamma_\varsigma\,\varsigma_k \\ \varsigma_k \end{pmatrix} \tag{13}$$

$$y_k = C_z\,z_k + v_k = \begin{pmatrix} 0 & C_z \end{pmatrix} \begin{pmatrix} x_k \\ z_k \end{pmatrix} + v_k \quad , \tag{14}$$

$$u_k = -K_z\,y_k = -K_z\,C_z\,z_k - K_z\,v_k \tag{15}$$

In order to determine necessary conditions for the case considered, we rewrite the general necessary conditions given in Eqs. (8) - (12) after partitioning the matrix equations according to the partition in Eq. (13). This results in the following equations.

$$P_{xx} = \phi_x^T\,P_{xx}\,\phi_x + Q_{xx} \quad , \tag{16}$$

$$P_{xx} = \phi_x^T P_{xx} \phi_x + \phi_x^T P_{xx}(\Gamma_x - \Gamma_x K_x C_x) + Q_{xx} \quad , \tag{17}$$

$$S_{xx} = \phi_x S_{xx} \phi_x^T + (\Gamma_x - \Gamma_x K_x C_x) S_{xx} \phi_x^T + \hat{W}_{xx} \quad , \tag{18}$$

$$S_{xx} = \phi_x S_{xx} \phi_x^T + \hat{W}_{xx} \quad , \tag{19}$$

$$K_x = \hat{P}_{xx}^{-1} \Gamma_x^T [P_{xx} \phi_x S_{xx} + (P_{xx} \Gamma_x + P_{xx} \phi_x) S_{xx}] C_x^T \hat{S}_{xx}^{-1} \quad , \tag{20}$$

where

$$\hat{P}_{xx} = \hat{P} = \Gamma_x^T P_{xx} \Gamma_x + R \quad , \tag{21}$$

$$\hat{S}_{xx} = \hat{S} = C_x S_{xx} C_x^T + \hat{V} \quad . \tag{22}$$

From these equations, it may be noted that the optimal feedforward control gain matrix, K_x, does not directly depend on P_{xx} nor S_{xx}. Furthermore, recall that, strictly speaking, the necessary conditions hold when the closed-loop system is output stabilizable. For the current problem this requires that ϕ_x be stable.

It should be noted that when ϕ_x is unstable, the covariance of the command vector grows without bounds; so that Eq. (19) does not have a non-negative definite solution, S_{xx}. On the other hand, Eq. (17) has a finite solution, P_{xx}, under relatively unrestricted conditions [13]. In particular, if

$$\rho(\phi_x)\, \rho(\phi_x^T) < 1, \tag{23}$$

then a finite P_{xx} satisfies Eq. (17), where $\rho(\phi)$ denotes the spectral radius of the matrix ϕ. Since ϕ_x is the closed-loop plant transition matrix, and is assumed to be stable $\rho(\phi_x^T)$

is strictly less than unity; if necessary, it could be designed to be smaller. On the other hand, in most cases of interest, a $\rho(\phi_z)$ value of unity is sufficient to model the desired trajectory class.

Similar comments apply to the solution of Eq. (18) since the matrices involved have the same eigenvalues; i.e., $\rho(\phi_z)\,\rho(\phi_z^T)$ is equal to $\rho(\phi_z^T)\,\rho(\phi_z)$. However, the forcing function in Eq. (18) contains S_{zz}. When S_{zz} grows without bounds, so will S_{xz}. However, this does not necessarily imply that the optimal feedforward gain, K_z, will also grow without bounds.

To investigate the nature of the optimal solution in the limiting case where the output stabilizability condition does not hold, we rewrite Eq. (18) in the following manner. Assuming that S_{zz} is nonsingular, let

$$\mathcal{S}_{xz} = S_{xz}\,S_{zz}^{-1} \qquad ; \tag{24}$$

then $\mathcal{S}_{xz}$ satisfies the equation

$$\mathcal{S}_{xz} = [\phi_x\,\mathcal{S}_{xz} + (\Gamma_x - \Gamma_x\,K_z\,C_z)][S_{zz}\,\phi_z^T\,S_{zz}^{-1}] + \hat{W}_{xz}\,S_{zz}^{-1} \tag{25}$$

Further assuming that ϕ_z is nonsingular, and manipulating Eq. (20) results in

$$S_{zz}\,\phi_z^T\,S_{zz}^{-1} = \phi_z^{-1}[I - \hat{W}_{zz}\,S_{zz}^{-1}] \qquad . \tag{26}$$

Substituting Eq. (26) into Eq. (25), and manipulating, we find that

$$\mathcal{S}_{xz}[I - \hat{W}_{zz}\,S_{zz}^{-1}]^{-1}\phi_z = \phi_x\,\mathcal{S}_{xz} + (\Gamma_x - \Gamma_x\,K_z\,C_z) + \hat{W}_{xz}[S_{zz} - \hat{W}_{zz}]^{-1}\phi_z \tag{27}$$

Now, in many cases of interest, when ϕ_z approaches an unstable matrix, the covariance of the command state, S_{zz}, grows without bounds, while S_{zz}^{-1} vanishes. In this report, we will limit attention to cases where the inverse of the covariance of the command state vanishes, unless stated otherwise. This results in simplifications in Eq. (27) and Eq. (20).

We will further assume that all the command state components are known without any error. This is certainly a reasonable assumption, since we cannot command a trajectory that we do not know; thus, we set the measurement noise covariance, $\hat{V}$, to zero; i.e.,

$$\hat{V} = 0 \quad , \quad \text{and} \quad C_z = I \quad . \tag{28}$$

The necessary conditions for optimality for this case can now be expressed as:

$$P_{xx} = \phi_x^T P_{xx} \phi_x + Q_{xx} \quad , \tag{29}$$

$$P_{xz} = \phi_x^T P_{xz} \phi_z + \phi_x^T P_{xz}(\Gamma_z - \Gamma_x K_z) + Q_{xz} \quad , \tag{30}$$

$$S_{xz} \phi_z - \phi_x S_{xz} = \Gamma_z - \Gamma_x K_z \quad , \tag{31}$$

$$K_z = \hat{P}_{xx}^{-1} \Gamma_x^T [P_{xx} \phi_x S_{xz} + P_{xx} \Gamma_z + P_{xz} \phi_z] \quad , \tag{32}$$

where $\hat{P}_{xx}$ is given by Eq. (21).

It should be noted that P_{xx} is independent of the feedforward gain matrix, K_z, but depends only on the (closed-loop) plant transition matrix, ϕ_x, and the weighting matrix, Q_{xx}. Similarly, the covariance matrix, S_{xz}, is also independent of the feedforward gain matrix, K_z. However, S_{xz} has been eliminated from the necessary conditions and does not explicitly appear in these equations.

It is of interest to note that the solutions of Eq. (30) and Eq. (31), P_{xz} and S_{xz}, respectively, are linear functions of the feedforward gain, K_z, as these are standard Lyapunov equations. Since P_{xx}, $\hat{P}_{xx}$ and ϕ_x are independent of K_z, Eq. (32) is also linear in the gain K_z. Thus, obtaining the optimal feedforward gain, K_z, does not require the solution of highly nonlinear matrix equations, but can be obtained by solving a set of coupled but

linear equations. An algorithm to solve for the optimal feedforward control gains, K_z, will be shown in a later section.

CASE 2. $u_k = -K_\varsigma(\varsigma_k + v_k)$.

In the preceding case, the feedforward control law was restricted to using only the command vector, z_k. In this section, we will consider the additional use of the command model forcing function (or vector), ς_k, in the feedforward law. Since ς_k is necessary to determine the succeeding command vector, z_{k+1}, it contains lead information and can play an important part in satisfactorily tracking the desired trajectory.

The augmented system for this problem

$$\begin{pmatrix} x_{k+1} \\ z_{k+1} \\ \varsigma_{k+1} \end{pmatrix} = \begin{pmatrix} \phi_x & \Gamma_z - \Gamma_x K_z & \Gamma_\varsigma \\ 0 & \phi_z & I \\ 0 & 0 & 0 \end{pmatrix} \begin{pmatrix} x_k \\ z_k \\ \varsigma_k \end{pmatrix} + \begin{pmatrix} \Gamma_x \\ 0 \\ 0 \end{pmatrix} u_k + \begin{pmatrix} w_{xk} \\ w_{zk} \\ w_{\varsigma k} \end{pmatrix} \quad , \tag{33}$$

$$y_k = \varsigma_k + v_k = (0\ 0\ I) \begin{pmatrix} x_k \\ z_k \\ \varsigma_k \end{pmatrix} + v_k \quad . \tag{34}$$

Partitioning the necessary conditions given by Eq. (8) – Eq. (12) according to the partition of Eq. (33), results in the necessary conditions for the problem considered here.

$$P_{xx} = \phi_x^T P_{xx} \phi_x + Q_{xx} \tag{35}$$

$$P_{xz} = \phi_x^T P_{xz} \phi_z + \phi_x^T P_{xz}(\Gamma_z - \Gamma_x K_z) + Q_{xz} \tag{36}$$

$$K_\varsigma = \hat{P}_{xx}^{-1} \Gamma_x^T [P_{xx} \Gamma_\varsigma + P_{xz}] \hat{W}_\varsigma [\hat{W}_\varsigma + \hat{V}_\varsigma]^{-1} \tag{37}$$

$$\hat{P}_{xx} = \Gamma_x^T P_{xx} \Gamma_x + R \tag{38}$$

It is important to note that the solutions P_{xx} and P_{xz} to Eq. (35) and Eq. (36), respectively, are precisely the same as the solutions to Eq. (29) and Eq. (30) in Case 1. Thus, if P_{xx} and P_{xz} are computed when obtaining the optimal gain for the command vector feedforward, the same matrices can be used in obtaining the optimal gain for the forcing vector feedforward.

Furthermore, it should be noted that the command forcing vector feedforward gain, K_ς, given by Eq. (35) - Eq. (38) is optimized for an arbitrary command vector feedforward gain, K_z. In other words, Eq. (35) - Eq. (38) hold for an arbitrary gain, K_z, not only for the optimal K_z.

Finally, note the simplicity of the expression for K_ς. Once the weighting matrices have been appropriately selected, and the feedback gains have been obtained so that satisfactory feedback characteristics are achieved, it is possible to compute K_ς on-line using the current values of the closed-loop plant transition matrix, ϕ_x, and the control effectiveness matrix, Γ_x. Thus, the simplicity of the necessary conditions for the optimal K_ς make it usable as a feedforward gain-scheduled controller. Similar comments apply to the optimal feedforward gain, K_z, for the command vector. However, in the latter case, the necessary conditions, although linear, are not as simple and easily computed as for K_ς.

It is of interest to consider the case where the command forcing vector is known with no error (i.e., $\hat{V}_\varsigma = 0$), so that ς_k can be fed forward without noise. In this case, Eq. (37) becomes

$$K_\varsigma = \hat{P}_{xx}^{-1}\Gamma_x^T[P_{xx}\Gamma_\varsigma + P_{xz}] \quad . \tag{39}$$

Thus, the optimal K_ς when ς_k is perfectly known at the k^{th} sampling instant is independent of the covariance, W_ς, of ς_k. From an alternate point of view, the gain K_ς can be decreased, or altered, by appropriate selection of the "measurement noise" associated with the forcing vector.

An Algorithm for K_z.

As mentioned earlier, the necessary conditions for Case 1 which considers the feedforward of the command vector, z_k, are linear functions of the gain K_z, which can be seen by observation of Eq. (29) - Eq. (32). Although linear, these matrix equations are coupled; so that an explicit expression for K_z cannot be easily obtained. In contrast, the gain K_ζ, the feedforward of the command forcing vector, can be easily solved for in an explicit expression as shown in Eq. (35) - Eq. (38).

In order to develop an algorithm which results in the optimal feedforward gain, K_z, we will make use of a basic principle of linear operators. Let ℓ be a linear transformation from some p-dimensional real linear space into itself, and let $\{e_i, 1 \leq i \leq p\}$ be an arbitrary set of basis vectors spanning the space. To an arbitrary vector K in the space, having the representation

$$K = \sum_{i=1}^{p} K_i \, e_i \qquad , \qquad K_i \epsilon R \tag{40}$$

associate the column vector $\tilde{K} \epsilon R^p$

$$\tilde{K} = \begin{pmatrix} K_1 \\ K_2 \\ \vdots \\ K_p \end{pmatrix} \qquad . \tag{41}$$

Then, the matrix representation, L, of the linear transformation, ℓ, satisfies the equation

$$\ell(e_j) = L_j = \sum_{i=1}^{p} L_{ij} \, e_i \qquad , \qquad 1 \leq j \leq p \qquad , \tag{42}$$

$$L = \left(\tilde{L}_1 | \tilde{L}_2 | \ldots | \tilde{L}_p \right) \qquad . \tag{43}$$

If K is given by Eq. (40), then

$$\widetilde{\ell(K)} = L \, \tilde{K} \qquad . \tag{44}$$

Now, rewrite Eq. (32) in the form

$$\Gamma_x^T[P_{xx}\,\phi_x\,S_{xx} + P_{xx}\,\Gamma_x + P_{xz}\,\phi_z] - \hat{P}_{xx}\,K_x = 0 \quad . \tag{45}$$

Equation (45) can be viewed as a linear transformation from the space of $r \times n_x$ matrices into itself. We will view Eq. (45) as corresponding to

$$\ell(K_x) + L_o = 0 \quad , \tag{46}$$

where L_o is a $r \times n_x$ matrix.

Consider the basis $\{e_j,\, 1 \le j \le rn_x\}$ defined by

$$e_1 = \begin{pmatrix} 1 & 0 & \dots & 0 \\ 0 & 0 & \dots & 0 \\ \vdots & \vdots & \ddots & \vdots \\ 0 & 0 & \dots & 0 \end{pmatrix} \quad , \quad e_2 = \begin{pmatrix} 0 & 0 & \dots & 0 \\ 1 & 0 & \dots & 0 \\ \vdots & \vdots & \ddots & \vdots \\ 0 & 0 & \dots & 0 \end{pmatrix} \tag{47}$$

$$e_{r+1} = \begin{pmatrix} 0 & 1 & \dots & 0 \\ 0 & 0 & \dots & 0 \\ \vdots & \vdots & \ddots & \vdots \\ 0 & 0 & \dots & 0 \end{pmatrix} \quad , \quad etc. \tag{48}$$

Of course, other basis selections are also possible.

From the preceding discussion, it follows that

$$L\tilde{K}_x + \tilde{L}_o = 0\,, \tag{49}$$

$$\tilde{K}_x = -L^{-1}\,\tilde{L}_o\,, \tag{50}$$

whenever L is invertible. This leads to the following algorithm.

ALGORITHM:

STEP 1. Solve the Lyapunov equations

$$P_{xzj} = \phi_x^T\,P_{xzj}\,\phi_x - \phi_x^T\,P_{xx}\,\Gamma_x\,e_j\,, \qquad 1 \le j \le rn_x \tag{51}$$

$$S_{xzj}\phi_z - \phi_x S_{xzj} = -\Gamma_x e_j\,, \qquad 1 \le j \le rn_z \tag{52}$$

STEP 2. Compute L

$$L_j = \Gamma_x^T[P_{xx}\,\phi_x\,S_{xzj} + P_{xzj}\,\phi_z] - \hat{P}_{xx}\,e_j \tag{53}$$

STEP 3. Form the L

$$L = (\,\tilde{L}_1|\tilde{L}_2|\ldots|\tilde{L}_{rn_z}\,)\,. \tag{54}$$

STEP 4. Solve the Lyapunov equations

$$P_{xzo} = \phi_x^T\,P_{xzo}\,\phi_z + \phi_x^T\,P_{xx}\,\Gamma_z + Q_{xz} \tag{55}$$

$$S_{xzo}\,\phi_z - \phi_x\,S_{xzo} = \Gamma_z \tag{56}$$

STEP 5. Compute L_o and form $\tilde{L}_o$

$$L_o = \Gamma_x^T[P_{xx}\,\phi_x\,S_{xzo} + P_{xx}\,\Gamma_z + P_{xzo}\,\phi_z] \tag{57}$$

STEP 6. Solve the linear equation

$$L\,\tilde{K}_z + \tilde{L}_o = 0 \tag{58}$$

STEP 7. Form K_z and compute the 'gradient' as a test

$$P_{xz} = \phi_x^T\,P_{xx}\,\phi_z + \phi_x^T\,P_{xx}(\Gamma_z - \Gamma_x\,K_z) + Q_{xz} \tag{59}$$

$$S_{xz}\,\phi_z - \phi_x\,S_{xz} = \Gamma_z - \Gamma_x\,K_z \tag{60}$$

$$\left\| \hat{P}_{xx} K_z - \Gamma_x^T [P_{xx} \phi_x S_{xx} + P_{xx} \Gamma_z + P_{xz} \phi_z] \right\| \tag{61}$$

STEP 8. Compute the forcing vector gain, K_ς.

$$K_\varsigma = \hat{P}_{xx}^{-1} \Gamma_x^T [P_{xx} \Gamma_\varsigma + P_{xz}] \hat{W}_\varsigma [\hat{W}_\varsigma + \hat{V}_\varsigma]^{-1} \tag{62}$$

The algorithm uses the fact that S_{xz} and P_{xz}, although 'linear', are not homogeneous functions of K_z; so that the non-homogeneous part is separated in the algorithm and combined in a single term, namely L_o.

It should be noted that the algorithm is not iterative, so that convergence questions do not arise. The problem solved is a set of coupled linear equations, and the solution is functionally obtained by inverting a $rn_z \times rn_z$ matrix, namely L.

On the other hand, the algorithm requires the solution of $2(rn_z + 1)$ Lyapunov equations and the inversion of a square matrix of dimension rn_z. When dealing with ill-conditioned matrices and high order problems, the accuracy of the solution may be of concern. Usual techniques to improve accuracy may be used in such, as yet hypothetical cases. Importantly, it is possible to test the accuracy of the solution, K_z, by computing the 'gradient' of the cost function with the exception that S_{zz} has been eliminated from the expression for the gradient. The norm of this pseudo-gradient which is computed in Step 7 of the algorithm provides an indication of the accuracy of the solution obtained.

The solution is unique if L is invertible. In this case, the feedforward gain obtained is the global solution to the stochastic optimization problem considered. It is desirable to obtain conditions which determine the invertibility of the matrix L in terms of parameters such as ϕ_x, ϕ_z, Γ_z, etc. which are more directly related to the physical aspects of the control problem under consideration. On the other hand, the author's experience on this problem which has been necessarily limited, has always resulted in an invertible L, hence a unique solution of the global optimal solution.

Finally, it may be of interest to note an identity which can be used in the algorithm as an alternate expression for Eq. (53), Eq. (57) and Eq. (59).

$$\Gamma_x^T[P_{xx}\,\phi_x\,S_{xz} + P_{xx}\,\Gamma_z + P_{xz}\,\phi_z] - \hat{P}_{xz}\,K_z$$
$$= \Gamma_x^T\{P_{xx}[\phi_x\,S_{xz} + \Gamma_z - \Gamma_x\,K_z] + P_{xz}\,\phi_z\} - R\,K_z \tag{63}$$

$$= \Gamma_x^T(P_{xx}\,S_{xz} + P_{xz})\,\phi_z - R\,K_z \quad . \tag{64}$$

where Eq. (31) has been used in Eq. (63). The expressions in Eq. (63) and Eq. (64) may be interchanged when desirable. The latter expression is somewhat simpler, particularly when the control weighting matrix, R, vanishes.

Constant Command, $\phi_z = I$.

The most straightforward way in which a constant command can be modeled would be to simply select a command model where

$$z_{k+1} = z_k + \varsigma_k \quad . \tag{65}$$

As a constant command is a commonly used desired trajectory, we will investigate this special case in more detail to obtain the feedforward control law for it. As will be seen, it is possible to obtain an explicit expression for the feedforward gain, K_z, for this special case.

The necessary conditions in Eq. (30) and Eq. (31) can now be solved explicitly for K_z to obtain

$$P_{xz} = (I - \phi_x^T)^{-1}[\phi_x^T\,P_{xz}(\Gamma_z - \Gamma_x\,K_z) + Q_{xz}] \quad , \tag{66}$$

$$S_{xz} = (I - \phi_x)^{-1}(\Gamma_z - \Gamma_x\,K_z) \quad . \tag{67}$$

Substituting these expressions into the necessary conditions expressed in Eq. (64) and manipulating, we obtain

$$K_x = (\Gamma_x^T p_{xx} \Gamma_x + R)^{-1} \Gamma_x^T [p_{xx} \Gamma_x + (I - \phi_x^T)^{-1} Q_{xx}] \quad , \tag{68}$$

$$p_{xx} = P_{xx}(I - \phi_x)^{-1} + (I - \phi_x^T)^{-1} \phi_x^T P_{xx} \quad , \tag{69}$$

$$p_{xx} = P_{xx} + P_{xx} \phi_x (I - \phi_x)^{-1} + (I - \phi_x^T)^{-1} \phi_x^T P_{xx} \quad , \tag{70}$$

where P_{xx} is given by Eq. (29).

It should be noted that since the closed-loop plant transition matrix, ϕ_x is stable, all its poles are strictly inside the unit circle. Therefore, $(I - \phi_x)$ is invertible. In this case, the existence and uniqueness of an optimal solution is determined by the singularity of the matrix $(\Gamma_x^T p_{xx} \Gamma_x + R)$.

For the constant command case considered here, it is therefore not necessary to use the algorithm given in the previous section. Finally, it is possible to obtain a similar expression for the command forcing vector feedforward gain, K_ς, by simply substituting Eq. (66) into Eq. (37).

A Simple Example.

To illustrate the stochastic feedforward control law optimization developed in the preceding sections, we will consider a simple 1^{st} order example with a constant command model.

$$x_{k+1} = \varphi x_k + \gamma u_k + w_k \quad , \quad |\varphi| < 1 \quad , \tag{71}$$

where $\{w_k\}$ is a white noise sequence with zero mean uncorrelated to the command state and forcing vector, z_k and ς_k, respectively. We model the class of desired trajectories by the 1^{st} order command model

$$z_{k+1} = z_k + \varsigma_k \quad , \tag{72}$$

where we model $\{\varsigma_k\}$ as a zero mean white noise sequence uncorrelated to the initial command z_o which may have a non-zero mean.

Suppose that we would like $h_x\, x_k$ to track $h_z\, z_k$ as closely as possible at all sampling instants irrespective of the control activity required. Now, using the results of the last section, we have

$$p_{xx} = \frac{Q_{xx}(1+\varphi)}{(1-\varphi^2)(1-\varphi)} = \frac{Q_{xx}}{(1-\varphi)^2} = \frac{h_x^2}{(1-\varphi)^2} \quad , \tag{73}$$

$$K_z = \frac{\dfrac{\gamma\, Q_{xz}}{(1-\varphi)} + \dfrac{\gamma\, Q_{xx}\, \gamma_z}{(1-\varphi)^2}}{\dfrac{\gamma^2\, Q_{xx}}{(1-\varphi)^2} + R} = \frac{(1-\varphi)\, Q_{xz}}{\gamma\, Q_{xx}} + \frac{\gamma_z}{\gamma} \quad , \tag{74}$$

where R has been assumed zero. If we further substitute $-h_x\, h_z$ for Q_{xz}, $h_x\, h_x$ for Q_{xx}, and null γ_z,

$$K_z = -\frac{(1-\varphi)}{\gamma}\, \frac{h_z}{h_x} \quad . \tag{75}$$

Using the optimal feedforward of the command vector, z_k,

$$x_{k+1} = \varphi\, x_k + (1-\varphi)\frac{h_z}{h_x}\, z_k + w_k \quad . \tag{76}$$

To see the effect of this control law, suppose that at some sampling instant k,

$$h_x\, x_k = h_z\, z_k \quad , \tag{77}$$

then

$$x_{k+1} = \varphi\frac{h_z}{h_x}\, z_k + (1-\varphi)\frac{h_z}{h_x}\, z_k + w_k = \frac{h_z}{h_x}\, z_k + w_k \quad . \tag{78}$$

It is seen that, as would be expected from an feedforward controller designed for a constant command, this control law maintains x_{k+1} at a constant desired value (with the exception of plant noise effects which are attenuated by the feedback design). This feedforward controller drives the state to the desired trajectory, based on the assumption that the command vector is most likely to remain constant. Note that

$$\hat{z}_{k+1} = E(z_{k+1}|z_k) = z_k \quad , \tag{79}$$

so that the least-squares estimate of the next command $h_z \hat{z}_{k+1}$ is in fact the last command $h_z z_k$.

Thus, when the feedforward controller is limited to using only the command vector, based on a constant command model, the design performs exactly as would be expected, and drives the state to the desired constant, and then maintains the commanded value. If the command state, z_k, is not completely constant, but moves slowly, the state will track the movement with some error. It may be noted that the Command-Generator-Tracker (CGT) deterministic feedforward controller for this problem is the same as the one obtained here; i.e., Eq. (75). It should also be noted that, for this example, non-zero control weighting (i.e., $R > 0$) produces less than perfect tracking.

Now we remove the restriction that only the present command value, z_k, be used in the feedforward law; by allowing the current value of ς_k to be used. Assuming that ς_k is perfectly known at sample k, we set $\hat{V}_\varsigma$ equal to zero. Using Eq. (39), the optimal gain for the forcing vector, ς_k, can be found to be

$$K_\varsigma = -\left[\frac{\varphi}{(1-\varphi)} K_z + \frac{(1+\varphi)}{\gamma} \frac{h_z}{h_x}\right] \tag{80}$$

Substituting the optimal K_z from Eq. (75) into Eq. (80), and manipulating

$$K_\varsigma = -\frac{1}{\gamma} \frac{h_z}{h_x} \quad . \tag{81}$$

The full feedforward control law now becomes

$$u_k = \frac{(1-\varphi)}{\gamma}\frac{h_z}{h_x} z_k + \frac{1}{\gamma}\frac{h_z}{h_x}\varsigma_k \quad , \tag{82}$$

$$x_{k+1} = \varphi x_k + (1-\varphi)\frac{h_z}{h_x} z_k + \frac{h_z}{h_x}\varsigma_k + w_k \quad . \tag{83}$$

Assume, as before, that at sample k perfect tracking was achieved; i.e., Eq. (77) holds. Then,

$$x_{k+1} = \frac{h_z}{h_x}(z_k + \varsigma_k) + w_k = \frac{h_z}{h_x} z_{k+1} + w_k \quad . \tag{84}$$

When the feedforward law is not restricted to z_k alone, it is seen that the state tracks the command perfectly, neglecting the plant noise effects. This improvement in the tracking performance is due to the availability of accurate lead information in ς_k. It is clear that, in this simple example, the feedforward law given by Eq. (82) will track the desired trajectory at every sampling instant, as long as the plant parameters φ and γ are perfectly known and do not vary.

Although illustrative of many true trends, this example is of low order and does not represent all the complexities of a realistic design problem.

B. A Stochastic Feedforward/Output Feedback Design Methodology

Having both feedforward and feedback control design techniques available for use, it is necessary to also have a methodology which combines these two control designs to solve realistic and practical control design problems. In particular, the control design methodology should have the capability to: 1) accommodate a variety of control law structures, 2) allow the use of different control design techniques to achieve desirable characteristics, and 3) have a simple and practical implementation free of the often-encountered problems.

In many control design problems, the specification of the control objectives also imply and sometimes require a particular structure for the control law. For example, if it is

necessary to have zero steady state tracking error in some variable in response to a constant command despite small variations in the plant parameters, then an error integral feedback structure is necessary to achieve this objective. Whereas if a bias error in that variable can be tolerated, then only an error feedback is sufficient.

Similarly, in many problems the unavailability of sensors which accurately measure every state variable makes it desirable to use dynamic compensation in the feedback loop. In other cases, a decentralized control structure may be desirable. A methodology which can accommodate a rich collection of the combined feedforward and feedback control law structures is desirable.

On the other hand, a large variety of feedback control design techniques are now available. These include modern control design methods such as stochastic output feedback or full state feedback techniques, multi-configuration control (MCC) techniques, decentralized control techniques [13], as well as classical control and frequency domain design techniques. As most of these design methods focus on achieving certain desirable control characteristics, it is desirable to have a methodology which accommodates the use of many design methods.

Finally, many modern control design techniques sometimes fail to adequately consider the digital implementation of the control law. For example, methods of avoiding the use of trim values, eliminating integrator wind up, minimizing the effects of control rate and control position limits, asynchronous sampling of sensor outputs, delays, etc. ought to be integral concerns of the design methodology. A design approach in which as many as possible of the practical implementation issues are explicitly treated is desirable.

To develop a methodology which formulates a combined feedforward and feedback control design problem which addresses most of the realistic issues raised above, consider a linearized plant model of the form

$$\bar{x}_{k+1} = \phi_x \bar{x}_k + \Gamma_x u_k + w_{xk} + d_x \quad , \tag{85}$$

where the state $\bar{x}_k$, the control u_k, correspond to the total values of the corresponding quantities rather than being perturbations about their trim values, w_k is the white plant noise and d_x is a constant vector arising from the linearization of the nonlinear plant about some operating point. When the plant operating point changes, all the plant parameters such as ϕ_x, Γ_x, Γ_z, Γ_ς and d_x may change; however, it is assumed here that the changes in these parameters occur at a much slower rate than the variations in the state x_k, controls u_k, etc., so that the plant parameters are assumed constant except when explicitly stated otherwise.

The feedback vector is assumed to admit a linearization of the form

$$\bar{y}_k = C_x \bar{x}_k + v_k + d_y \quad , \tag{86}$$

where d_y again is a constant vector which depends on the point about which the linearization is obtained, and v_k represents the measurement noise assumed to be a white noise sequence.

As in the previous section, we will limit attention to the class of command models which admit a discrete stochastic model of the form

$$z_{k+1} = \phi_z z_k + \varsigma_k \quad , \tag{87}$$

where $\{\varsigma_k\,,\, k \geq 0\}$ is a sequence of uncorrelated random vectors with zero mean, such that

$$E(\varsigma_k v_k^T) = 0 \quad , \quad E(\varsigma_k w_k^T) = 0 \quad , \tag{88}$$

$$E(\varsigma_k \bar{x}_o^T) = 0 \quad , \quad E(\varsigma_k z_o^T) = 0 \quad . \tag{89}$$

We consider the basic control objective to be the design of a combined feedforward/feedback control law where only the vector, $\bar{y}_k$, is used in the feedback law, and

$H_x \bar{x}_k$ tracks $H_z z_k$ as closely as possible for a given class of commanded trajectories in the presence of disturbances and despite uncertainties about the plant.

In many applications, the designer may be interested in a control law structure which contains dynamic compensation and integral feedback to achieve certain objectives. Furthermore, it may be desirable to have an inner loop/outer loop structure or to have some fixed (previously designed) filter provide some state estimates. Such dynamic subsystems as an inner loop or a filter can be included in the plant model described in Eq. (85).

Furthermore, in many cases it is desirable and important to distinguish between the variable describing the commanded control value and the actual position of the control (the physical quantity such as an elevator position, or an electrical current). These two quantities, the commanded and the actual control values, are usually related through an actuator subsystem which should be modeled and included in the plant dynamics model in Eq. (85).

In other cases, the designer may decide on a control rate command structure rather than using control position commands. This has a variety of advantages such as low-pass filtering the control command thus reducing unnecessary control activity, and providing the commanded control position for feedback when the actual control position is not measured and used for feedback.

In most of these cases, it is necessary to use a formulation which accommodates output feedback for the controller. Here, it is assumed that the types of control structures mentioned above have been included in the plant dynamics and the feedback vector models given by Eq. (85) and Eq. (86), respectively.

Error Formulation.

While the plant and feedback vector models can be used in the form given by Eq. (85) and Eq. (86), it is often convenient and desirable to have state variables which represent the error in some of these variables instead of their values with respect to some fixed frame of reference. In cases where a plant state variable is being commanded by a command

model state variable, defining the error as the difference is straight forward. Also state variables corresponding to the time rate of change of already defined error terms can be easily obtained. However, since many variables are not directly commanded, only some of the state variable errors terms can readily be defined in this manner, while the remaining ones maintain their previous representations.

Let H be a $n \times n_z$ dimensional matrix relating the command model state, z_k, to the plant model state, $\bar{x}_k$, and let

$$x_k = \bar{x}_k - H z_k \tag{90}$$

Substituting Eq. (85) and Eq. (87) into Eq. (90) and manipulating, the dynamics equations for the new state vector, x_k, can be obtained.

$$x_{k+1} = \phi_x x_k + \Gamma_x u_k + (\phi_x H - H \phi_z) z_k - H \varsigma_k + w_{xk} + d_x \quad . \tag{91}$$

It is seen that while the plant model in Eq. (85), as is usually the case, does not depend on the commanded model state and forcing vectors, the description of the plant in terms of errors introduces such terms; hence, the inclusion of command state and forcing vector terms in the previous section dealing with the design of feedforward control. It should also be noted that the control vector u_k in the plant representations given by Eq. (85) and Eq. (91) is the same. So that the new plant representation still deals with the same control values that drive the plant.

Now consider the feedback vector in Eq. (86). The components of the feedback generally correspond to sensor outputs, filter outputs, dynamic compensation states, control command values, etc. It is possible to use the vector $\bar{y}_k$ by substituting Eq. (90).

$$\bar{y}_k = C_x(x_k + H z_k) + v_k + d_y = C_x x_k + C_x H z_k + v_k + d_y \tag{92}$$

On the other hand, it is often convenient to think in terms of error feedback. So that

a new feedback vector consisting of the error terms defined in Eq. (90) may also be used in the form of $\bar{y}_k - C_x H z_k$; i.e.,

$$\bar{y}_k - C_x H z_k = C_x x_k + v_k + d_y \tag{93}$$

Since the command state, z_k, is known at the k^{th} sampling instant, implementation of the error feedback vector in real time is clearly possible.

To maintain further generality, we will consider the plant and feedback models in the form given below

$$x_{k+1} = \phi_x x_k + \Gamma_x u_k + \Gamma_z z_k + \Gamma_\zeta \zeta_k + w_{xk} + d_x \tag{94}$$

$$y_k = C_x x_k + C_z z_k + v_k + d_y \quad , \tag{95}$$

where the standard error feedback case shown above would correspond to C_z being null.

From the limited experience and experimentation performed in this study, it appears that better performance is achieved when the error formulation is used in as many variables as applicable. Due to the limited time available, the reasons for the differences in performance or methods for best selection of H were not investigated in this study.

Dynamic Compensation and Integral Feedback.

In many cases, it is of interest to include dynamic compensation in the control law to achieve particular objectives. The objective may be to estimate a variable for purposes of feedback, or to provide more robustness or insensitivity.

Similarly, it is usually of interest to have integral feedback of the tracking error, or of equivalent variables, in order to obtain a type 1 system. To accommodate these often used control structures, augment the plant state model given in Eq. (94) by the compensator and integral error models

$$c_{k+1} = \phi_c\, c_k + u_{ck} + w_{ck} \quad , \tag{96}$$

$$I_{k+1} = I_k + \Delta t(H_y\, y_k - H_z\, z_k) + w_{Ik} \quad , \tag{97}$$

$$H_x = H_y\, C_x \quad . \tag{98}$$

Note that the "integrator" is a digitally implementable accumulator. Also note that the tracking variables, $H_y\, y_k$, have been assumed to be a linear combination of known or measured, y_k, rather than possible unavailable state variables in x_k.

The dynamic compensator is assumed to be of order n_c which can be selected arbitrarily, according to the desired objectives. The compensator state transition matrix, ϕ_c, is also arbitrary, and should be selected in accordance to the cost function which will produce the closed-loop compensator. The white noise sequences w_{ck} and w_{Ik} are included largely for generality. They could be interpreted as round-off error, variations in H_y, jitter, etc.; however, most importantly, they can be used as design parameters which modulate the optimal feedback gains.

The basic form of the combined feedforward/feedback control law is assumed to be

$$u_{xk} = -K_{xy}\, y_k - K_{xc}\, c_k - K_{xI}\, I_k - K_{xz}\, z_k - K_{x\varsigma}\, \varsigma_k + \bar{u}_x \quad , \tag{99}$$

$$u_{ck} = -\bar{K}_{cy}\, y_k - \bar{K}_{cc}\, c_k - \bar{K}_{cI}\, I_k - \bar{K}_{cz}\, z_k - \bar{K}_{c\varsigma}\, \varsigma_k + \bar{u}_c \quad . \tag{100}$$

Note that, for the augmented problem, the feedback vector, y_k, is also augmented by the compensator state, c_k, and the error integral variables, I_k. The feedforward control law has been constrained to use only the command state and forcing vectors, z_k and ς_k, respectively. Finally, $\bar{u}_x$ and $\bar{u}_c$ are unknown constant (with respect to k) variables arising

from the fact that the variables used are not the perturbed values, but correspond to the total values including the trim values of the variables. As an incremental implementation will be used, it is not necessary to actually compute the constant vectors.

It should also be noted that the control vector, may be selected to be the rate of the actual control position variables by augmenting the plant model accordingly. This would result in a control rate command structure.

Feedback Design Model.

Suppose that the feedforward control sequences $\{u^*_{xk}, k \geq 0\}$ and $\{u^*_{ck}, k \geq 0\}$ produce a satisfactory trajectory. Then, when no plant noise or measurement noise is present, then trajectory will be given by

$$x^*_{k+1} = \phi_x x^*_k + \Gamma_x u^*_{xk} + \Gamma_z z_k + \Gamma_\varsigma \varsigma_k + d_x \quad , \tag{101}$$

$$c^*_{k+1} = \phi_c c^*_k + u^*_{ck} \quad , \tag{102}$$

$$I^*_{k+1} = I^*_k + \Delta t(H_y y^*_k - H_x z_k) \quad , \tag{103}$$

$$y^*_k = C_x x^*_k + C_z z_k + d_y \quad . \tag{104}$$

Since the actual plant, compensator and integral states evolve according to Eq. (94), Eq. (96) and Eq. (97), respectively, the deviations, or error, in these variables can be defined as

$$\tilde{x}_k = x_k - x^*_k, \qquad \tilde{u}_{xk} = u_{xk} - u^*_{xk}, \qquad \tilde{u}_{ck} = u_{ck} - u^*_{ck} \tag{105}$$

$$\tilde{y}_k = y_k - y^*_k, \qquad \tilde{I}_k = I_k - I^*_k, \qquad \tilde{c}_k = c_k - c^*_k. \tag{106}$$

Manipulating, it is seen that the error in the state has the dynamics

$$\tilde{x}_{k+1} = \phi_k \tilde{x}_k + \Gamma_x \tilde{u}_{xk} + w_{xk} \quad , \tag{107}$$

$$\tilde{c}_{k+1} = \phi_c \tilde{c}_k + \tilde{u}_{ck} + w_{ck} \quad , \tag{108}$$

$$\tilde{I}_{k+1} = \tilde{I}_k + \Delta t\, H_x \tilde{x}_k + (w_{Ik} + \Delta t\, H_y v_k) \quad , \tag{109}$$

$$\tilde{y}_k = C_x \tilde{x}_k + v_k \quad . \tag{110}$$

The deviations in the actual state relative to the desired trajectory are seen to be due to plant and measurement noise, and initial condition mismatch. Of course, in practice these deviations are also due to changing plant parameter values, unmodeled nonlinearities, unmodeled dynamics, sampling errors, etc.

Since all the terms containing the command model have canceled, the deviation about the desired trajectory is seen to be independent of the command state. Thus, the possibly unstable command model has no direct impact on the feedback control law design. Where highly nonlinear effects which involve the command state exist, the command may not cancel; however, this is not a usually encountered case.

Therefore, the design of the feedback control law can be done largely independently of the feedforward control law. The usual major objectives of feedback, such as stability about the desired trajectory in the presence of disturbances and despite uncertainties about, and variations in, the plant models, can thus be pursued using the dynamical system describing the deviations about the desired trajectory in Eq. (107) – Eq. (110).

The feedback vector, in this case, is taken to be $(\tilde{y}_k^T \ \tilde{c}_k^T \ \tilde{I}_k^T)^T$. So that a control law of the form

$$\tilde{u}_{xk} = -K_{xy}\,\tilde{y}_k - K_{xc}\,\tilde{c}_k - K_{xI}\,\tilde{I}_k \tag{111}$$

$$\tilde{u}_{ck} = -K_{cy}\,\tilde{y}_k - K_{cc}\,\tilde{c}_k - K_{cI}\,\tilde{I}_k \tag{112}$$

can be designed using any modern or classical control design technique. In particular, note that stochastic output feedback [11], [12], multi-configuration control or decentralized control techniques [13] can be used for this purpose. In the following, it will be assumed that the feedback control law thus designed stabilizes the closed-loop system.

Feedforward Control Model.

Having designed a satisfactory feedback control law, recall that the feedforward control in Eq. (101) - Eq. (104) is arbitrary, and can now be selected using a stable closed-loop system.

Consider the following change of variables in the control vectors u^*_{xk} and u^*_{ck}.

$$\mu^*_{xk} = u^*_{xk} + K_{xy}\,y^*_k + K_{xc}\,c^*_k + K_{xI}\,I^*_k \tag{113}$$

$$\mu^*_{ck} = u^*_{ck} + K_{cy}\,y^*_k + K_{cc}\,c^*_k + K_{cI}\,I^*_k \tag{114}$$

Substituting these expressions into Eq. (101) - Eq. (104), we obtain the feedforward control model

$$\begin{aligned} x^*_{k+1} = (\phi_x - \Gamma_x\,K_{xy}\,C_x)x^*_k \; &- \Gamma_x\,K_{xc}\,c^*_k - \Gamma_x\,K_{xI}\,I^*_k + \Gamma_x\,\mu^*_{xk} \\ &+ (\Gamma_z - \Gamma_x\,K_{xy}\,C_z)z_k + \Gamma_\varsigma\,\varsigma_k + d^*_x \end{aligned} \tag{115}$$

$$c^*_{k+1} = -K_{cy}\,C_x\,x^*_k + (\phi_c - K_{cc})\,c^*_k - K_{cI}\,I^*_k + \mu^*_{ck} - K_{cy}\,C_z\,z_k + d^*_c \tag{116}$$

$$I^*_{k+1} = I^*_k + \Delta t\, H_x\, x^*_k - (H_z - \Delta t\, H_y\, C_z)\, z_k + d^*_I \tag{117}$$

$$z_{k+1} = \phi_z\, z_k + \varsigma_k \tag{118}$$

where

$$d^*_x = d_x - \Gamma_x\, K_{xy}\, d_y \quad , \quad d^*_c = -K_{cy}\, d_y \quad , \quad d^*_I = \Delta t\, H_y\, d_y \quad , \tag{119}$$

are constant vectors depending on the trim conditions for the particular operating points used.

From the discussion above, it is clear that the feedforward control design problem is one finding control sequences $\{\mu^*_{xk}\,,\ k \geq 0\}$ and $\{\mu^*_{ck}\,,\ k \geq 0\}$ in terms of a given subset of the augmented state variables x^*_k, c^*_k, I^*_k, and z_k, ς_k, when the command state transition matrix ϕ_z, is not necessarily stable, such that $\{H_y\, y^*_k - H_z\, z_k\,,\ k \geq 0\}$ is as "small" as possible.

A full analysis of the many interesting cases where different subsets of the augmented feedforward model state are selected is beyond the scope of the current study. Only the two cases solved in the preceding section will be treated in some detail. However, the full state feedback case is worthy of note.

Consider the case where the feedforward control law form is unrestricted and $\{\varsigma_k\,,\ k \geq 0\}$ is a Gaussian white noise process, with all initial conditions also being jointly Gaussian. With a quadratic cost function, it is well-known [4] that the optimal control is the solution to the LQG problem. The case where the plant contains unstable and uncontrollable modes, has been treated by the author as a disturbance accommodation problem [8], [7]. It is clear that the most accurate feedforward control law would be obtained by this unconstrained solution.

While this solution has a variety of desirable characteristics, it also has a disadvantage. It requires the computation of the augmented desired trajectory x_k^*, c_k^*, I_K^*, z_k, ς_k as a part of the feedforward controller. With the increasing speed and memory capabilities of flight computers, this is not necessarily impractical, but will not be pursued further in this study.

Now consider the case where the feedforward control is restricted to the form

$$\mu_{xk}^* = -K_{xz}\, z_k - K_{x\varsigma}\, \varsigma_k - \mu_x^* \tag{120}$$

$$\mu_{ck}^* = -K_{cz}\, z_k - K_{c\varsigma}\, \varsigma_k - \mu_c^* \tag{121}$$

Using a quadratic cost function of the form of Eq. (5) which includes the most common case

$$J = \lim_{N\to\infty} \frac{1}{2(N+1)} E \sum_{k=0}^{N} \|H_y\, y_k^* - H_z\, z_k\|_E^2 \quad , \tag{122}$$

it is possible to obtain the optimal feedforward gains K_{xz}, $K_{x\varsigma}$, K_{cz}, and $K_{c\varsigma}$.

It is important to note that the treatment of the feedforward control law in the preceding section accommodates the cases where any one of the feedforward gains is set to zero or some other constant.

To obtain the total control law, recall that from Eq. (105),

$$u_{xk} = \tilde{u}_{xk} + u_{xk}^* \quad , \quad u_{ck} = \tilde{u}_{ck} + u_{ck}^* \quad . \tag{123}$$

$$u_{xk} = -K_{xy}\, y_k - K_{xc}\, c_k - K_{xI}\, I_k + \mu_{xk}^* \tag{124}$$

$$u_{ck} = -K_{cy}\, y_k - K_{cc}\, c_k - K_{cI}\, I_k + \mu_{ck}^* \tag{125}$$

The combined feedforward/feedback control law with dynamic compensation and integral error feedback can be obtained by closing the loop on the compensation in Eq. (96) with Eq. (125).

$$c_{k+1} = (\phi_c - K_{cc})c_k - K_{cI}\, I_k - K_{cy}\, y_k - K_{cz}\, z_k - K_{c\varsigma}\, \varsigma_k - \mu_c^* \qquad (126)$$

$$I_{k+1} = I_k + \Delta t(H_y\, y_k - H_z\, z_k) \qquad (127)$$

$$u_{xk} = -K_{xy}\, y_k - K_{xc}\, c_k - K_{xI}\, I_k - K_{xz}\, z_k - K_{x\varsigma}\, \varsigma_k - \mu_c^* \qquad (128)$$

Of course, it is also necessary to compute and update the command state and forcing vectors, z_k and ς_k, respectively, according to the desired trajectory. Note that since the feedforward law only uses the current values z_k and ς_k, these commands need not be available ahead of time and could be real-time pilot inputs or may be computed from real-time pilot inputs.

C. Implementation

While Eq. (126) - Eq. (128) with the addition of the command state and forcing vector constitute the combined feedforward/feedback control law, there are a number of advantages to implementing the control law in incremental form.

First note that the constant terms μ_x^* and μ_c^* have not been determined. Even though it is possible to compute these vectors using trim conditions, it is more convenient if the control law were not to require these vectors. A second advantage to an incremental implementation is the elimination of the integral terms. When the tracking error is, at least temporarily, large, the integral state I_k can reach very high values. This usually leads to the control commands reaching limits. Even though the tracking error may have been reduced to small levels, it can take a considerable amount of time before the integral state

reaches reasonable levels, and the limiting of the controls is eliminated. The unnecessary effects of this phenomenon, referred to as "integral wind-up" can largely be eliminated by an incremental implementation.

By simply differencing the control law,

$$\Delta I_k = \Delta t(H_y\, y_{k-1} - H_z\, z_{k-1}) \tag{129}$$

$$\begin{aligned}\Delta c_{k+1} = (\phi_c - K_{cc})\Delta c_k - K_{cy}(y_k - y_{k-1}) - K_{cI}\,\Delta I_k \\ - K_{cx}(z_k - z_{k-1}) - K_{c\varsigma}(\varsigma_k - \varsigma_{k-1})\end{aligned} \tag{130}$$

$$\begin{aligned}u_{xk} = u_{xk-1} - K_{xy}(y_k - y_{k-1}) - K_{xc}\,\Delta c_k - K_{xI}\,\Delta I_k \\ - K_{xx}(z_k - z_{k-1}) - K_{k\varsigma}(\varsigma_k - \varsigma_{k-1})\end{aligned} \tag{131}$$

$$z_{k+1} = f(z_k, \varsigma_k) \quad , \quad \varsigma_k = g_k \tag{132}$$

When u_{xk} has been modeled as a control rate command with a zero order hold, the actual control position commanded is given by δ_k.

$$\delta_{k+1} = \delta_k + \Delta t\, u_{xk} \quad , \tag{133}$$

where the control position command δ_k is part of the state x_k. Other holds will result in similar expressions.

Thus, the actual implemented digital control law is given by Eq. (129) - Eq. (133). It is seen that the constant terms depending on the trim conditions have canceled out and do not appear in this implementation.

It should be noted that the initial condition for the error integrator states, I_o, is not needed in this implementation. Only the initial control variables u_{xo}, and sometimes δ_o, and the initial compensator increment Δc_o are needed at initialization. The initial conditions for the control variables can be set equal to the actual control values at initialization. When a dynamic compensator is designed, the best selection of the initial compensator value is not clear; however, in many cases, the objective of the compensator and the initial plant operating point provide a good choice. For example, when the plant initially is in trim (i.e., in a steady state condition), the initial compensator increment, Δc_o, would be selected as zero. According to circumstances, other choices are possible. A more detailed study of the selection of the initial conditions, particularly when obvious choices are not available, is necessary.

When the plant, due to mechanical reasons, has limiting effects on the movement of the actual control variables, it is desirable not to command the controls to exceed these limits since such commands will not be followed. Therefore, it is often desirable to have control rate and control position limits set in the control law. In this implementation, such limits are easy to implement and generally have little negative impact. Rate limits can be applied to u_{xk} and position limits to δ_k.

It is important to distinguish between limiting action due to the feedforward commands as opposed to feedback related commands. It is important to note that, in a satisfactory design, there should be no plant limiting due to feedforward commands, except in some circumstances. The feedforward control design should include an analysis of maximum control commands implied by the class of commanded trajectories. In general, the plant limiting conditions should be avoided by appropriate changes in the command state and forcing vector.

In other words, the feedforward design philosophy proposed taken here is to command only trajectories which can physically be achieved by the plant, and avoid using up the control authority in the feedforward control, thus leaving some control authority to the

feedback controller. This has two desirable effects. The first is to allow the feedback controller to close the loop and provide its main objective; i.e., stability. This is of utmost importance in plants which are open-loop unstable or have relaxed static stability, as is the case with many high performance aircraft. If the feedforward commands were to reach the plant control limits, the feedback law would not be able to close the loop and perform its critical objectives. The second effect of this philosophy is to maintain the nonlinearities in the command model generating the desired trajectory. If an unachieveable trajectory is commanded, the precise outcome is not clear; i.e., the actual and desired trajectories will diverge; however, the nature of the divergence is no longer controlled, and how to recover from the divergence is not clear. Whereas by commanding and tracking a trajectory which may be somewhat different than originally desired, tracking control is maintained, and can be used to converge with the originally desired trajectory. The ease with which such nonlinear command models can be implemented digitally, as opposed to analog designs, is also worthy of note.

Finally, the usual type of "integrator wind-up" is eliminated in this implementation since the integral itself is not explicitly computed. Of course, when no limiting occurs, the effect of the integrator is unchanged; the integration is simply performed at a different location, namely in Eq. (131). However, when (nonlinear) limiting occurs, the effects are usually much more benign.

Eigenvalues of Implementation.

Since the implementation is obtained by differencing the control law designed, it would result in the same numerical control commands when all initial conditions are appropriately matched, no nonlinearities and no random disturbances are present. However, since these conditions rarely, if at all, hold, the implemented and designed control commands are not the same.

It is important to note that the implemented control law is closely related to but different than the designed law. For example, the implemented law depends on both y_k

and y_{k-1}, whereas the designed law only uses y_k. It is therefore necessary to investigate the closed-loop characteristics of the implemented control law.

After some manipulation, the implemented closed-loop system can be written as

$$\begin{pmatrix} x_{k+1} \\ \Delta c_{k+1} \\ \Delta I_{k+1} \\ x_k \\ u_{xk} \end{pmatrix} = \begin{pmatrix} \phi_x - \Gamma_x K_{xy} C_x & -\Gamma_x K_{xc} & -\Gamma_x K_{xI} & \Gamma_x K_{xy} C_x & \Gamma_x \\ -K_{cy} C_x & \phi_c - K_{cc} & -K_{cI} & K_{cy} C_x & 0 \\ \Delta t H_y C_x & 0 & 0 & 0 & 0 \\ I & 0 & 0 & 0 & 0 \\ -K_{xy} C_x & -K_{xc} & -K_{xI} & K_{xy} C_x & I \end{pmatrix} \begin{pmatrix} x_k \\ \Delta c_k \\ \Delta I_k \\ x_{k-1} \\ u_{xk-1} \end{pmatrix} \tag{134}$$

where the command model state and forcing vector, z_k and ς_k, and the constant vector d_k have been set to zero as they do not affect or modify the closed-loop eigenvalues.

It is clear that the stability of the implemented closed-loop system is determined by the eigenvalues of the matrix, Φ_I, rather than the eigenvalues of the designed closed-loop system shown below.

$$\begin{pmatrix} x_{k+1} \\ c_{k+1} \\ I_{k+1} \end{pmatrix} = \begin{pmatrix} \phi_x - \Gamma_x K_{xy} C_x & -\Gamma_x K_{xc} & -\Gamma_x K_{xI} \\ -K_{cy} C_x & \phi_c - K_{cc} & -K_{cI} \\ \Delta t H_y C_x & 0 & I \end{pmatrix} \begin{pmatrix} x_k \\ c_k \\ I_k \end{pmatrix} \quad , \tag{135}$$

where the vectors z_k, ς_k and the trim related constant vectors, which do not influence the closed-loop eigenvalues have again been set to zero for convenience.

The state transition matrix in Eq. (135) will be denoted by Φ_D, while the implemented state transition matrix in Eq. (134) will be denoted by Φ_I. Now, to investigate the relationship between the eigenvalues of Φ_I and Φ_D, consider

$$\Phi_I X = \lambda X \quad , \quad X^T = (x^T \; c^T \; I^T \; x_-^T \; u^T) \tag{136}$$

where X has $n + n_c + n_I + n + r$ components.

THEOREM 1. *Any eigenvalue of Φ_D is an eigenvalue of Φ_I.*

PROOF: Suppose that $(\tilde{x}^T \; \tilde{c}^T \; \tilde{I}^T)^T$ is an eigenvector of Φ_D corresponding to the eigenvalue λ. Note that there is at least one eigenvector for each eigenvalue, no matter its multiplicity. Let

$$x = \lambda\tilde{x} \quad , \quad c = (\lambda - 1)\tilde{c} \quad , \quad I = (\lambda - 1)\tilde{I} \quad , \quad x = \tilde{x} \quad , \tag{137}$$

$$u = -K_{xy}\, C_x\, \tilde{x} - K_{xc}\, \tilde{c} - K_{xI}\, \tilde{I} \quad , \tag{138}$$

for the augmented vector X according to the partition shown in Eq. (136).

To show that X is eigenvector of Φ_I corresponding to the eigenvalue λ, we write $\Phi_I\, X$ according to the partition and manipulate using the fact that λ is also an eigenvalue of Φ_D.

$$\begin{aligned}(\phi_x - \Gamma_x K_{xy} C_x)(\lambda\tilde{x}) - \Gamma_x K_{xc}(\lambda - 1)\tilde{c} - \Gamma_x K_{xI}(\lambda - 1)\tilde{I} + \Gamma_x K_{xy} C_x \tilde{x} + \Gamma_x u \\ = \lambda(\phi_x - \Gamma_x K_{xk} C_x)\tilde{x} - \lambda\Gamma_x K_{xc}\tilde{c} - \lambda\Gamma_x K_{xI}\tilde{I} \\ = \lambda(\lambda\tilde{x}) = \lambda x\end{aligned} \tag{139}$$

$$\begin{aligned}-K_{cy} C_x(\lambda\tilde{x}) + (\phi_c - K_{cc})(\lambda - 1)\tilde{c} - K_{cI}(\lambda - 1)\tilde{I} + K_{cy} C_x \tilde{x} \\ = (\lambda - 1)(\lambda\tilde{c}) = \lambda x\end{aligned} \tag{140}$$

$$\Delta t H_y C_x(\lambda\tilde{x}) = \lambda(\lambda\tilde{I} - \tilde{I}) = \lambda(\lambda - 1)\tilde{I} = \lambda I \tag{141}$$

$$Ix = \lambda\tilde{x} = \lambda x \tag{142}$$

$$\begin{aligned}-K_{xy} C_x(\lambda\tilde{x}) - K_{xc}(\lambda - 1)\tilde{c} - K_{xI}(\lambda - 1)\tilde{I} + K_{xy} C_x \tilde{x} + u \\ = (\lambda - 1)u + u = \lambda u\end{aligned} \tag{143}$$

Therefore, X is eigenvector of Φ_I corresponding to the eigenvalue λ, and the assertion is proved.

Thus, the designed eigenvalues are maintained in this implementation. Note that we have further shown that the eigenvectors of the implementation are very closely related to those designed; i.e., Eq. (137), Eq. (138). Note that other incremental implementations also maintain the designed eigenvalues [10].

It should be noted that the case of eigenvalues with multiplicity greater than one has not been considered, although, it would seem that the multiplicity may also be preserved.

THEOREM 2. *Φ_I has exactly $n + n_I + n_c - r_c$ zero eigenvalues, where*

$$r_c = \text{rank}\,(\phi_c - K_{cc} \quad - K_{cI} \quad K_{cy}C_x) \tag{144}$$

PROOF: Using Eq. (136) for λ of zero, we obtain

$$\phi_x x + \Gamma_x \bar{u} = \lambda x = 0 \tag{145}$$

$$-K_{cy}c_x x + (\phi_c - K_{cc})c - K_{cI}I + K_{cy}C_x x_- = \lambda c = 0 \tag{146}$$

$$\Delta t H_y C_x x = \lambda I = 0 \tag{147}$$

$$Ix = \lambda x_- = 0 \tag{148}$$

$$\bar{u} = -K_{xy}C_x x - K_{xc}C - K_{xI}I + K_{xy}C_x x_- + u = \lambda u = 0 \tag{149}$$

From Eq. (148) and Eq. (149), it is seen that x and $\bar{u}$ must vanish. Then, Eq. (145), Eq. (147), Eq. (148) and Eq. (149) are automatically satisfied. The remaining constraints are

$$(\phi_c - K_{cc})c - K_{cI}I + K_{cy}C - x_- = 0 \tag{150}$$

$$u = K_{xc}c + K_{xI}I - K_{xy}C_x x_- \tag{151}$$

$$X^T = (0^T \quad C^T \quad I^T \quad x_-^T \quad u^T) \tag{152}$$

where u is given by Eq. (151) and (c, I, x_-) satisfies Eq. (150) is an eigenvector of Φ_I corresponding to the zero eigenvalue. Since Eq. (150) has $n_c + n_I + n - R_c$ linearly independent solutions, there are as many linearly independent vectors X satisfying Eq. (150) - Eq. (152), which is the desired result.

Note that since $r_c \leq n_c$, the implementation has at least $n + n_I$ zero eigenvalues. When, as is usual, the number of integrals is selected to be the number of plant controls, all eigenvalues are accounted by the two theorems.

COROLLARY. *Let Φ_D have distinct non-zero eigenvalues and $n_I = r$; then the eigenvalues of Φ_I consist of those of Φ_D and zero.*

PROOF: By Theorem 1, the $n+n_c+n_I$ eigenvalues of Φ_D also belong to Φ_I. By Theorem 2, Φ_I has $n + r$ zero eigenvalues, which are necessarily different than those of Φ_D. Thus, all $2(n + r) + n_c$ eigenvalues of Φ_D are accounted for.

It is interesting to note that if the number of integrators used is greater than the number of plant controls, then some of the eigenvalues of Φ_D must necessarily be zero. This seems to provide a further implication that the number of integrators should be selected to be no greater than the number of plant controls, irrespective of the order of the dynamic compensator.

On the other hand, if the number of integrators is smaller than the number of plant controls, all the eigenvalues of Φ_I are not necessarily accounted for by Theorems 1 and 2.

In such cases, it is necessary to investigate the implemented closed-loop eigenvalues further, to ascertain that unstable eigenvalues (e.g., $\lambda = 1$) are not introduced in the process. To accommodate some cases, it is sometimes possible to use different implementations which circumvent implementation instabilities [14].

To illustrate the possibility of unstable eigenvalues, the following Theorem will be stated without proof.

THEOREM 3. *Φ_I has an eigenvalue of unity if, and only if, the matrix below is singular.*

$$\begin{pmatrix} \phi_x - I & 0 & \Gamma_x \\ \Delta t K_{cI} H_y C_x & I - \phi_c + K_{cc} & 0 \\ \Delta t K_{xI} H_y C_x & K_{xc} & 0 \end{pmatrix} \tag{153}$$

This theorem illustrates that when no integrators are used in the design, so that H_y vanishes, the matrix in Eq. (153) becomes singular, and the implementation has eigenvalues equal to unity which may, and often do, cause problems. This effect of the use of integrators provides a further incentive for their use in the control law.

III. DESIGN OF DIGITAL AUTOMATIC LANDING SYSTEM

In this section, the design of a digital integrated automatic landing system for NASA's Advanced Transport Operating Systems (ATOPS) Research Aircraft will be described. The ATOPS aircraft is a Boeing 737-100 which is used by Langley Research Center as a research vehicle equipped with special equipment and flight computers with which automatic control systems can be implemented in flight tests.

The automatic landing system described in this report is the successor to the Digital Integrated Automatic Landing System (DIALS) designed by the author using full state feedback techniques and random disturbance accommodation results [14], [8]. This system was successfully flight tested by NASA Langley Research Center [15]. The automatic control system described here uses stochastic output feedback [12], [11] and the stochastic feedforward techniques developed in the previous section.

A. Lateral Control Law Design

The design of the lateral control system follows the basic approach described in the previous section; i.e., the stochastic feedforward and output feedback design methodology. This requires the development of the design model, the feedback and the feedforward controller designs.

Lateral Plant Design Model.

As described in the previous section, the design model is needed for both the feedback and the feedforward control law designs. This model contains the aircraft's lateral aerodynamic and kinematic model, as well as the control actuator models, any inner loop control law and filtering which is already present and is intended to be part of the overall controller. The design model also includes basic elements of the control law structure such

as the open-loop models of any desired dynamic compensation, error integral feedback and control rate command.

The aerodynamic aircraft model can be obtained by linearizing the general nonlinear equations of motion (e.g., [16], [17]) about a flight condition with level wings, constant airspeed, constant flight path angle corresponding to the desired glideslope, flaps and gear down in the landing configuration. The linearized equations obtained are of the following form.

$$\dot{v}' = a_{11}v' + a_{12}p + a_{13}r + a_{14}\phi + a_{11}W_v' + b_{11}\delta A + b_{12}\delta R + b_{13}\delta s_p + d_v \tag{154}$$

$$\dot{p} = a_{21}v' + a_{22}p + a_{23}r + a_{21}W_v' + b_{21}\delta A + b_{22}\delta R + b_{23}\delta s_p + d_p \tag{155}$$

$$\dot{r} = a_{31}v' + a_{32}p + a_{33}r + a_{31}W_v' + b_{31}\delta A + b_{32}\delta R + b_{33}\delta s_p + d_r \tag{156}$$

$$\dot{\phi} = p + tan\,\theta_o\ r + d_\phi \tag{157}$$

$$\dot{\psi} = r + d_\psi \tag{158}$$

where ϕ, ψ, θ are the roll, yaw and pitch angles, respectively, p and r the roll rate and the yaw rate, respectively, v' is the inertial velocity of the aircraft c.g. along the y body-axis normalized by the nominal airspeed; δA, δR and δs_p are the aileron, rudder and spoiler

control surface positions, respectively; θ_o is the nominal value of the pitch angle. The coefficients a_{ij} and b_{ij} are functions of the aircraft's stability and control derivatives at the flight condition used in the linearization.

The lateral wind model included in the design model is a simple first order system describing the normalized lateral wind velocity, w'_v, driven by white noise.

$$W'_v = -0.1 W'_v + \omega_v \tag{159}$$

The kinematics in the lateral axis consist of the y-position of the aircraft c.g. relative to some fixed axis. Figure 2 shows the lateral geometry and the definition of some of the relevant angles and distances. The Earth-fixed set of axes has its origin at the glide path intercept point (GPIP), with the positive x-axis pointing along the runway centerline in the direction of the aircraft velocity at landing. The z-axis is along the local vertical positive downwards; with the y-axis selected so as to make a right-handed coordinate frame.

Let V_o be the nominal airspeed of the aircraft and $L_{EB} = L$ be the 3×3 matrix representing the transformation from the aircraft body axes to the Earth-fixed coordinate frame described above. If L_{ij} is the (i,j) element of the matrix L, then

$$\dot{y}' = L_{21}\, u' + L_{22}\, v' + L_{23}\, w' \quad , \tag{160}$$

where u', v' and w' are the normalized inertial velocity components along x, y and z body axes, respectively, and

$$L_{21} = cos\theta\, sin\psi \tag{161}$$

$$L_{22} = sin\varphi\, sin\theta\, sin\psi + cos\varphi\, cos\psi \tag{162}$$

$$L_{23} = cos\varphi\, sin\theta\, sin\psi - sin\varphi\, cos\psi \quad . \tag{163}$$

The general expression in Eq. (160) can be approximated using small angle approximations to give

$$\dot{y}' = v' - w'_o \varphi + u'_o \cos\theta_o \psi + d_y \quad , \tag{164}$$

where u'_o and w'_o are the normalized nominal velocity components along the x and y body axes, respectively.

The lateral actuator models used for control law design purposes are given below

$$\delta\dot{A} = -12.378\,\delta A + \frac{(11)(1.531)}{1 + .0015\bar{q}}\,\delta A_c \quad , \tag{165}$$

$$\delta\dot{R} = -32.67\,\delta R + 32.67(r_1 + r_2) + 32.67\,\delta R_c \quad , \tag{166}$$

where δA and δR represent the actual aileron and rudder surface positions, while δA_c and δR_c represent the aileron and rudder commands generated by the control law, respectively, and $\bar{q}$ is the dynamic pressure. The variables r_1 and r_2 are inner loop (yaw damper) variables which will be discussed in more detail later. The aileron and rudder actuator models given above are linearized and approximated versions of nonlinear systems containing servomechanisms, hydraulic and mechanical systems with usual nonlinearities such as hysteresis and limiting effects. A more detailed discussion of the actuator systems on the ATOPS research vehicle can be found in [18]. The spoiler is not used as an independent control surface, but rather as an aid in producing further rolling moment during turns in cooperation with the aileron surface. This is achieved as a nonlinear programmed gain on the flight computers, which is approximated to a simple linear relation in the design model.

$$\delta s_p = 1.73\,\delta A \quad . \tag{167}$$

The ATOPS research aircraft incorporates a yaw damper. In the design of the automatic landing system, the yaw damper is taken to be part of the basic airplane stability control system and interpreted as an inner loop system which will be part of the overall controller. The yaw damper model given below is therefore included in the design model of the open-loop plant.

$$\dot{r}_1 = -0.3(r_1 + r_2) \quad , \tag{168}$$

$$\dot{r}_2 = -6.993\, r_2 + 10.7485\, r \quad , \tag{169}$$

where r is the yaw rate, modeled by Eq. (156). The variables r_1 and r_2 are then used to generate the overall rudder command as shown in the rudder actuator model in Eq. (165).

Another system that is included in the design model as part of the open-loop plant is a third order complementary filter. This filter uses a body-mounted accelerometer triad along with position information from the Microwave Landing System (MLS) to obtain estimates of the aircraft velocity in the Earth coordinate system. The complementary filter is approximated as follows.

$$\hat{a}'_y = \dot{x}_{10} = -10\, x_{10} + 10\, a'_y \quad , \tag{170}$$

$$\hat{y}' = \dot{x}_{11} = x_{12} + .8(y - x_{11}) \quad , \tag{171}$$

$$\dot{y}' = \dot{x}_{12} = a'_y + .32(y - x_{11}) \quad , \tag{172}$$

$$a'_y = \frac{a_y}{U_o} \cong \dot{\beta} + r \quad , \tag{173}$$

where a_y is the body-mounted accelerometer reading for the x-axis, while a'_y is its normalized form and x_{10} the filtered acceleration, x_{11} and x_{12} are the filtered aircraft distance from the runway centerline and x_{12} its rate of change.

As mentioned earlier, the control variables are the aileron and rudder commands δA_c and δR_c, respectively. A rate command structure is used in the design of the control law, even though the actual implementation will command the surface positions.

$$\delta A_{ck+1} = \delta A_{ck} + \Delta t\, u_{1k} \quad , \tag{174}$$

$$\delta R_{ck+1} = \delta R_{ck} + \Delta t\, u_{2k} \quad , \tag{175}$$

where Δt is the sampling interval of the control law.

The design model accommodates a second order dynamic compensator, even though the actual design does not use the dynamic compensator. However, the model is given here for completeness.

$$c_{1k+1} = e^{-5\Delta t} c_{1k} + \Delta t\, u_{c1k} \quad , \tag{176}$$

$$c_{2k+1} = e^{-5\Delta t} c_{2k} + \Delta t\, u_{c2k} \quad , \tag{177}$$

Finally, the control law structure is modeled with two integrators, shown below as digital accumulators.

$$I_{1k+1} = I_{1k} + \Delta t(x_{11k} + 5\, x_{12k} - y'_{ck} - 5\, \dot{y}'_{ck}) \quad , \tag{178}$$

$$I_{2k+1} = I_{2k} + \Delta t(\varphi_k - \varphi_{ck}) \quad , \tag{179}$$

where y_{ck}, $\dot{y}_{ck}$ and φ_{ck} are the commanded values for y_k, $\dot{y}_k$ and φ_k, respectively. These commanded values will be defined in the command model.

The open-loop plant model used for the design of the lateral control law is obtained by the augmented system consisting of the state equations (154) - (159), (164) - (166), (168) - (172) and (174) - (179). It is important to note that Eqs. (174) - (179) which contain the digital controller structure are defined in discrete form in exactly the way that they will be implemented. Whereas the remaining equations of the design model are given in differential equation form as they model continuous processes. The latter set of equations must first be discretized using the usual sampled-data formulation [19] based on the assumption that δA_c and δR_c remain constant over the sampling interval. Then this set of discrete equations are augmented by the already discrete set (174) - (179) to obtain the complete discrete design model for the open-loop plant of 20^{th} order.

$$\bar{x}_{k+1} = \phi_x \bar{x}_k + \Gamma_x u_k + \bar{\Gamma}_x z_k + \omega_k + d_x \tag{180}$$

Lateral Command Design Model.

While the design model of the open-loop plant developed in the preceding is sufficient to design the feedback control law, the feedforward control law design requires the command design model. The command design model is used to obtain the structure and gains of the control law; however, the implementation of the actual commands may use a somewhat different set of equations as will be discussed in more detail in the following.

The lateral command model is selected to be the 4^{th} order system given by

$$y'_{ck+1} = y'_{ck} + \Delta t\, \dot{y}'_{ck} + \frac{\Delta t^2}{2} \ddot{y}'_{ck} \quad , \tag{181}$$

$$\dot{y}'_{ck+1} = \dot{y}'_{ck} + \Delta t\, \ddot{y}'_{ck} \quad , \tag{182}$$

$$\varphi_{ck+1} = \varphi_{ck} + \Delta t\, \dot{\varphi}_{ck} + \frac{\Delta t^2}{2} \ddot{\varphi}_{ck} \quad , \tag{183}$$

$$\dot{\varphi}_{ck+1} = \dot{\varphi}_{ck} + \Delta t\, \ddot{\varphi}_{ck} \quad . \tag{184}$$

The command model state vector, z_k, is

$$z_k = \left(y'_{ck} \;\; \dot{y}'_{ck} \;\; \varphi_{ck} \;\; \dot{\varphi}_{ck} \right)^T \quad , \tag{185}$$

$$\varsigma_{1k} = \frac{\Delta t^2}{2} \ddot{y}'_{ck} \;\; , \;\; \varsigma_{2k} = \Delta t\, \ddot{y}'_{ck} \;\; , \;\; \varsigma_{3k} = \frac{\Delta t^2}{2} \ddot{\varphi}_{ck} \;\; , \;\; \varsigma_{4k} = \Delta t\, \ddot{\varphi}_{ck} \tag{186}$$

The resulting command model is

$$z_{k+1} = \phi_z\, z_k + \varsigma_k \tag{187}$$

$$\phi_z = \begin{pmatrix} 1 & \Delta t & 0 & 0 \\ 0 & 1 & 0 & 0 \\ 0 & 0 & 1 & \Delta t \\ 0 & 0 & 0 & 1 \end{pmatrix} \quad . \tag{188}$$

As can be seen from the open-loop plant design model integral feedback equations (178) and (179), the tracking variables are the lateral position y and the roll angle φ. In the case of the y-position, a linear combination of the position and velocity is used as the error integral feedback. Furthermore, since the actual position and velocity are not known, their estimates as obtained from the third order complementary filter are used in the feedback loop; thus, the position tracking error is defined to be

$$(\hat{y}'_k - y'_{ck}) + 5(\dot{y}'_k - \dot{y}'_{ck}) \quad , \tag{189}$$

while the bank angle error is simply the difference $\varphi_k - \varphi_{ck}$.

An error formulation of the type described in the previous section is used for the design of the controller. The variables in which error terms are formed are the roll angle φ, the roll rate p, the lateral position y, the yaw angle ψ, and the lateral position and

velocity estimates from the complementary filter. The yaw angle command used is the desired track angle. With this definition of H in the error formulation Eq. (180) becomes

$$x_k = \bar{x}_k - H\, z_k \tag{190}$$

$$x_{k+1} = \phi_x\, x_k + \Gamma_x\, u_k + (\bar{\Gamma}_z + \phi_x\, H - H\, \phi_z)\, z_k - H\, \zeta_k + \omega_k + d_x \tag{191}$$

The error formulation of the open-loop plant model thus obtained is then used in designing the feedforward and feedback control laws. Table 1 shows the feedback vector and summarizes the structure of the controller. Table 2 shows the feedforward matrices Γ_z and Γ_ζ which apply to the error formulation of the open-loop design model.

While the command design model is given by Eqs. (181) - (188), the on-line generation of the actually commanded path is obtained using a more complex procedure. The lateral trajectory followed by the aircraft may be divided into two portions: the localizer capture path and the localizer. The localizer beam is assumed to be on the runway centerline.

Figure 2 shows the basic geometry of lateral maneuvers. When the controller is engaged, the aircraft heading ψ_o, is extended until it intersects the runway centerline (hence the localizer) at x_I. It is assumed that the initial aircraft position and heading are such that the aircraft would intersect the runway centerline if the heading remained constant. A new independent variable, R, is defined as follows.

$$R = (x - x_I)\, cos\, \frac{\psi_o}{2} + y\, sin\, \frac{\psi_o}{2} \quad , \tag{192}$$

As can be seen from Figure 2, R is measured along the bisector of the heading ψ_o at the localizer intercept point, x_I; it is the position component of the aircraft along this bisector; i.e., R is the distance between the localizer intercept point, x_I, and the intersection of the perpendicular to the bisector. The localizer capture command path is defined with R as the independent variable.

The command path prior to the initiation of the localizer capture mode simply follows a straight line along the initial heading of ψ_o. The localizer capture path is commanded when the capture criterion is satisfied, at $R = R_o$. The localizer capture path is a smooth curve with continuous first and second derivatives at both capture initiation and termination. At $R = R_o + P$, the commanded localizer capture path smoothly transitions into the straight-in localizer portion. The decrab mode is initiated when the decrab altitude is reached and continues until touchdown.

Thus, the actual lateral command path is generated using the equations

$$y_c = \begin{cases} (\hat{x} - x_I)\tan\psi_o & , \; R < R_0 \text{ or } JLOC = F \\ f_0(R) & , \; R_0 \le R \le R_0 + P \\ 0 & , \; R > R_0 + P \end{cases} \tag{193}$$

$$\dot{y}_c = \begin{cases} \hat{V}_G \sin\psi_o & , \; R < R_0 \text{ or } JLOC = F \\ \dot{R}\, f_1(R) & , \; R_0 \le R \le R_0 + P \\ 0 & , \; R > R_0 + P \end{cases} \tag{194}$$

$$\dot{R} = \dot{x}\cos\frac{\psi_o}{2} + \dot{y}\sin\frac{\psi_o}{2} \quad , \quad \hat{V}_G = \sqrt{\dot{x}^2 + \dot{y}^2} \quad , \tag{195}$$

where $\hat{V}_G$ is the estimated ground speed.

The smoothness of the localizer capture path is due to the selection of the functions $f_0(R)$ and $f_1(R)$. Over the interval $[-\frac{P}{2}, \frac{P}{2}]$, these functions are defined by

$$f_0(R) = f_0(R_0) + f_1(R_0)(R - R_0) + \frac{A}{2}(R - R_0)^2 - A\left(\frac{P}{2\pi}\right)^2\left(1 + \cos\frac{2\pi R}{P}\right) \tag{196}$$

$$f_1(R) = f_1(R_0) + A\left[(R - R_0) + \frac{P}{2\pi}\sin\frac{2\pi R}{P}\right] \quad , \tag{197}$$

$$f_2(R) = A\left(1 + \cos\frac{2\pi R}{P}\right) \quad , \tag{198}$$

where $f_0(R_0)$, $f_1(R_0)$, R_0, P and A are arbitrary parameters. These parameters are selected so as to satisfy the boundary conditions of continuity of the first and second derivatives of $f_0(R)$, namely $f_1(R)$ and $f_2(R)$, at both ends of the interval $[-\frac{P}{2}, \frac{P}{2}]$ with the adjoining paths, resulting in

$$P = -\frac{2}{A} sin \frac{\psi_o}{2} \quad , \quad R_0 = \frac{1}{A} sin \frac{\psi_o}{2} \quad , \tag{199}$$

$$f_0(R_0) = \frac{2}{A} sin^2 \frac{\psi_o}{2} \quad , \quad f_1(R_0) = 2 sin \frac{\psi_o}{2} \quad , \tag{200}$$

$$A = -sgn(\psi_o) \frac{|\ddot{y}|_{max}}{2 V_0^2} \quad , \tag{201}$$

where V_0 is the commanded airspeed and $|\ddot{y}|_{max}$ is the maximum inertial lateral acceleration which will be required to track y_c perfectly. Since $|\ddot{y}|_{max}$ is a measure of the sharpness of the capture and of the maximum bank angle required, it is left as a parameter to be selected by the flight experimenter. When $|\ddot{y}|_{max}$ is increased the localizer capture maneuver will be engaged closer to the localizer and will be performed more quickly using a higher bank angle.

The localizer capture criterion resulting from this trajectory is to engage the capture mode when

$$|\hat{y}| \leq \frac{1}{|\ddot{y}|_{max}} \left(2 V_0 sin \frac{\psi_o}{2} \right)^2 \tag{202}$$

is satisfied for the first time.

The commands for the roll angle, φ_c, are chosen so as to produce a coordinated turn when perfect tracking is achieved. The commanded track angle can be found to be

$$\psi_c = tan^{-1} \frac{f_1(R) cos \frac{\psi_o}{2}}{1 - f_1(R) sin \frac{\psi_o}{2}} \quad , \quad R_0 \leq R \leq R_0 + P \quad . \tag{203}$$

Accordingly, the commanded roll is selected to be

$$\varphi_c = tan^{-1}\left(\frac{\hat{V}_G}{g}\dot{\psi}_c\right) \quad , \quad p_c = \dot{\varphi}_c \tag{204}$$

When the decrab altitude is reached, the commanded roll angle is selected so as to roll into the wind and perform a sideslip maneuver

$$\dot{\varphi}_{ck} = G_d\,\hat{\psi}_k \quad , \quad \varphi_{ck+1} = \varphi_{ck} + \Delta t\,\dot{\varphi}_{ck} \quad . \tag{205}$$

The actual command vector used on-line is thus obtained using the set of equations described above. On the other hand, the design of the control gains uses the command design model given by Equations (181) - (184). Using the design models for the open-loop plant and controller structure and the command trajectory, the feedback and feedforward design for the lateral control law is obtained using the stochastic feedforward and output feedback approach described in the previous section. The analysis and simulation results will be described in the next section.

B. Longitudinal Control Law Design

The longitudinal control law design is performed following the same approach as the lateral control law. Although the flight maneuvers performed in the longitudinal vertical plane are different than the lateral maneuvers, command path models similar to the lateral capture can be used in the glideslope capture and flare maneuvers. As in the lateral case, a longitudinal plant design model and a command design model are needed to obtain the longitudinal control law.

Longitudinal Plant Design Model.

The plant design model is obtained by combining the aircraft's longitudinal aerodynamics and kinematics model with the control actuator and complementary filter models, and then augmenting the resulting model with the controller model consisting of dynamic

compensation, integral feedback and control rate models. An inner loop controller is not included in the longitudinal open-loop plant model. However, dynamic models for the vertical position and velocity estimates of the third order complementary filter and for the elevator and engine dynamics are included.

The aircraft's longitudinal aerodynamic model is obtained by linearizing the nonlinear aircraft equations of motion ([16], [17]) about the desired flight condition. The resulting equations are of the form

$$\dot{V}' = a_{11} V' + a_{12} w' + a_{13} q + a_{14} \theta + a_{11} W'_V + a_{12} W'_w + b_{11} \delta e + b_{12} \delta T + d_V \quad , \tag{206}$$

$$\dot{w}' = a_{21} V' + a_{22} w' + a_{23} q + a_{24} \theta + a_{21} W'_V + a_{22} W'_w + b_{21} \delta e + b_{22} \delta T + d_w \quad , \tag{207}$$

$$\dot{q} = a_{31} V' + a_{32} w' + a_{33} q + a_{34} \theta + a_{31} W'_V + a_{32} W'_w + b_{31} \delta e + b_{32} \delta T + d_q \quad , \tag{208}$$

$$\dot{\theta} = q + d_\theta \quad , \tag{209}$$

where V' is the normalized inertial speed of the aircraft e.g., w' the normalized velocity along the body z-axis, q the pitch rate, θ the pitch angle, W'_V and W'_w the normalized wind velocities along the x and z axes, respectively, δe the elevator surface position, δT the engine thrust, d_V, d_w, d_p and d_θ constants depending on the linearization point. The coefficients a_{ij} and b_{ij} are constants depending on the aircraft stability and control derivatives [16],

[17], [14]. The normalization factor for the affected variables is the aircraft's nominal airspeed, V_o.

It should be noted that, due to the presence of the linearization constants d_V, d_w, d_q and d_θ, the state variables V', W', q and θ are not the usual perturbations but the total value of these variables.

The design model for the longitudinal wind velocity components W'_V and W'_w is taken to consist of first order dynamics in each of the velocity components. Thus,

$$\dot{W}'_V = -0.1\, W'_V + \omega_V \quad , \tag{210}$$

$$\dot{W}'_w = -0.1\, W'_w + \omega_w \quad , \tag{211}$$

where ω_V and ω_w are assumed to be independent white noise processes driving the wind model.

The position of the aircraft c.g. along the Earth-fixed x and z axes can be obtained from the kinematic equations. The general kinematic equations can be expressed as

$$\dot{x}' = V'_G \cos \psi_T = V' \cos \gamma \cos \psi_T \quad , \tag{212}$$

$$\dot{z}' = -V' \sin \gamma \quad , \tag{213}$$

where V'_G is the normalized ground speed, ψ_T the track angle and γ the flight path angle. In the plant design model used here, the position along the Earth-fixed x-axis is taken as the independent variable, and is not modeled as a state variable. Accordingly, the expression for $\dot{x}$ given in Eq. (212) is not a state equation. On the other hand, the vertical position z is modeled as a state variable. After some manipulation, Eq. (213) can be approximated in the form

$$\dot{z}' = cos\ \gamma_o\, w' - cos\ \gamma_o\, \theta - sin\ \gamma_o\, V' + d_z \quad , \tag{214}$$

where γ_o is the nominal flight path angle.

The longitudinal controls used are the elevator surface position, δe, and the engine thrust, δT. The control actuator models used for design purposes are given by

$$\delta\dot{e} = -23.23\ \delta e + 2.0779\ \frac{10.76}{1 + 0.0023\bar{q}}\ \delta e_c \quad , \tag{215}$$

$$\delta\dot{T} = -0.5\ \delta T + 0.298\ \delta th \quad , \tag{216}$$

$$\delta\dot{th} = -\delta th + \delta th_c \quad , \tag{217}$$

where δe_c and δth_c represent the commanded elevator and throttle positions, respectively, and δth the throttle position. The elevator actuator model includes the effect of cable stretch due to aerodynamic loading on the surface. It is also important to note that the engine dynamics are actually rather nonlinear, and respond faster when reducing thrust than when increasing thrust. A linear approximation to the latter condition has been used in the design model in Eq. (216). A 1 second time constant is used to model the throttle servo dynamics. Rate limiting and other nonlinear effects are not included in the open-loop plant design model.

The third order complementary filter is modeled by

$$\hat{z} = 0.8\, z - 0.8\, \hat{z} + \dot{z} \tag{218}$$

$$\dot{z} = 0.4\, z - 0.4\, \hat{z} + \hat{a}_z \tag{219}$$

$$\hat{a}_z = -10\, \hat{a}_z + 10\, a_z \tag{220}$$

$$\dot{\hat{a}}_x = -10\,\hat{a}_x + 10\,a_x \tag{221}$$

where $\hat{a}_x$ and $\hat{a}_z$ are the filtered versions of the actual accelerations a_x and a_z, respectively.

As in the case of the lateral design model, a second order dynamic compensator is included in the plant model; however, the design does not use dynamic compensator and purposefully results in vanishingly small gains. The open-loop compensator model is shown here for completeness.

$$c_{1k+1} = u_{c1k} \quad , \tag{222}$$

$$c_{2k+1} = u_{c2k} \quad , \tag{223}$$

where u_{c1k} and u_{c2k} are the compensator control variables.

To obtain a Type-1 system in the commanded variables, integral feedback of the error in altitude and airspeed is included in the control structure as follows.

$$I_{1k+1} = I_{1k} + \Delta t(\hat{z}'_k + 5\,\dot{z}'_k - z'_{ck} - 5\,\dot{z}'_{ck}) \quad , \tag{224}$$

$$I_{2k+1} = I_{2k} + \Delta t(V'_k + W'_{vk} - V'_{ck}) \quad , \tag{225}$$

where Δt is the sampling interval of the control law. Note that although the inertial speed V' is not known, the sum $(V' + W'_v)$ is the airspeed which is measured and therefore available for feedback. V'_{ck} here represents the normalized airspeed rather than inertial speed command.

Finally, the design model uses a rate command structure for the control variables. Thus,

$$\delta e_{ck+1} = \delta e_{ck} + \Delta t\; u_{1k} \quad , \tag{226}$$

$$\delta th_{ck+1} = \delta th_{ck} + \Delta t \; u_{2k} \quad , \tag{227}$$

where u_{1k} and u_{2k} are the control variables of the open-loop plant design model thus obtained.

When the continuous system model described by linear differential equations are discretized using the standard stochastic sampled-data formulation and the digital controller model is added, the discrete plant design model of 20^{th} order is obtained.

$$\bar{x}_{k+1} = \phi_x \bar{x}_k + \Gamma_x u_k + \bar{\Gamma}_z Z_k + \omega_k + d_x \quad . \tag{228}$$

To avoid confusing the vertical position variable, z, with the command state vector, the latter is denoted by Z in Eq. (228) and in the following.

Longitudinal Command Design Model.

The longitudinal variables used in the design, as indicated by the error integral feedback variables in Eqs. (224) and (225), are the airspeed and a linear combination of the vertical position and its rate of change. Note that this linear combination may be interpreted as the predicted value of the vertical position in 5 seconds. Also recall that since the Earth-fixed z-axis is defined positive downward, the vertical position, z, is the negative of the c.g. altitude, h.

The longitudinal command model selected for designing the feedforward control gains is the 2^{nd} order system given by

$$Z_{1k+1} = Z_{1k} + \varsigma_{1k} \quad , \tag{229}$$

$$Z_{2k+1} = Z_{2k} + \varsigma_{2k} \quad , \tag{230}$$

$$Z_{k+1} = I \, Z_k + \varsigma_k \quad . \tag{231}$$

The command state vector Z_k corresponds to $(z'_{ck}\ V'_{ck})^T$, where z'_{ck} is the normalized vertical position command and V'_{ck} is the normalized airspeed command.

An error formulation is also used in the longitudinal control law. Thus, error terms are formed in the normalized vertical position, z, the complementary filtered estimate of the vertical position, $\hat{z}$, and the airspeed, V. With this definition of the matrix H, the plant equations become

$$x_k = \bar{x}_k = H\ Z_k \tag{232}$$

$$x_{k+1} = \phi_x\, x_k + \Gamma_x\, u_k + (\bar{\Gamma}_x + \phi_x\, H - H\, \phi_x) Z_k - H\, \varsigma_k + \omega_k + d_x \quad . \tag{233}$$

While the command design model given by Eqs. (229) and (230) are used to design the feedforward control gains, the actually commanded path is obtained as follows. Initially, the aircraft is assumed to be in level flight prior to the glideslope capture maneuver. The initial altitude of the aircraft is maintained until the glideslope capture criterion is satisfied, at which time the desired glideslope capture path is commanded. When the capture is completed, the desired glideslope is the vertical path commanded until the flare initiation criterion is satisfied. At that time, the altitude profile corresponding to the flare path is commanded until touchdown.

The same functions f_0, f_1 and f_2 which have been used in the lateral command path generation are used in generating the glideslope capture and flare path. An important characteristic of these paths is their smoothness. The independent variable used in the longitudinal path command is the x-position of the aircraft c.g. in the Earth-fixed coordinate frame. The commanded path is given here as the altitude, h, which corresponds to the negative of the vertical position, z. Thus, the glideslope capture and flare vertical profiles are generated using the basic form

$$h_0(x) = h_0(x_0) + h_1(x_0)(x - x_0) + \frac{1}{2} A(x - x_0)^2 - A\left(\frac{P}{2\pi}\right)^2 \left(1 + cos\ \frac{2\pi(x + \Delta x)}{P}\right) \quad , \tag{234}$$

$$h_1(x) = h_1(x_0) + A\left[(x - x_0) + \frac{P}{2\pi}\ sin\ \frac{2\pi(x + \Delta x)}{P}\right] \quad , \tag{235}$$

$$h_2(x) = A\left(1 + cos\ \frac{2\pi(x + \Delta x)}{P}\right) \quad , \tag{236}$$

where x_0 corresponds to the initiation of the maneuver, and the constants are selected according to whether the glideslope capture or flare maneuver is to be performed. The altitude, sink rate and vertical acceleration are given by

$$h(x) = h_0(x) \quad , \quad \dot{h}(x) = \dot{x}\, h_1(x) \quad , \quad \ddot{h}(x) = \ddot{x}^2\, h_2(x) + \ddot{x}\, h_1(x) \quad . \tag{237}$$

The glideslope capture path starts from level flight and smoothly transitions to the desired glideslope angle γ_{GS}. When the capture path starts at an altitude h_{GC} and requires a vertical acceleration no larger than $|\ddot{h}|_{max}$, the parameters of the path given by Eqs. (234) - (235) are

$$A_{GC} = -\frac{|\ddot{h}|_{max}}{2V_0^2} \quad , \quad P_{GC} = \frac{tan\,\gamma_{GS}}{A_{GC}} \quad , \tag{238}$$

$$x_0 = x_{GC} = \frac{h_{GC}}{tan\,\gamma_{GS}} - \frac{P_{GC}}{2} \quad , \quad \Delta x = -\frac{h_{GC}}{tan\,\gamma_{GS}} \quad , \tag{239}$$

$$h_0(x_{GC}) = h_{GC} \quad , \quad h_1(x_{GC}) = 0 \tag{240}$$

Thus, when the aircraft is at an initial altitude h_{GC} and must track the glideslope γ_{GS} without exceeding $|\ddot{h}|_{max}$ of vertical acceleration the vertical profile given by Eq. (234)

using the parameters in Eqs. (238) - (240) will be denoted by $h_{GC}(x) = h_{0GC}(x)$, $h_{1GC}(x)$ and $h_{2GC}(x)$. It should be noted that the smoothness of the glideslope capture can be easily adjusted by selecting the appropriate value for $|\bar{h}|_{max}$.

The criterion for initiating the glideslope capture can be expressed as follows. Command the path $h_{0GC}(x)$ when the inequality

$$\hat{x}_k \tan\gamma_{GS} - \hat{h}_k \leq -\frac{P_{GC}}{2} \tan\gamma_{GS} \tag{241}$$

is satisfied.* Here $\hat{x}_k$, and $\hat{h}_k$ are the current estimates of the aircraft's x-position and altitude.

For the flare maneuver, the constraints are placed at touchdown. It is desired that the aircraft touch down at x_{td} with a flight path angle γ_{td}. Since flare must also initiate on the glideslope, the parameters for the flare profile $h_F(x)$ are uniquely determined.

$$A_F = \frac{(\tan\gamma_{td} - \tan\gamma_{GS})^2}{2(h_{td} - x_{td}\tan\gamma_{GS})} \quad , \qquad P_F = \frac{\tan\gamma_{td} - \tan\gamma_{GS}}{A_F} \quad . \tag{242}$$

$$x_0 = x_F = x_{td} - P_F \quad , \qquad \Delta x = -\frac{P_F}{2} - x_F \quad , \tag{243}$$

$$h_0(x_F) = x_F \tan\gamma_{GS} \quad , \qquad h_1(x_F) = \tan\gamma_{GS} \quad . \tag{244}$$

The flare initiation criterion resulting from this trajectory is to command the flare path $h_F(x)$ when

$$\hat{h}_k \leq x_F \tan\gamma_{GS} + 12.75 \tag{245}$$

is satisfied for the first time. Note that the constant 12.75 allows for the fact that the altitude of interest for touchdown is measured to the bottom of the wheels on the landing

*The glideslope capture criterion was later changed, replacing $\hat{h}_k$ by $h_o(\hat{x}_k)$ to eliminate a spike in the elevator.

gear rather than the aircraft c.g.. The overall vertical profile of the commanded path starting at level flight prior to glideslope capture until touchdown can be expressed as

$$h(x) = \begin{cases} h_{GC} & , x < x_{GC} \\ h_{GC}(x) & , x_{GC} \leq x < x_{GS} = x_{GC} + P_{GC} \\ x\,tan\,\gamma_{GS} & , x_{GS} \leq x < x_F \\ h_F(x) & , x \geq x_F \end{cases} \tag{246}$$

$$h_1(x) = \begin{cases} 0 & , x < x_{GC} \\ h_{1GC}(x) & , x_{GC} \leq x < x_{GS} = x_{GC} + P_{GC} \\ tan\,\gamma_{GS} & , x_{GS} \leq x < x_F \\ h_{1F}(x) & , x \geq x_F \end{cases} \tag{247}$$

$$h_2(x) = \begin{cases} 0 & , x < x_{GC} \\ h_{2GC}(x) & , x_{GC} \leq x < x_{GS} = x_{GC} + P_{GC} \\ 0 & , x_{GS} \leq x < x_F \\ h_{2F}(x) & , x \geq x_F \end{cases} \tag{248}$$

Recall that the sink rate and vertical acceleration can be easily obtained using Eq. (237).

The airspeed command is generated as follows. Let V_o be the commanded airspeed, $\hat{V}_o$ the initial measured airspeed and V_{ck} the airspeed commanded at the k^{th} sample by the command model. Since a sudden jump in airspeed is undesirable, any difference between the initial and desired airspeeds, $V_o - \hat{V}_o$, is gradually eliminated starting with an initial command equal to the actually measured airspeed.

$$V'_{ck+1} = V'_{ck} + \varsigma_{2k} \quad , \quad V'_{co} = \hat{V}'_o \quad , \quad V'_{ck} = \frac{V_{ck}}{V_o} \tag{249}$$

$$\varsigma_{2k} = \begin{cases} sgn(V_o - \hat{V}_o)\dfrac{\dot{V}_{max}}{V_o} & , \text{ if } |1 - V'_{ck}| > \dfrac{\dot{V}_{max}}{V_o} \\ 1 - V'_{ck} & , \text{ otherwise} \end{cases} \tag{250}$$

where $\dot{V}_{max}$ is the maximum acceleration or deceleration desired during the approach. Thus, the commanded airspeed starts from the actual one and commands a constant deceleration or acceleration until the desired airspeed command is reached.

During flare, the airspeed command decelerates the aircraft for touchdown as long as the airspeed remains above the minimum desirable airspeed V_{min} which is selected higher than the stall speed and consistent with contingencies such as go-around maneuvers.

$$V'_{ck+1} = \begin{cases} V'_{ck} + \varsigma_{2k} & , V'_{ck} > V'_{min} \\ V'_{min} & , V'_{ck} \leq V'_{min} \end{cases} \tag{251}$$

$$\varsigma_{2k+1} = \begin{cases} \varsigma_{2k} - \Delta t \dfrac{25}{V_o T n} & , \varsigma_{2k+1} > -\Delta t \dfrac{25}{V_o T} \text{ and } V'_{ck} > V'_{min} \\ -\Delta t \dfrac{25}{V_o T} & , \varsigma_{2k+1} \leq -\Delta t \dfrac{25}{V_o T} \text{ and } V'_{ck} > V'_{min} \\ 0 & , V'_{ck} \leq V'_{min} \end{cases} \tag{252}$$

where T is the period of time in which a 25 ft/sec. decrease in airspeed will be commanded.

Thus, during flare the commanded airspeed is reduced to aid in the maneuver and in touchdown as long as a safe speed of V_{min} is maintained.

IV. ANALYSIS AND NONLINEAR SIMULATION

The lateral and longitudinal/vertical control laws designed use the open-loop plant design models and the command design models described in the last section. The design approach used is the Stochastic Feedforward/Output Feedback methodology described in Section II. In this section, the design is analyzed by obtaining the closed-loop eigenvalues and singular values, and by simulating the digital automatic landing system obtained to control a nonlinear computer simulation of the ATOPS Research Vehicle, a B-737-100 aircraft.

A. Closed-Loop System Analysis

The open-loop plant design models for the lateral and longitudinal/vertical dynamics have been discussed in Section III. As can be seen by simple observation of the equations making up the design models, both the lateral and longitudinal/vertical open-loop plants can be expressed in the form

$$x_{k+1} = \phi_x x_k + \Gamma_x u_k + \Gamma_z Z_k + \Gamma_\varsigma \varsigma_k + \omega_k + d_x \tag{253}$$

The lateral design model state consists of the twenty components:

$$\{v', p, r, \varphi, \psi, y', W_v', \delta A, \delta R, \hat{a}_y', \hat{y}', \hat{\dot{y}}', r_1, r_2, c_1, c_2, I_1, I_2, \delta A_c, \delta R_c\}$$

The control law structure is selected so that 13 out of the 20 lateral states are used in the feedback. In particular, the actual aileron and rudder surface positions, the yaw damper inner loop system states and the lateral wind velocity are not used for feedback, although some of these are measured and available for use. The feedback vector for lateral controller consists of

$$\{p, r, \varphi, \psi, \hat{a}'_y, \hat{y}', \hat{\dot{y}}', c_1, c_2, I_1, I_2, \delta A_c, \delta R_c\}$$

The control vector consists of the aileron and rudder rate commands $\delta \dot{A}_c$ and $\delta \dot{R}_c$, respectively. Integral feedback is used for errors in lateral position and roll angle. The lateral control structure is summarized in Table 1. Table 2 summarizes the lateral command model parameters needed in designing the feedforward control gains. Table 3 shows the designed lateral gains for the feedforward and feedback control laws. The control gains in Table 3 follow the terminology of Eq. (128).

It should be noted that the feedforward command state gain corresponds to the case of error feedback. This is obtained intentionally to aid in steady state offset reduction. The reasoning can be illustrated as follows. Suppose that the altitude and sink rate errors and the airspeed error are null, and that the command system does not contemplate a maneuver, then it is reasonable to maintain the control surfaces at their current position, since changing the control commands to different values is likely to result in a non-zero error. The same approach is used in both the lateral and longitudinal feedforward controllers.

Closing the loop with the feedback control gains given in Table 3 results in the closed-loop discrete system. The s-domain equivalent eigenvalues of the closed-loop lateral system are shown in Table 4. The singular values for the discrete plant with the loop broken at the input is shown in Table 5.

The longitudinal/vertical design model state consists of the following twenty components:

$$\{V', w, q, \theta, z', W'_V, W'_w, \delta T, \delta e, \delta th, \hat{a}'_x, \hat{a}'_z, \hat{z}', \hat{\dot{z}}' c_1, c_2, I_1, I_2, \delta th_c, \delta e_c\}$$

The longitudinal feedback vector excludes some of the components of the state vector such as the inertial speed in vertical body axis w', the longitudinal and vertical wind velocities, the true aircraft altitude, the engine thrust and the elevator surface position.

On the other hand, the complementary filtered altitude ($-\hat{z}$), sink rate and accelerations are used by the controller, as can be seen by the feedback vector components

$$\{V', q, \theta, \hat{a}'_x, \hat{a}'_y, \hat{z}', \hat{\dot{z}}', c_1, c_2, I_1, I_2, \delta th_c, \delta e_c\}$$

In the longitudinal/vertical control law, the commanded variables are predicted vertical position and airspeed. Thus, the integral of the error in the predicted vertical position and the airspeed are used in the feedback law. The throttle rate and elevator rate are, the control components; however, as discussed in Section II C, the actual control commands are the throttle and elevator positions δth_c and δe_c, respectively. The longitudinal/vertical feedback control structure is summarized in Table 6.

The command design model parameters required for the feedforward control of the longitudinal/vertical trajectory is summarized in Table 7. The gains designed for the feedforward and feedback controllers are shown in Table 8.

Closing the loop with the output feedback gains obtained results in the closed-loop equivalent s-domain eigenvalues shown in Table 9. The singular value, eigenvalue and Bode plots of the closed-loop system are shown in Figure 4.

B. Nonlinear Simulation

The performance of the digital automatic landing system described above is evaluated in this part through a digital computer simulation. The ATOPS B-737-100 aerodynamics, actuator systems, kinematics, servo, hydraulic and other systems have been simulated in considerable detail in a nonlinear digital computer simulation. In this simulation, dynamic systems such as the complementary filter, the yaw damper, the spoiler-aileron coupling, the engine, etc. are modeled as nonlinear systems which accurately describe their actual behavior rather than their linearized versions used in the open-loop plant model.

The digital automatic control system described in the preceding sections is simulated in detail. The control law simulation is then interfaced with the aircraft simulation so that

the control commands computed by the design become the input to the aircraft control actuator systems. Numerous simulations of the closed-loop aircraft system were performed under a variety of different conditions. The aircraft response in simulations are shown in Figures 5 - 16.

The digital control system simulates the incremental implementation shown in Section II. C Eqs. (129) - (133). While other incremental implementations are possible, they are not used here. It should be noted that, since both lateral and longitudinal/vertical controllers designed used a control rate structure, Eq. (133) is, in fact, implemented to obtain the commands for the aileron, rudder, elevator and throttle positions. The actual outputs of the control system are the control position commands δ_k.

The Boeing 737 aircraft used here has a baseline stabilizer automatic trim logic. The auto-trim logic drives the stabilizer surface so as to minimize the moment on the elevator hinge, thus providing maximum authority for the elevator to react to sudden changes in the flight parameters. The stabilizer movement is much slower than that of the elevator and does not introduce further dynamic modes in the models. The use of the incremental implementation is very suitable to accommodate such slow moving surfaces. In the nonlinear simulations of the automatic landing system designed here, the stabilizer automatic trim logic is turned on; so that the stabilizer automatically trims the aircraft even though the plots shown do not include the stabilizer position.

The control system iteration rate used in the simulation is 10 Hz which is also the sampling rate used in the control law design. Since the control law is digital, this update rate must be used for the controller simulation. However, the simulation of the aircraft aerodynamic and on-board systems is performed at 20 Hz. Since these system describe continuous processes with some modes of high natural frequency, their simulation requires a higher update rate for accuracy. It is also important to note from Eqs. (129) - (133) that the control system output δ_k at time t_k uses only variables available at time t_{k-1}. Therefore, as long as the real-time computation of the commands, δ_k, require no more

than 100 msecs, no computational delay will be present. It is assumed that a sufficiently fast flight computer will be used to compute the incremental implementation commands. Thus, the accuracy of the digital control system simulation is expected to be restricted to round-off errors due to limitations in the word length of the flight computer, possible mismatches in obtaining exactly a 10 Hz rate, input-output limitations, etc.

The feedforward and feedback control gains used in the simulation are given in Tables 3 and 8. The simulation of the actual commanded path shown by Eq. (132) in the incremental implementation equations is performed as described in Section III. It should be noted that the actual command model uses estimates of the position and of the velocity of the aircraft c.g.. thus, the feedforward control law implementation actually contains nonlinear feedback. The coupling is usually rather low and may be neglected. However, a more complete evaluation should include these feedback effects as well as the effect of the feedback control law.

The simulations shown in Figures 5 - 16 are initialized at an estimated altitude of 950 ft. At initialization, the aircraft is flying a constant altitude path with level wings and a heading so as to intercept the localizer or the runway centerline at some point, x_I. The automatic landing system is engaged at the initialization of the simulation. At that point, the control law checks to see whether the localizer glideslope capture criteria are satisfied. The initial conditions have been selected so that neither the localizer nor the glideslope capture criterion will be met at this point. Thus, according to the command path generated, the aircraft continues along the same track angle with level wings and maintains a constant altitude.

At initialization, the aircraft calibrated airspeed is selected to be 135 knots. On the other hand, in most of the simulations, the commanded airspeed V_o is 125 knots. Accordingly, the control law experiences an instantaneous error of about 10 knots at initialization. As described in Section III, the feedforward command model generates a linearly decreasing airspeed profile from this initial speed to its commanded speed. As seen in the simulations,

the aircraft decelerates, following the commanded airspeed, until V_o is reached. When the commanded airspeed V_o is 135 knots, as shown in Figure 6, then the initial airspeed error is zero, and the airspeed command is a constant value of V_o. As can bee seen from Figure 6, the control law accurately maintains the commanded speed of 135 knots rather than reducing it to 125 knots as it does when the commanded airspeed is 125 knots.

As the control law continually tests to see if the glideslope or localizer capture criteria are satisfied, whether the glideslope or the localizer capture will be the first to engage depends on the aircraft's position, its heading relative to the runway centerline and the commanded glideslope angle, with other parameters having generally a lesser effect. In almost all the simulations shown here, one capture mode is engaged soon after the other, so that the aircraft flight path is a curved 3D path in both the lateral and vertical planes. Ability to perform both localizer and glideslope captures simultaneously is described in order to achieve close-in captures, as it is no longer necessary to perform localizer capture first and then engage the glideslope capture.

When the desired glideslope angle is 3^o, the glideslope capture criterion is satisfied first in most of the simulations. The initiation of the glideslope capture maneuvers can be clearly seen in the commanded and actual sink rate plots. Both commanded and actual sink rate smoothly transition from level flight to the sink rate required to remain on the desired glideslope at the desired airspeed. Also note the pitch angle and angle of attack movements during the glideslope capture maneuvers. Whereas the angles coincide when flying a constant altitude path, when glideslope capture is engaged automatically, the control law smoothly pitches the aircraft down to capture the glideslope. Note that there is no initial tendency to pitch in the "wrong" direction.

Also note that prior to glideslope capture, the pitch and angle of attack have to increase slightly when the aircraft is decelerating in order to compensate for the reduction of lift due to the airspeed, hence dynamic pressure, reduction. The needed extra lift is obtained by pitching up and increasing the angle of attack, albeit with lag which results

in a small altitude offset. On the other hand, when the aircraft does not decelerate, as shown in Figure 6, the aircraft pitch and angle of attack remain essentially constant as it is not necessary to obtain extra lift to maintain altitude.

It should be noted that since maneuvers are principally performed by the feedforward controller, the glideslope capture performance is an indication that the feedforward controller is satisfactory for this type of maneuver. Observation of the throttle and elevator positions shows that the feedforward controller pitches down by initially lowering the throttle rather than using the elevator. For the B-737 which has a thrust line considerably lower than the c.g., reducing thrust has the added effect of reducing the pitching moment. This control strategy is precisely the one that best suits this aircraft, since simply using the elevator to pitch would have the unwanted result of increasing the airspeed. Thus, the stochastic feedforward control approach is indeed making use of the plant design model information as would be desired.

At the end of the glideslope capture, the altitude error is redefined causing an instantaneous move in its value. This causes a corresponding sudden and undesired transient in the elevator and throttle commands when the altitude error move is appreciable. This glitch can be removed in a number of ways, including the use of a simple easy-on function at the appropriate time.

It should be noted that the smoothness of the glideslope capture maneuver and its duration are directly related to the parameter $|\tilde{h}|_{max}$; i.e., the maximum vertical acceleration of the commanded altitude profile. By simply varying this parameter at any time prior to glideslope capture, the commanded capture path may be changed on-line to a smoother or faster maneuver as desired.

In Figures 7 and 8, the automatic landing system captures steep glideslope of 4° and 4.5°, respectively. The glideslope capture path generated by the feedforward model given in the previous section by Eqs. (234) - (248) is automatically modified to result in a vertical profile which captures a steeper glideslope, tracks it and flares from this steeper glideslope.

Since the same maximum vertical acceleration value is used for all glideslope angles, it may be noted that the duration of the steeper glideslope captures is slightly longer. However, the basic characteristics of the response and of the control law remain unchanged.

It should also be noted that the feedforward and feedback control gains remain unchanged while the commanded vertical path varies according to speed or glideslope angle. Thus, the feedforward control law tracks the commanded path within the class of commanded trajectories. It is clear that if the commanded paths are sufficiently different from each other, feedforward controllers adapted to the specific characteristics of each path would result in "better" performance. One such approach would be to extend the stochastic feedforward approach to include optimal gain scheduling.

In the simulation of the steep glideslope cases, it may be noted that glideslope capture occurs later. This is a consequence of the geometry, as the initial aircraft altitude is the same. In the case of the 4^o glideslope both localizer and glideslope capture occur in the same period of time. Localizer capture occurs mostly before the aircraft captures the steeper 4.5^o glideslope in part due to a larger localizer intercept angle of 47^o. In all cases, the control law captures the desired glideslope by satisfactorily tracking the commanded capture path.

When the glideslope capture is performed, the aircraft tracks the desired glideslope until the flare mode is engaged. As can be seen from the simulations of different glideslope angles (i.e., Figures 5 - 8), the aircraft remains on the desired glideslope with essentially the same precision for shallow and steep glideslopes.

The flare mode is engaged when the flare criterion in Eq. (245) is satisfied. In this mode, both the flare vertical profile generated as well as the airspeed reduction profile are commanded. As can be seen from the simulations, the aircraft pitches up increasing its angle of attack and the lift as desired; this results in a corresponding reduction in the sink rate and the airspeed until touchdown. This is achieved by using the elevator to pitch up while lowering the throttle to reduce the airspeed.

It can be seen that in all cases, the pitch angle at touchdown is comfortable above zero and still rising. This pitch attitude at touchdown is necessary to avoid landing on the nose wheel which is not designed for the high load at touchdown.

As the flare maneuver is significantly sharper than the glideslope capture maneuver, it requires faster control action. Thus, the measurement noise covariance, $\hat{V}_\zeta$, for the command model forcing vector was reduced to obtain the flare gains, resulting in a higher forcing vector gain, K_ζ, during flare as shown in Table 8. Due to the complexity of the flare maneuver and the high accuracy needed in tracking the altitude profile, a higher order altitude command model would model this profile more accurately.

The localizer capture for a 3^o glideslope and localizer intercept angle of 32^o, as shown in Figure 5, is initiated near the end of the glideslope capture maneuver. As can be seen from the heading and roll plots, the aircraft yaw and roll angles track their commanded trajectories closely and capture the localizer. The lateral position is also seen to track its commanded profile accurately. Although a small deviation from the localizer is present, this does not resemble a usual overshoot pattern as it occurs after reaching the localizer. In all cases, this offset is quite small and tends not to exceed 3 m. As in the case of the glideslope capture, the high accuracy of the tracking of the lateral position indicates that the stochastic feedforward controller can produce satisfactory feedforward control law designs.

During the maneuver, the roll angle and the lateral position commands are selected so as to produce a coordinated turn when perfect tracking occurs. The sideslip angle plots indicate that the sideslip angle remains well within 1^o of sideslip during the whole final approach excluding, of course, the decrab maneuver shown in Figure 14. The maximum sideslip tends to occur during localizer capture slightly after the peak bank angle. On the other hand, note that the lateral acceleration is plotted on the same set of axes and follows the roll angle quite closely, as expected during a coordinated turn, whereas the lateral specific force in the body axes remains near zero in a coordinated turn.

The smoothness and duration of the localizer capture path command can be varied by varying the maximum commanded lateral acceleration $|\ddot{y}|_{max}$. This maximum acceleration is set to 10 ft/sec^2 in most of the simulations shown. However, Figure 10 shows a simulation where $|\ddot{y}|_{max}$ is set to a value of 5 ft/sec^2. Observation of the lateral variables shows that the localizer capture is smoother, lasts longer, requires a lower maximum roll angle to capture as well as resulting in a lower maximum lateral acceleration as expected. The turn coordination, although acceptable for $|\ddot{y}|_{max}$ value of 10, appears to be improved as indicated by a lower maximum sideslip angle. The tracking of the lateral position also shows some improvement. Thus, the feedforward control law can clearly track lateral command paths where the lateral acceleration does not exceed 10 ft/sec^2 with no change in the feedforward control gains.

A number of simulations are shown in Figures 5 - 16 where the sensitivity of the automatic landing system to various parameters is shown. For example, the aircraft weight is varied among 85,000 lbs, 90,000 lbs, and 95,000 lbs. The center of gravity of the aircraft is also varied in tandem with the weight. Figures 13 - 16 shows the sensitivity to winds and noise including bias errors. The wind gust standard deviation used in the simulations containing gusts is 2 ft/sec. (0.61 m/sec.). The airspeed command is varied between 125 and 135 knots, while the commanded glideslope angles simulated are 3^o, 4^o and 4.5^o.

V. CONCLUSIONS AND RECOMMENDATIONS

In this study, a combined stochastic feedforward/feedback control design methodology is developed, and a digital automatic landing system is designed using this approach. It is considered that the main objective of a control law is to enable the plant to track a desired or commanded trajectory selected from a given class of trajectories as closely as possible in the presence of random and deterministic disturbances and despite uncertainties about the plant. The feedforward controller tries to track the desired or commanded trajectory, whereas the feedback controller tries to maintain the plant state near the desired trajectory despite the presence of random, and possibly deterministic, disturbances and uncertainties about the plant. Modern control theory has concentrated more attention on the important feedback control problem, while the feedforward control problem has received less attention.

The feedforward control problem is formulated as a stochastic output feedback problem where the plant contains unstable and uncontrollable modes. As the standard output feedback algorithm requires an initial gain which stabilizes the plant, a new algorithm is developed to obtain the feedforward control gains. The necessary conditions are shown to result in coupled linear matrix equations, implying that when a solution exists, it is indeed the globally optimal control gain.

The formulation of the feedforward problem in a stochastic, rather than the standard deterministic, setting is significant in two ways. First, the class of desired trajectories from which the actually commanded path is selected can be effectively described as a random process generated by a dynamical system driven by a white noise process. The second, and more important, implication of a stochastic optimization formulation is the tacit understanding that "perfect tracking" is often not possible due to various reasons including uncertainties about, or variation in the, plant parameters, the presence of plant

nonlinearities and unmatched initial conditions. Thus, questions about the robustness and sensitivity of the feedforward controller arise naturally in this context.

A combined stochastic feedforward/feedback control methodology is developed where the main objectives of the feedforward and feedback control laws are clearly seen. Furthermore, the inclusion of error integral feedback, dynamic compensation, rate command control structure, etc. is an integral element of the methodology. Another advantage of the methodology is the flexibility that a variety of feedback control design techniques with arbitrary structures may be employed to obtain the feedback controller; these include stochastic output feedback, multi-configuration control, decentralized control or frequency and classical control methods.

Finally, a specific incremental implementation is recommended for the combined feedforward/feedback controller. Some advantages of this digital implementation are the simplicity of implementation, the fact that trim values are not needed and that problems such as integrator wind-up can be largely avoided. The closed-loop eigenvalues using this implementation are shown to contain the designed closed-loop eigenvalues which would result if an incremental implementation were not used. It is further shown that when using an incremental implementation, it is advantageous to design the controller with as many integrators as the number of controls. Using fewer integrators results in marginally stable eigenvalues of unity, while using more integrators constrains the placement of eigenvalues. The choice of the same number of integrators as controls is also an intuitively pleasing one.

A digital automatic landing system for the ATOPS Research Vehicle (a Boeing 737-100) is designed using the stochastic feedforward controller and stochastic output feedback. The system control modes include localizer and glideslope capture, localizer and glideslope track, crab, decrab and flare. Using the recommended incremental implementation, the control laws are simulated on a digital computer and interfaced with a nonlinear digital simulation of the aircraft and its systems.

In this study, the feedforward controller takes an equal place along the feedback con-

troller in achieving the overall control objective. While the stochastic feedforward/feedback approach has been successfully developed and applied to a significant problem, some significant questions and extensions of the problem remain unanswered, and are recommended for further study and experimentation. Three general areas of study are worthy of further investigation:

- **the structure of the feedforward controller**
- **the robustness and sensitivity of the feedforward controller**
- **optimal gain scheduling of the feedforward controller**

The structure of the feedback controller considers questions about the role of feedforward dynamic compensation, the use of the "future values of the desired trajectory" in the current control command, the use of the full-state feedforward controller when fast flight computers are available. An argument can be effectively made that since a pilot knows the future desired trajectory and uses this information in his current control commands, the optimal feedforward controller should also take advantage of such information.

The uncertainties about complex system parameters and nonlinear effects bring forth uncertainties about the trajectory which would be tracked when the actual plant parameter are different than those used in the feedforward design. Since the feedforward controller does not determine the stability of the closed-loop plant, instability does not generally result from such mismatching. However, since unsatisfactory performance would generally result from a high sensitive feedforward law, it is of interest to study measures of robustness and design methods which incorporate low sensitivity criteria.

In applications where the plant will vary over a wide range of conditions resulting in large changes in plant model parameters, or in cases where the command model parameter vary to achieve some objective, it is necessary to adapt the feedforward control gains according to varying conditions. This can be achieved by extending the optimal gain scheduling studies to include feedforward controller. Due to the relative simplicity of the coupled linear necessary conditions, gain scheduling with respect to all the plant parameters

rather than a selected few may be feasible. In particular, the feedforward gain of the command model forcing vector seems extremely appropriate for such application.

REFERENCES

1. Ogata, K., Modern Control Engineering, Prentice-Hall, Englewood Cliffs, New Jersey, 1970.
2. Schultz, D. G. and J. L. Melsa, State Functions and Linear Control Systems, McGraw-Hill, New York, 1967.
3. Anderson, B. D. O. and J. B. Moore, Linear Optimal Control, Prentice-Hall, Englewood Cliffs, New Jersey, 1971.
4. Kwakernaak, H. and R. Sivan, Linear Optimal Control Systems, John Wiley & Sons, Inc., New York, 1972.
5. Kailath, T., Linear Systems, Prentice-Hall, Englewood Cliffs, New Jersey, 1980.
6. O'Brien, M. J. and J. R. Broussard, "Feedforward Control to Track the Output of a Forced Model", The 17th IEEE Conference on Decision and Control, San Diego, CA, January 1979.
7. Halyo, N., "Development of a Digital Automatic Control Law for Steep Glideslope Capture and Flare", NASA CR-2834, June 1977.
8. Halyo, N. and R. E. Foulkes, "On the Quadratic Sampled-Data Regulator with Unstable Random Disturbances", IEEE SMC Cos. Proc. 1974 International Conf. on Syst., Man and Cybern., October 1974.
9. Broussard, J. R., "Extensions to PIFCGT: Multirate Output Feedback and Optimal Disturbance Suppression", NASA CR-3968, March 1986.
10. Maybeck, P. S., Stochastic Models, Estimation and Control, Vol. 3, Academic Press, New York, 1982.
11. Halyo, N. and J. R. Broussard, "A Convergent Algorithm for the Stochastic Infinite-Time Discrete Optimal Output Feedback Problem", Proc. 1981 Joint Auto. Control Conference, Charlottesville, VA, June 1981.

12. Halyo, N. and J. R. Broussard, "Investigation, Development, and Application of Optimal Output Feedback Theory, Volume I - A Convergent Algorithm for the Stochastic Infinite-Time Discrete Optimal Output Feedback Problem", NASA CR-3828, August 1984.

13. Halyo, N. and J. R. Broussard, "Algorithms for Output Feedback, Multiple Model and Decentralized Control Problems", NASA Aircraft Controls Research - 1983, NASA CP-2296, October 25-27, 1983.

14. Halyo, N., "Flight Tests of the Digital Integrated Automatic Landing System (DIALS)", NASA CR-3859, December 1984.

15. Hueschen, R. M., "The Design, Development, and Flight Testing of a Modern-Control-Designed Autoland System", American Control Conference, Boston, Massachusetts, June 1985.

16. Etkin, B., Dynamics of Atmospheric Flight, John Wiley & Sons, Inc., New York, 1972.

17. Roskam, J., Flight Dynamics of Rigid and Elastic Airplanes, Parts I & II, Roskam Aviation and Engineering Corp., 519 Boulder, Lawrence, KS, 1972.

18. Broussard, J. R. and S. T. Stallman, "Modification and Verification of an ACSL Simulation of the ATOPS B-737 Research Aircraft", NASA CR-166049, February 1983.

19. Halyo, N. and A. K. Caglayan, "A Separation Theorem for the Stochastic Sampled-Data LQG Problem", International J. of Control, Vol. 23, No. 2, February 1976, pp. 237-244.

TABLE 1

LATERAL CONTROL STRUCTURE

• STATES :	$V', p, r, \varphi, \psi, y', W'_V, \delta A, \delta R, \hat{a}'_y, \hat{y}', \hat{\dot{y}}',$ $r_1, r_2, c_1, c_2, I_1, I_2, \delta A_c, \delta R_c$
• FEEDBACK :	$p, r, \varphi, \psi, \hat{a}'_y, \hat{y}', \hat{\dot{y}}', c_1, c_2, I_1, I_2, \delta A_c, \delta R_c$
• CONTROLS :	$\delta \dot{A}_c, \delta \dot{R}_c$
• INTEGRATORS :	$I_1 : (\hat{y}' + 5\hat{\dot{y}}') - (y'_c + 5\dot{y}'_c)$ $I_2 : \varphi - \varphi_c$

TABLE 2

LATERAL FEEDFORWARD DESIGN MODEL

$$\phi_x = \begin{pmatrix} 1 & \Delta t & 0 & 0 \\ 0 & 1 & 0 & 0 \\ 0 & 0 & 1 & \Delta t \\ 0 & 0 & 0 & 1 \end{pmatrix} \qquad H_x = 0$$

$$H_x = \begin{pmatrix} 0 & 0 & 0 & 0 & 0 & 0 & 0 & 0 & 0 & 0 & 1 & 5 & 0 & 0 & 0 & 0 & 0 & 0 & 0 & 0 \\ 0 & 0 & 0 & 1 & 0 & 0 & 0 & 0 & 0 & 0 & 0 & 0 & 0 & 0 & 0 & 0 & 0 & 0 & 0 & 0 \end{pmatrix}$$

$$\Gamma_x = \begin{pmatrix} 0 & 0 & \phi_{1,4} & \phi_{1,2} \\ 0 & 0 & \phi_{2,4} & \phi_{2,2} - 1 \\ 0 & 0 & \phi_{3,4} & \phi_{3,2} \\ 0 & 0 & 0 & \phi_{4,2} - \Delta t \\ 0 & 0 & \phi_{5,4} & \phi_{5,2} \\ 0 & 0 & \phi_{6,4} & \phi_{6,2} \\ 0 & 0 & \phi_{7,4} & \phi_{7,2} \\ 0 & 0 & \phi_{8,4} & \phi_{8,2} \\ 0 & 0 & \phi_{9,4} & \phi_{9,2} \\ 0 & 0 & \phi_{10,4} & \phi_{10,2} \\ 0 & 0 & \phi_{11,4} & \phi_{11,2} \\ 0 & 0 & \phi_{12,4} & \phi_{12,2} \\ 0 & 0 & \phi_{13,4} & \phi_{13,2} \\ 0 & 0 & \phi_{14,4} & \phi_{14,2} \\ 0 & 0 & 0 & 0 \\ 0 & 0 & 0 & 0 \\ 0 & 0 & 0 & 0 \\ 0 & 0 & 0 & 0 \\ 0 & 0 & 0 & 0 \\ 0 & 0 & 0 & 0 \end{pmatrix} \qquad \Gamma_\zeta = \begin{pmatrix} 0 & 0 & 0 & 0 \\ 0 & 0 & 0 & -1 \\ 0 & 0 & 0 & 0 \\ 0 & 0 & -1 & 0 \\ 0 & -1 & 0 & 0 \\ -1 & 0 & 0 & 0 \\ 0 & 0 & 0 & 0 \\ 0 & 0 & 0 & 0 \\ 0 & 0 & 0 & 0 \\ 0 & 0 & 0 & 0 \\ -1 & 0 & 0 & 0 \\ 0 & -1 & 0 & 0 \\ 0 & 0 & 0 & 0 \\ 0 & 0 & 0 & 0 \\ 0 & 0 & 0 & 0 \\ 0 & 0 & 0 & 0 \\ 0 & 0 & 0 & 0 \\ 0 & 0 & 0 & 0 \\ 0 & 0 & 0 & 0 \end{pmatrix}$$

TABLE 3

LATERAL FEEDFORWARD AND FEEDBACK CONTROL GAINS

$$K_{xy} = \begin{array}{cccccccccc} & p & r & \varphi & \psi & \hat{a}'_y & \hat{y}' & \dot{y}' & \delta A_c & \delta R_c \\ & 3.20 & 8.58 & 6.96 & 23.1 & -12.9 & 2.61 & 6.36 & 8.10 & -1.37 \\ & 0.874 & -3.91 & 1.79 & -4.01 & -4.67 & 0.164 & -2.75 & 0.658 & 3.0 \end{array}$$

$$K_{xI} = \begin{array}{ccc} & I_1 & I_2 \\ & 0.136 & -0.974 \\ & 0.087 & 0.709 \end{array}$$

$$K_{xc} = 0$$

$$K_{xz} = \begin{array}{ccccc} & z_1 & z_2 & z_3 & z_4 \\ & -2.61 & -29.40 & -6.96 & -3.20 \\ & -0.164 & 6.75 & -1.79 & -0.874 \end{array}$$

$$K_{x\zeta} = \begin{array}{ccccc} & \zeta_1 & \zeta_2 & \zeta_3 & \zeta_4 \\ & -15.8 & -94.0 & 0 & 0 \\ & 6.37 & 42.4 & 0 & 0 \end{array}$$

TABLE 4.

LATERAL EQUIVALENT s-DOMAIN EIGENVALUES

REAL	IMAGINARY	DAMPING RATIO ζ	NATURAL FREQUENCY ω_n
-30.528 -30.528	10.231 -10.231	0.948	32.197
-10.309	0.000	---	---
- 5.919	0.000	---	---
- 5.000	0.000	---	---
- 5.000	0.000	---	---
- 2.991 - 2.991	2.565 - 2.565	0.759	3.940
- 1.813	0.000	---	---
- 1.298 - 1.298	2.206 - 2.206	0.507	2.560
- 0.400 - 0.400	0.399 - 0.399	0.708	0.565
- 0.320 - 0.320	0.383 - 0.383	0.641	0.499
- 0.221 - 0.221	0.159 - 0.159	0.812	0.272
- 0.101	0.000	---	---
- 0.100	0.000	---	---
- 0.045	0.000	---	---

TABLE 5

LATERAL SINGULAR VALUES

DISCRETE PLANT MODEL
LOOP BROKEN AT INPUT
ADDITIVE DISTURBANCES - I + G(z)

FREQUENCY RAD/SEC	SINGULAR VALUES (DB)		FREQUENCY RAD/SEC	SINGULAR VALUES (DB)	
.100	38.96317	4.78900	1.096	7.51139	3.65942
.120	34.17652	4.06872	1.202	7.28880	3.51846
.132	31.94145	3.65855	1.318	6.95444	3.37497
.145	29.82154	3.20361	1.445	6.55861	3.24136
.158	27.82184	2.69623	1.585	6.13864	3.11803
.174	25.94473	2.13010	1.738	5.71874	3.00086
.191	24.18936	1.50043	1.905	5.31367	2.88429
.289	22.55143	.80378	2.089	4.93203	2.76257
.229	21.02349	.03714	2.291	4.57867	2.63037
.251	19.59549	- .80331	2.512	4.25595	2.48330
.275	18.25574	-1.72397	2.754	3.96424	2.31841
.302	16.99190	-2.73499	3.020	3.70189	2.13494
.331	15.79191	-3.84906	3.311	3.46516	1.93470
.363	14.64492	-5.07103	3.631	3.24856	1.72195
.398	13.54220	-6.35644	3.981	3.04569	1.50253
.437	12.47835	-7.48516	4.365	2.85016	1.28290
.479	11.45294	-7.85899	4.786	2.65619	1.06925
.525	10.47290	-6.80808	5.248	2.45896	.86701
.575	9.55562	-4.59673	5.754	2.25473	.68047
.631	8.73253	-2.06160	6.310	2.04096	.51261
.692	8.05380	.25371	6.919	1.81659	.36501
.759	7.59327	2.06794	7.586	1.58224	.23791
.832	7.42464	3.20706	8.318	1.34069	.13031
.912	7.49358	3.68497	9.120	1.09716	.04016
1.000	7.57524	3.75444	12.000	.85950	- .03544

TABLE 6

LONGITUDINAL/VERTICAL CONTROL STRUCTURE

• STATES :	V', α, q, θ, z', W'_u, W'_α, δT, δe, δth, $\hat{a}_x$, $\hat{a}_n$, $\hat{z}$, $\dot{\hat{z}}$, c_1, c_2, I_1, I_2, δth_c, δe_c
• FEEDBACK :	V', q, θ, $\hat{a}_x$, $\hat{a}_n$, $\hat{z}$, $\dot{\hat{z}}$, c_1, c_2, I_1, I_2, δth_c, δe_c
• CONTROLS :	$\delta \dot{th}_c$, $\delta \dot{e}_c$
• INTEGRATORS :	$\hat{z} + 5\,\dot{\hat{z}}$, V'

TABLE 7

LONGITUDINAL/VERTICAL FEEDFORWARD DESIGN MODEL

$$\phi_x = I \qquad H_x = 0$$

$$H_x = \begin{pmatrix} 0 & 0 & 0 & 0 & 0 & 0 & 0 & 0 & 0 & 0 & 0 & 0 & 1 & 5 & 0 & 0 & 0 & 0 & 0 & 0 \\ 1 & 0 & 0 & 0 & 0 & 0 & 0 & 0 & 0 & 0 & 0 & 0 & 0 & 0 & 0 & 0 & 0 & 0 & 0 & 0 \end{pmatrix}$$

$$\Gamma_x = \begin{pmatrix} 0 & \phi_{1,1} - 1 \\ 0 & \phi_{2,1} \\ 0 & \phi_{3,1} \\ 0 & \phi_{4,1} \\ 0 & \phi_{5,1} \\ 0 & \phi_{6,1} \\ 0 & \phi_{7,1} \\ 0 & \phi_{8,1} \\ 0 & \phi_{9,1} \\ 0 & \phi_{10,1} \\ 0 & \phi_{11,1} \\ 0 & \phi_{12,1} \\ 0 & \phi_{13,1} \\ 0 & \phi_{14,1} \\ 0 & 0 \\ 0 & 0 \\ 0 & 0 \\ 0 & 0 \\ 0 & 0 \\ 0 & 0 \end{pmatrix} \qquad \Gamma_\zeta = \begin{pmatrix} 0 & -1 \\ 0 & 0 \\ 0 & 0 \\ 0 & 0 \\ -1 & 0 \\ 0 & 0 \\ 0 & 0 \\ 0 & 0 \\ 0 & 0 \\ 0 & 0 \\ 0 & 0 \\ 0 & 0 \\ -1 & 0 \\ 0 & 0 \\ 0 & 0 \\ 0 & 0 \\ 0 & 0 \\ 0 & 0 \\ 0 & 0 \end{pmatrix}$$

TABLE 8

LONGITUDINAL/VERTICAL FEEDFORWARD AND FEEDBACK CONTROL GAINS

$$K_{xy} = \begin{array}{cccccccccc} & CAS' & q & \theta & a'_x & a'_n & \hat{z}' & \dot{z}' & \delta th_c & \delta e_c \\ & 9.01 & -0.16 & 1.14 & 8.9 & 1.24 & -1.18 & -0.81 & 1.0 & 1.05 \\ & -5.75 & -8.04 & -9.10 & -11.7 & -5.90 & 3.39 & 7.69 & -0.03 & 4.81 \end{array}$$

$$K_{xI} = \begin{array}{cc} \hat{z}' + 5\,\dot{\hat{z}}' & CAS' \\ -0.082 & 0.56 \\ 0.36 & 0.093 \end{array}$$

$$K_{xc} = \begin{array}{cc} -2.8E-05 & -9.1E-05 \\ -1.3E-05 & 2.0E-05 \end{array}$$

$$K_{xx} = \begin{array}{cc} 0.0 & 0.0 \\ 0.0 & 0.0 \end{array}$$

$$K_{x\zeta} = \begin{array}{cccc} & \text{GLIDESLOPE} & & \text{FLARE} \\ & \underline{\qquad} & & \underline{\qquad} \\ & \zeta_1 & \zeta_2 & \zeta_1 \quad \zeta_2 \\ - & 67.97 & -527.6 & -203.9 \quad -527.6 \\ & 101.2 & -116.0 & 303.6 \quad -116.0 \end{array}$$

TABLE 9.

LONGITUDINAL EQUIVALENT s-DOMAIN EIGENVALUES

REAL	IMAGINARY	DAMPING RATIO ζ	NATURAL FREQUENCY ω_n
-42.9	0.000	---	---
-29.9	0.000	---	---
-10.0	0.000	---	---
- 8.4	0.000	---	---
- 6.4	0.000	---	---
- 6.4	0.000	---	---
- 1.79 - 1.79	3.3 - 3.3	0.477	3.754
- 0.97	0.000	---	---
- 0.70	0.000	---	---
- 0.42 - 0.42	0.27 - 0.27	0.841	0.499
- 0.40	0.000	---	---
- 0.37 - 0.37	0.67 - 0.67	0.483	0.765
- 0.2	0.000	---	---
- 0.2	0.000	---	---
- 0.10 - 0.10	0.088 - 0.088	0.751	0.133
- 0.095	0.000	---	---

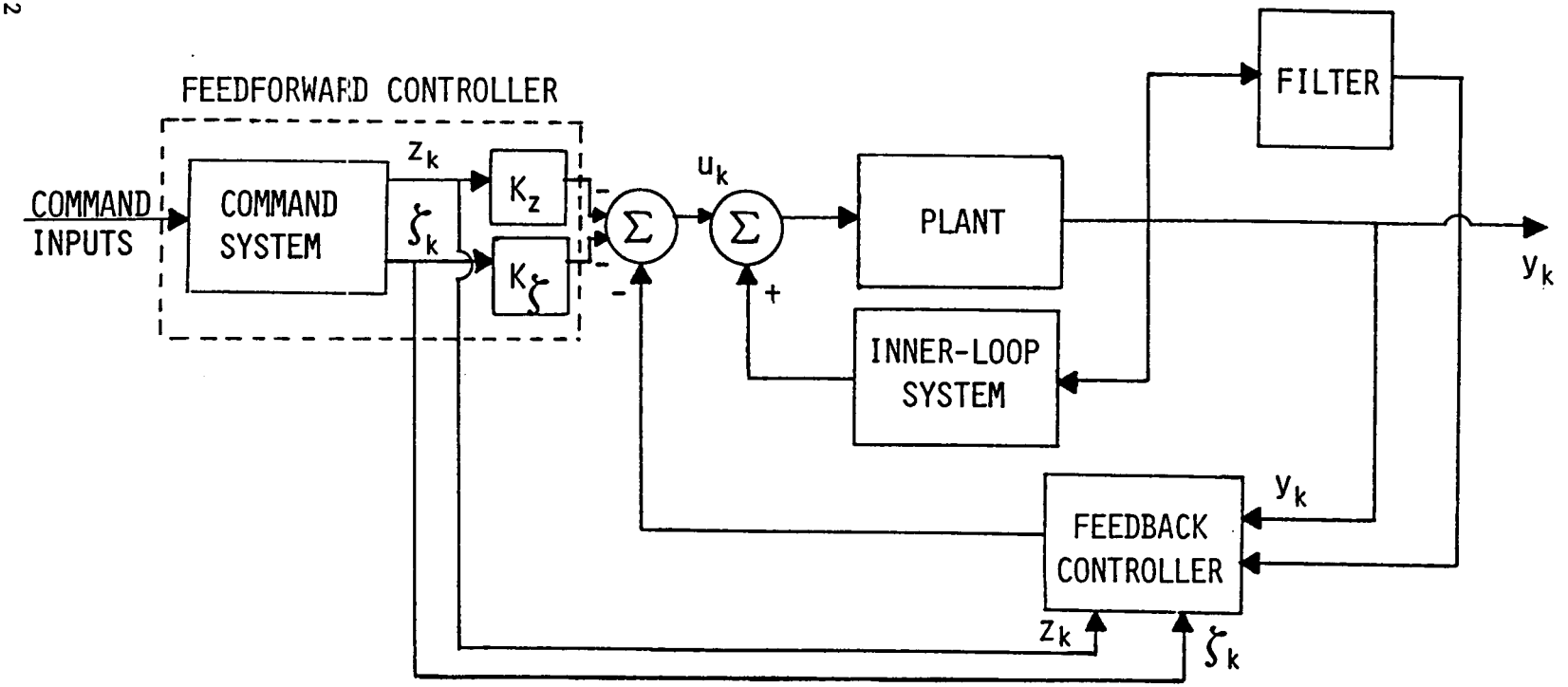

FIGURE 1. FUNCTIONAL CLOSED-LOOP BLOCK DIAGRAM

$$R = (x - x_I)\cos\frac{\psi_o}{2} + y\sin\frac{\psi_o}{2}$$

$$\dot{R} = \dot{x}\cos\frac{\psi_o}{2} + \dot{y}\sin\frac{\psi_o}{2}$$

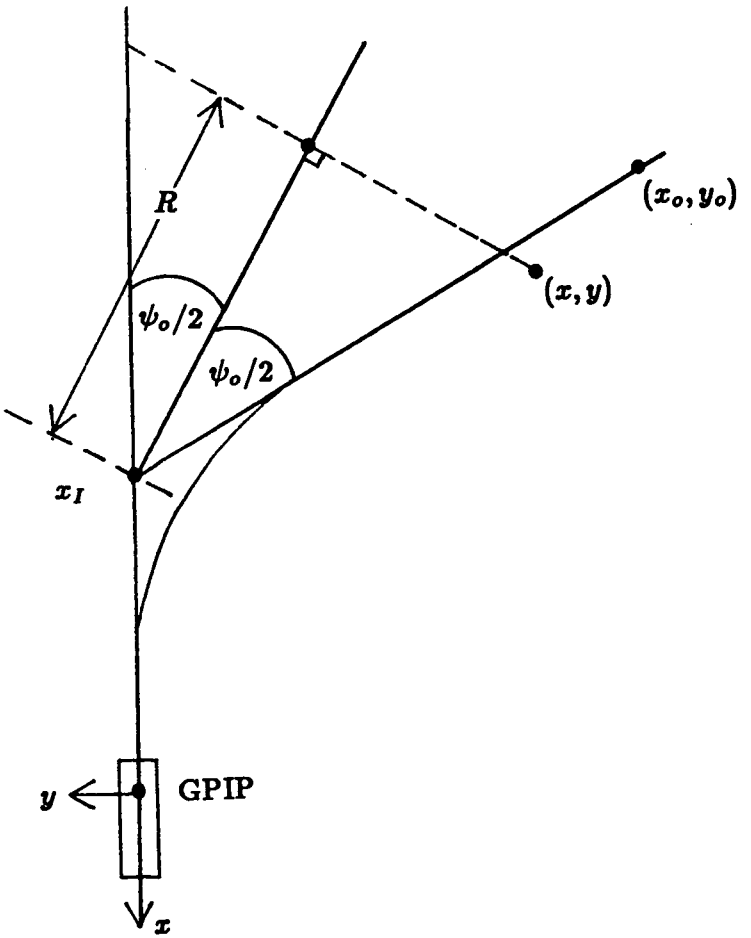

FIGURE 2. LATERAL PATH GEOMETRY

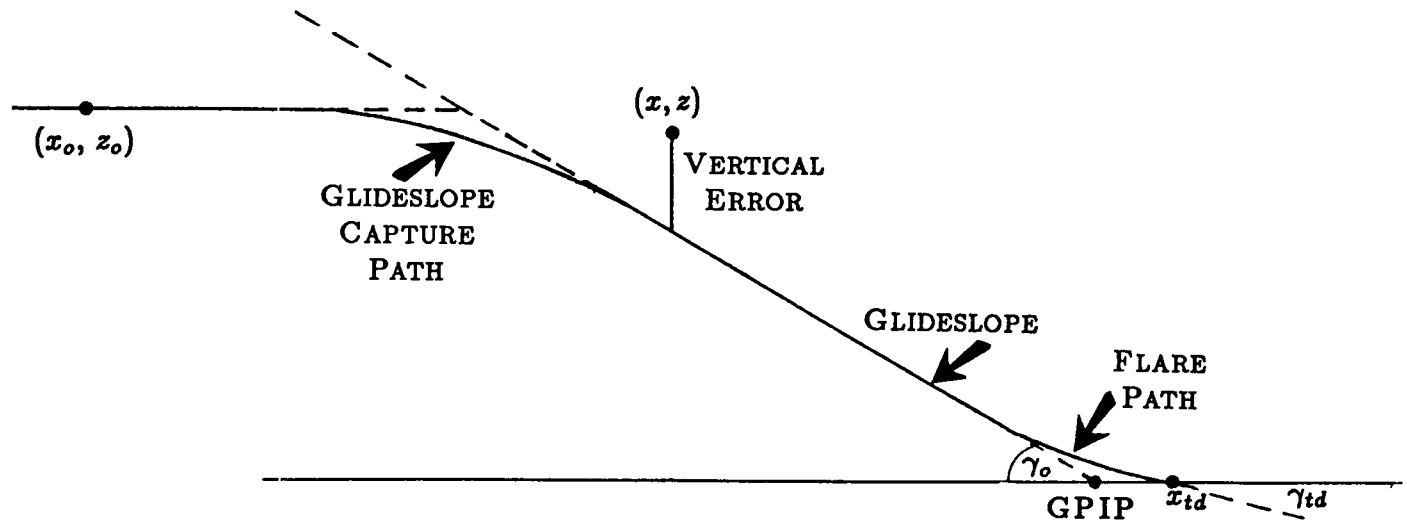

FIGURE 3. LONGITUDINAL/VERTICAL PATH GEOMETRY

- LOOP IS BROKEN AT CONTROL INPUT
- ADDITIVE DISTURBANCES

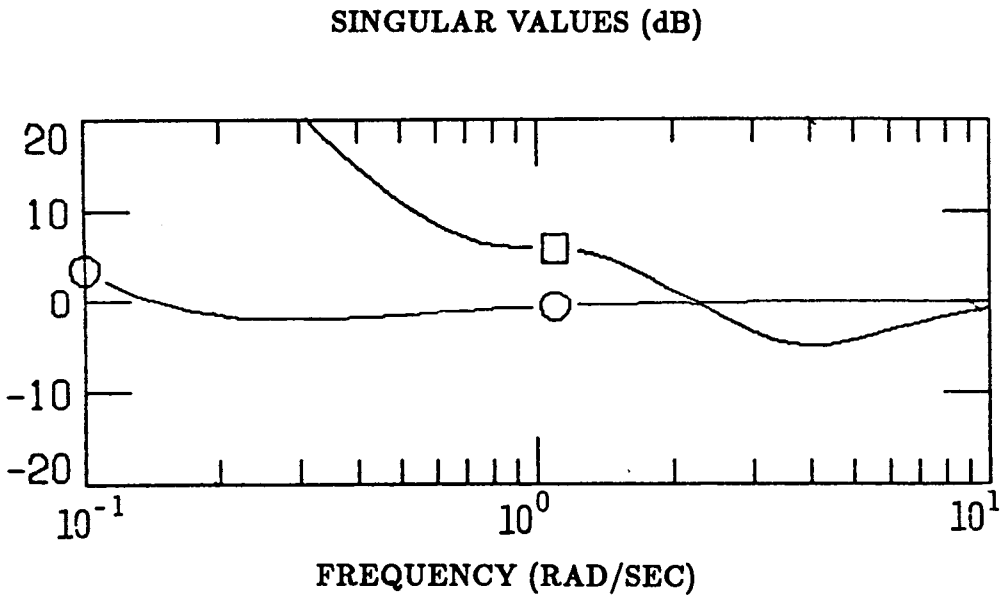

MINIMUM SINGULAR VALUE

-5.2 dB AT 4.0 rad/sec

FIGURE 4a. EIGENVALUE AND SINGULAR VALUE ANALYSIS OF CONTROL DESIGN AT 125 kt, γ = - 3 deg, FLAPS = 40 deg, HEIGHT = SEA LEVEL

- LOOP IS BROKEN AT CONTROL INPUT
- ADDITIVE DISTURBANCES

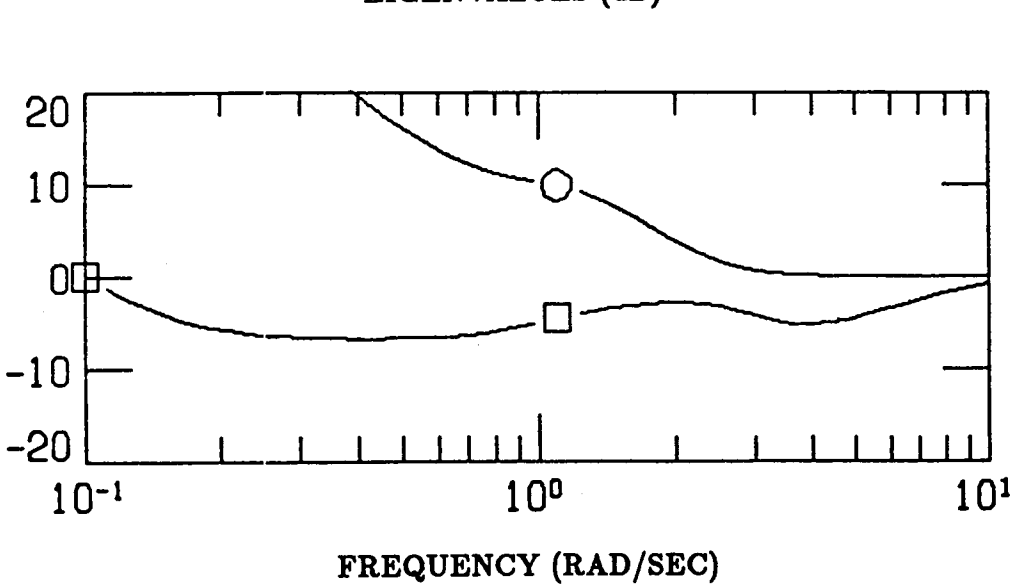

MINIMUM EIGENVALUE

-5.0 dB AT 4.0 rad/sec

FIGURE 4b. EIGENVALUE AND SINGULAR VALUE ANALYSIS OF CONTROL DESIGN AT 125 kt, γ = - 3 deg, FLAPS = 40 deg, HEIGHT = SEA LEVEL

THROTTLE LOOP OPEN

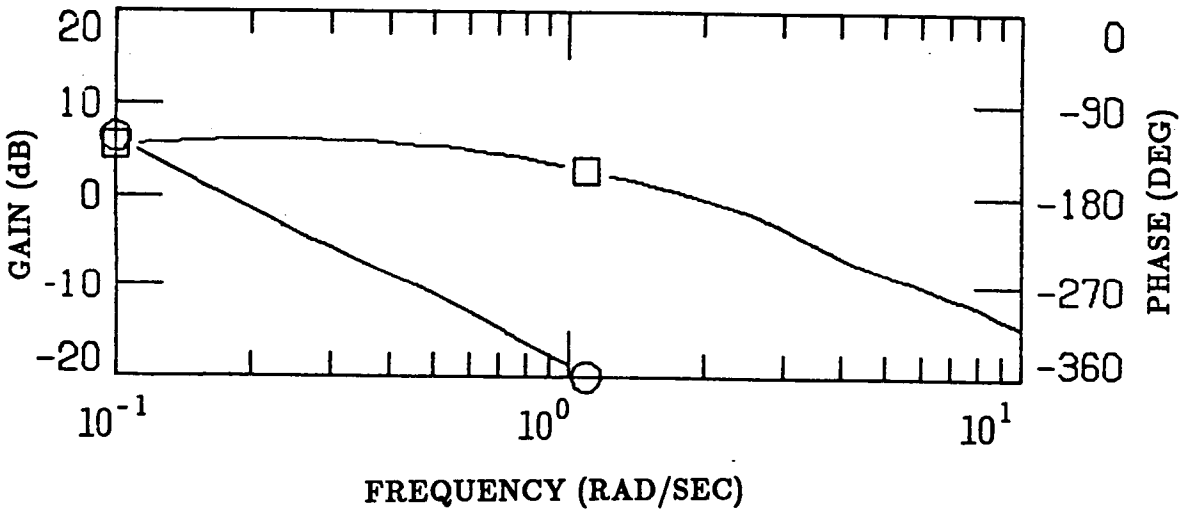

PHASE MARGIN

55 deg AT 0.17 rad/sec

GAIN MARGIN

-27 dB AT 2.0 rad/sec

FIGURE 4c. BODE PLOT OF CONTROL DESIGN

SAME FLIGHT CONDITIONS

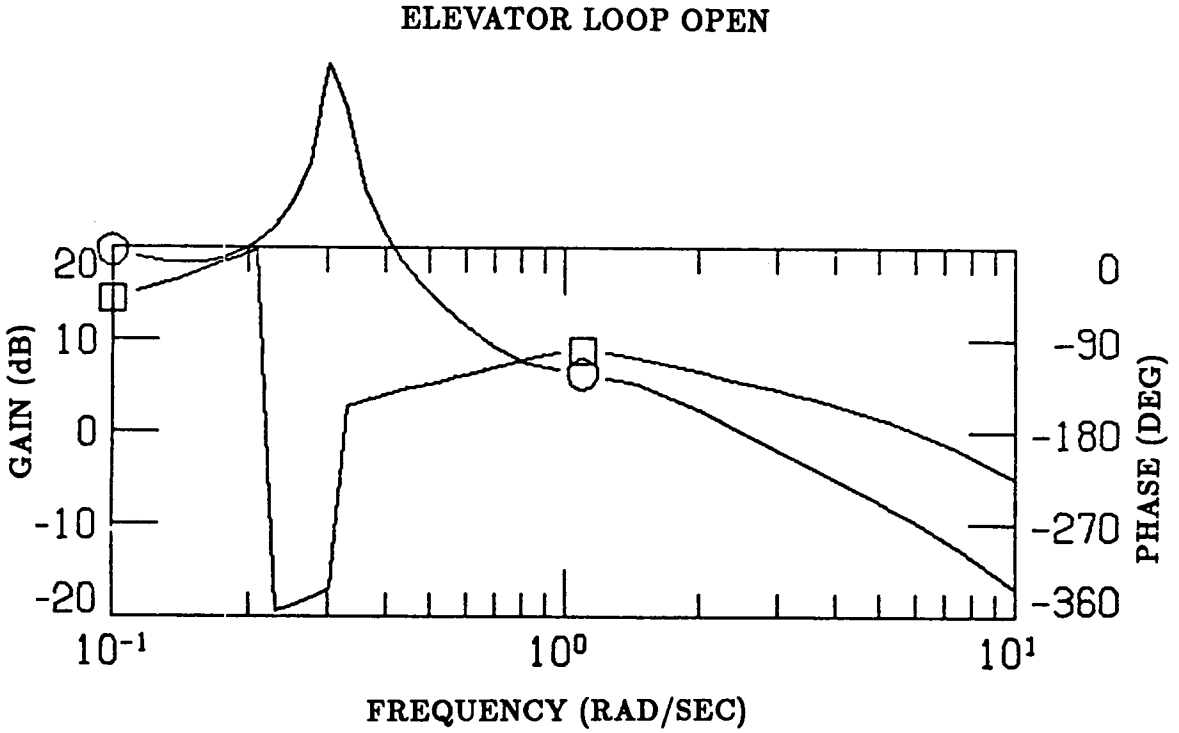

PHASE MARGIN

49 deg AT 2.5 rad/sec

GAIN MARGIN

-10 dB AT 6.3 rad/sec

FIGURE 4d. BODE PLOT OF CONTROL DESIGN

SAME FLIGHT CONDITIONS

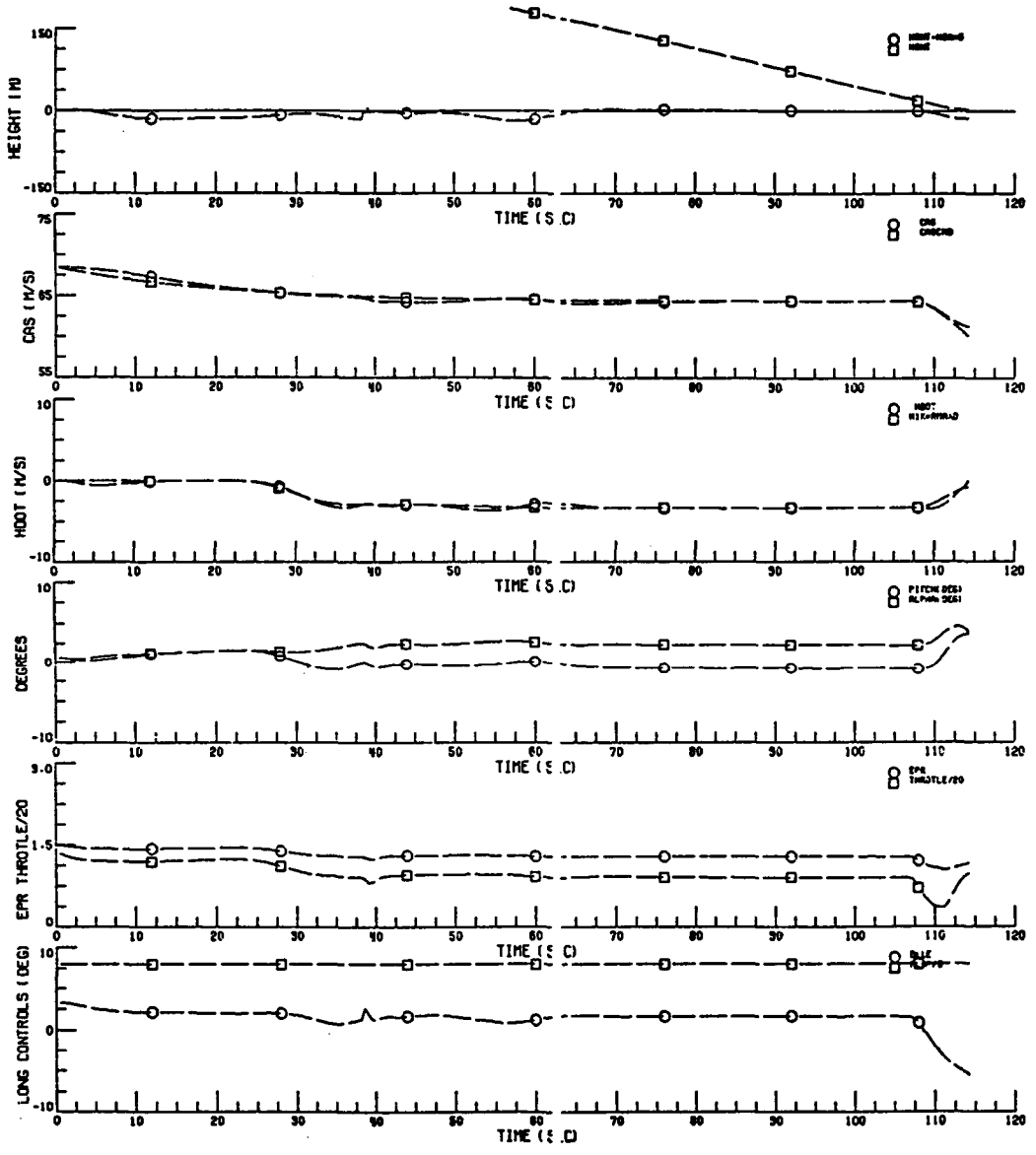

FIGURE 5a. NONLINEAR SIMULATION:

$$\mathrm{GS} = -3^{\circ},\ U_o = 125\,\mathrm{KTS},\ \psi_I = -32^{\circ}\ \mathrm{WT} = 85{,}000\,\mathrm{LBS}$$

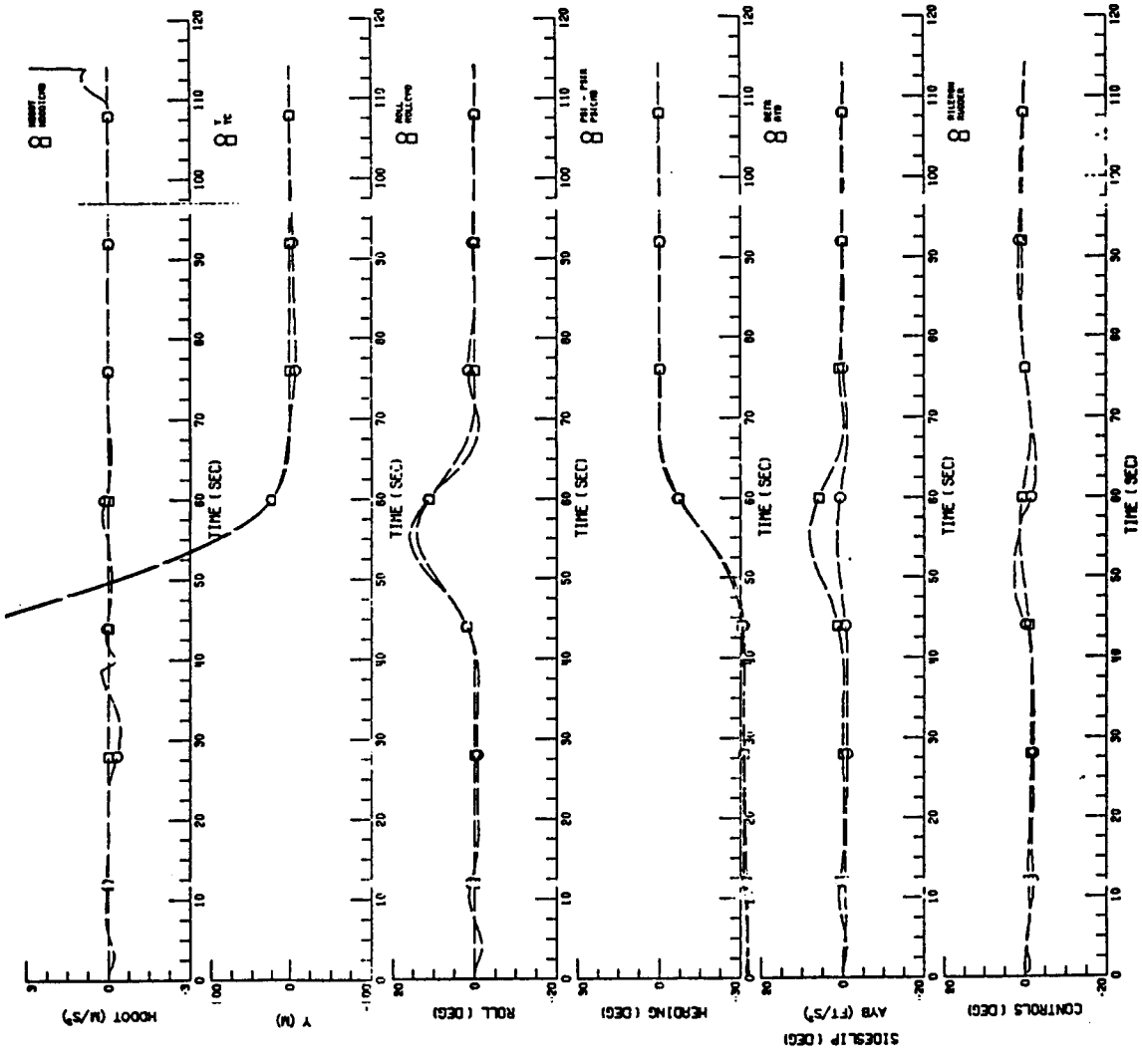

FIGURE 5b. NONLINEAR SIMULATION:

$GS = -3°$, $U_o = 125$ KTS, $\psi_T = -32°$ WT = 85,000 LBS

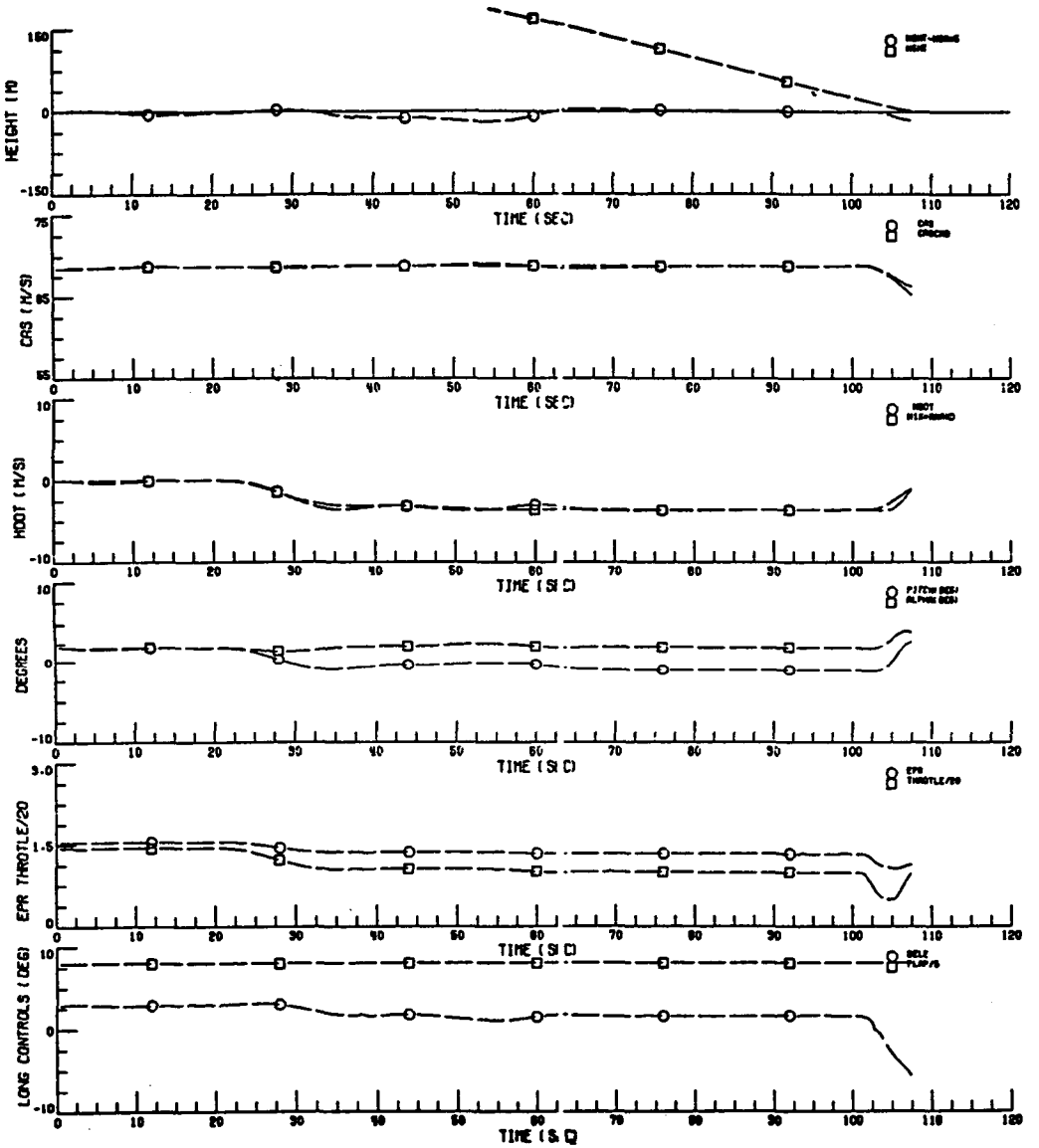

FIGURE 6a. NONLINEAR SIMULATION:

$\mathrm{GS} = -3°$, $U_o = 135\,\mathrm{KTS}$, $\psi_I = -32°$, $\mathrm{WT} = 95{,}000\,\mathrm{LBS}$, C.G. = .19

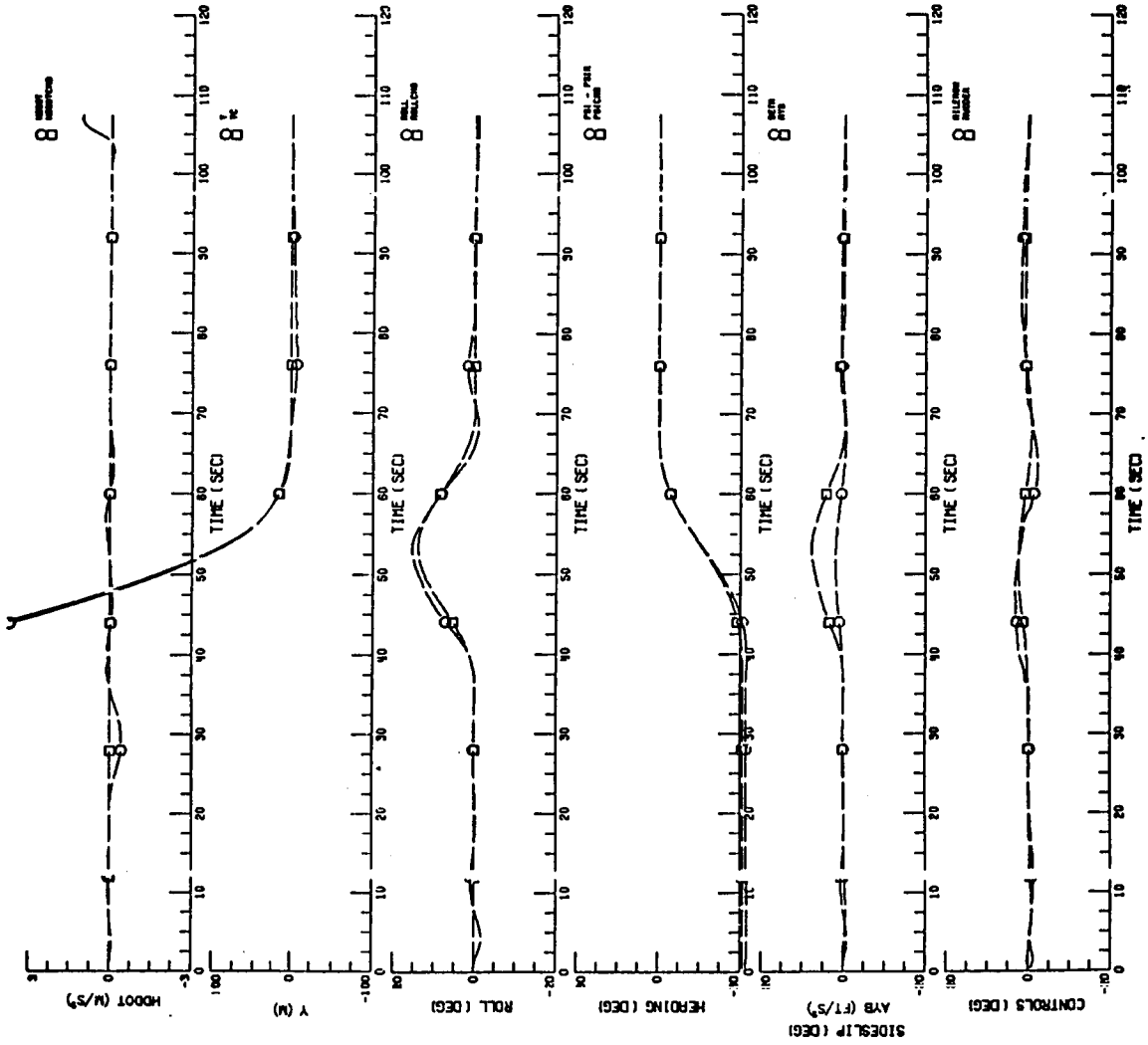

FIGURE 6b. NONLINEAR SIMULATION:

$GS = -3°$, $U_o = 135$ KTS, $\psi_I = -32°$, WT = 95,000 LBS, C.G. = .19

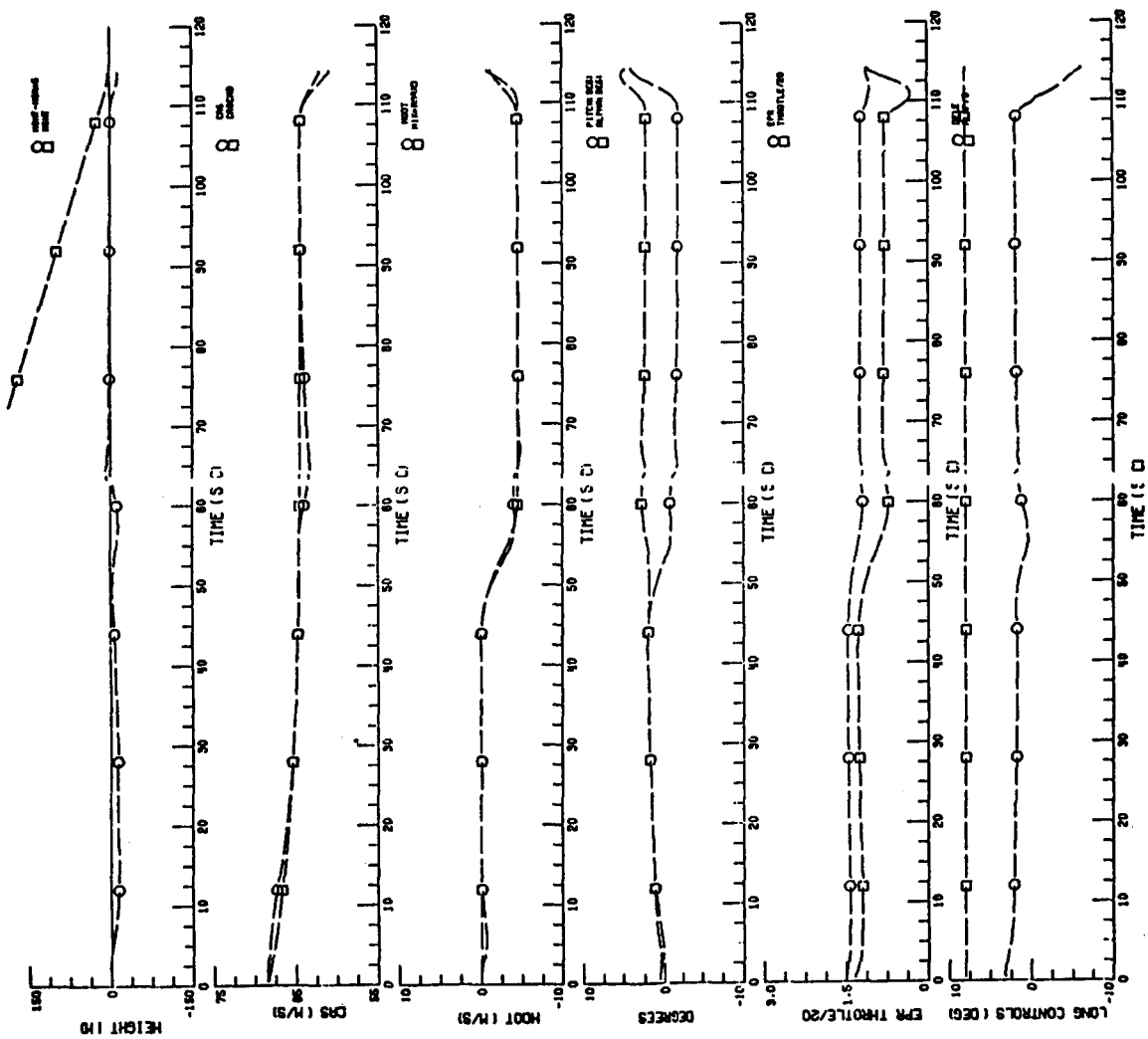

FIGURE 7a. NONLINEAR SIMULATION:

$GS = -4°$, $U_o = 125$ KTS, $\psi_I = -32°$ WT $= 85{,}000$ LBS

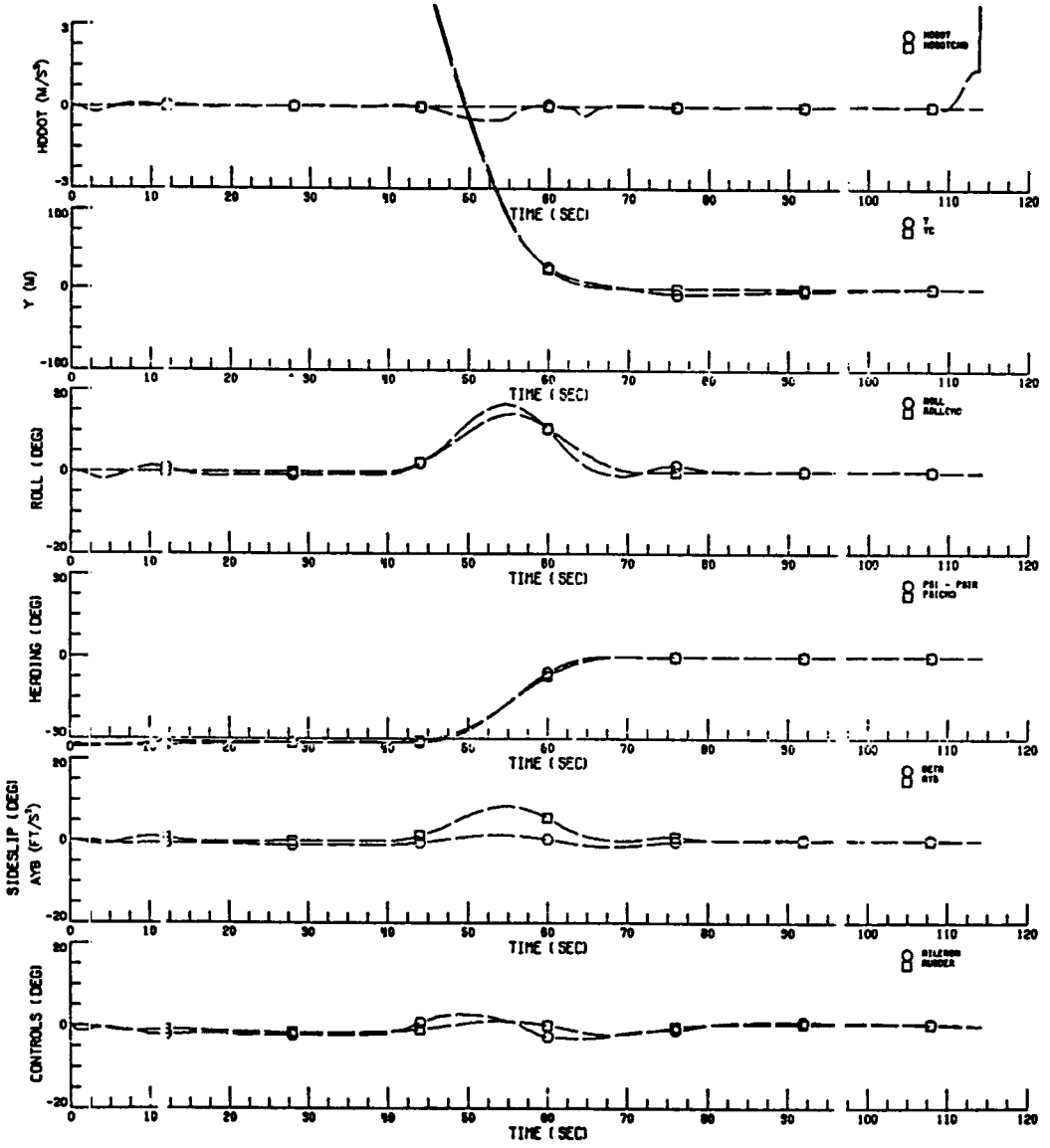

FIGURE 7b. NONLINEAR SIMULATION:

$$\mathrm{GS} = -4^{o},\ U_o = 125\,\mathrm{KTS},\ \psi_I = -32^{o}\ \mathrm{WT} = 85{,}000\,\mathrm{LBS}$$

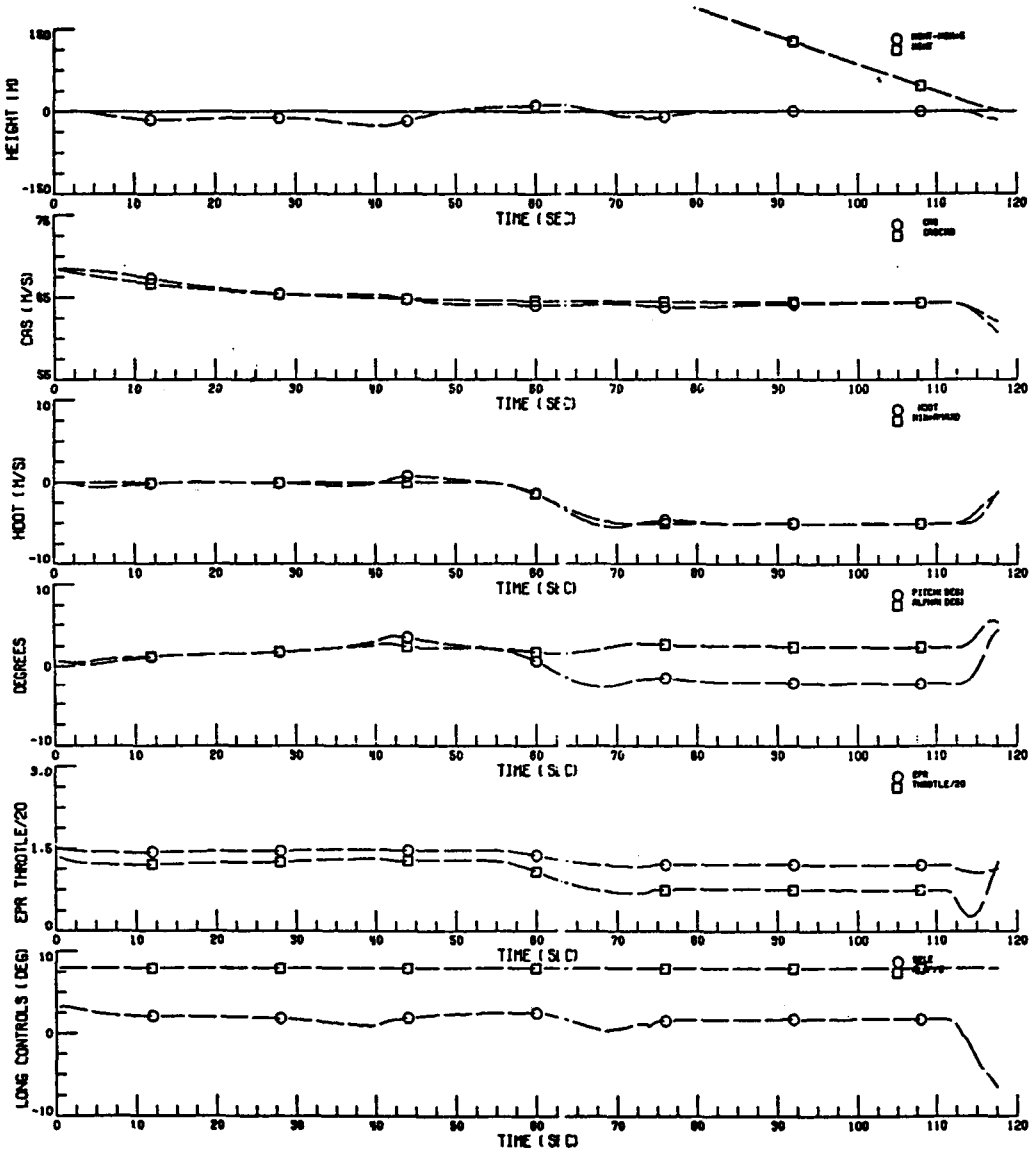

FIGURE 8a. NONLINEAR SIMULATION:

$$\mathrm{GS} = -4.5°,\ U_o = 125\,\mathrm{KTS},\ \psi_I = -47°\ \mathrm{WT} = 85{,}000\,\mathrm{LBS}$$

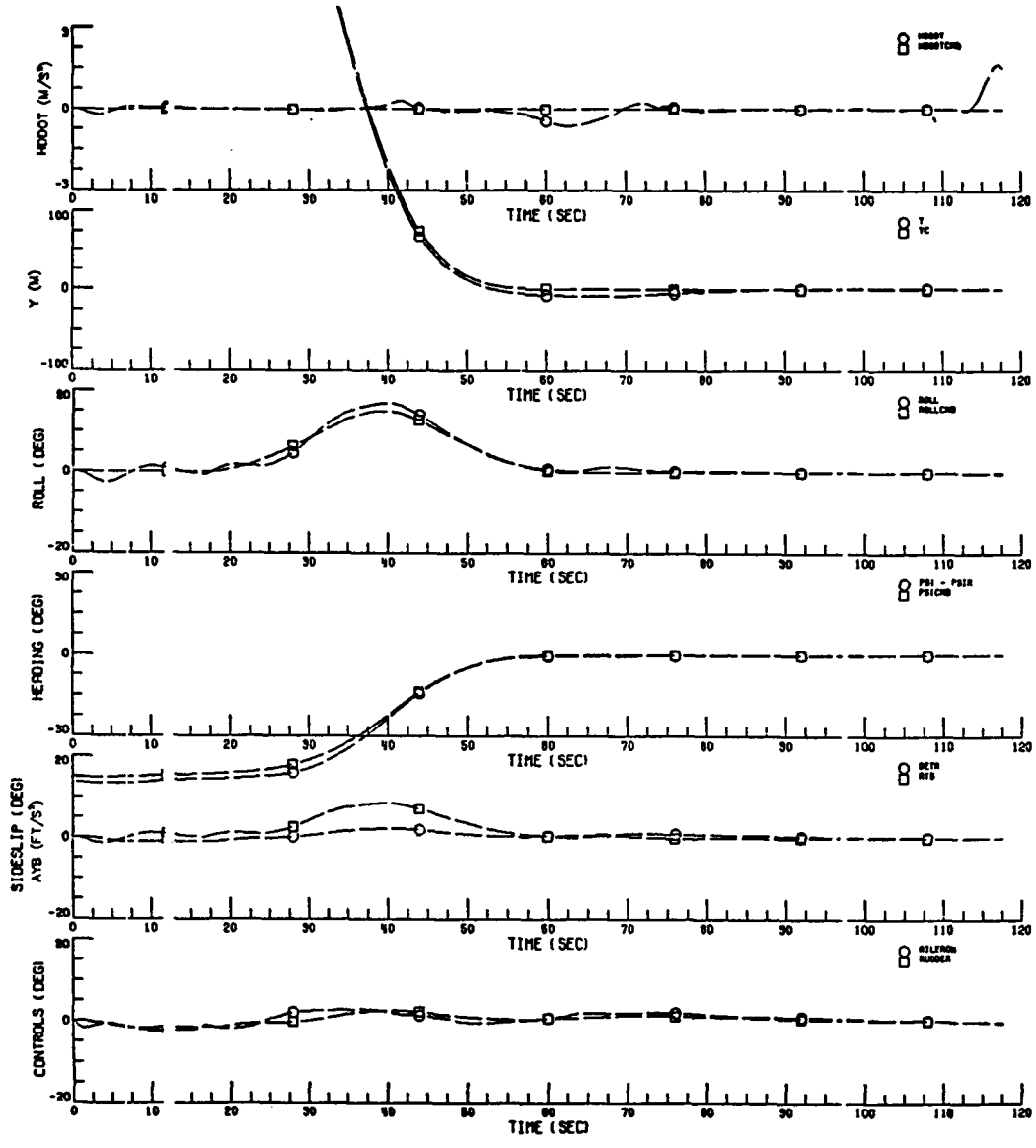

FIGURE 8b. NONLINEAR SIMULATION:

$$\mathrm{GS} = -4.5°,\ U_o = 125\ \mathrm{KTS},\ \psi_I = -47°\ \mathrm{WT} = 85{,}000\ \mathrm{LBS}$$

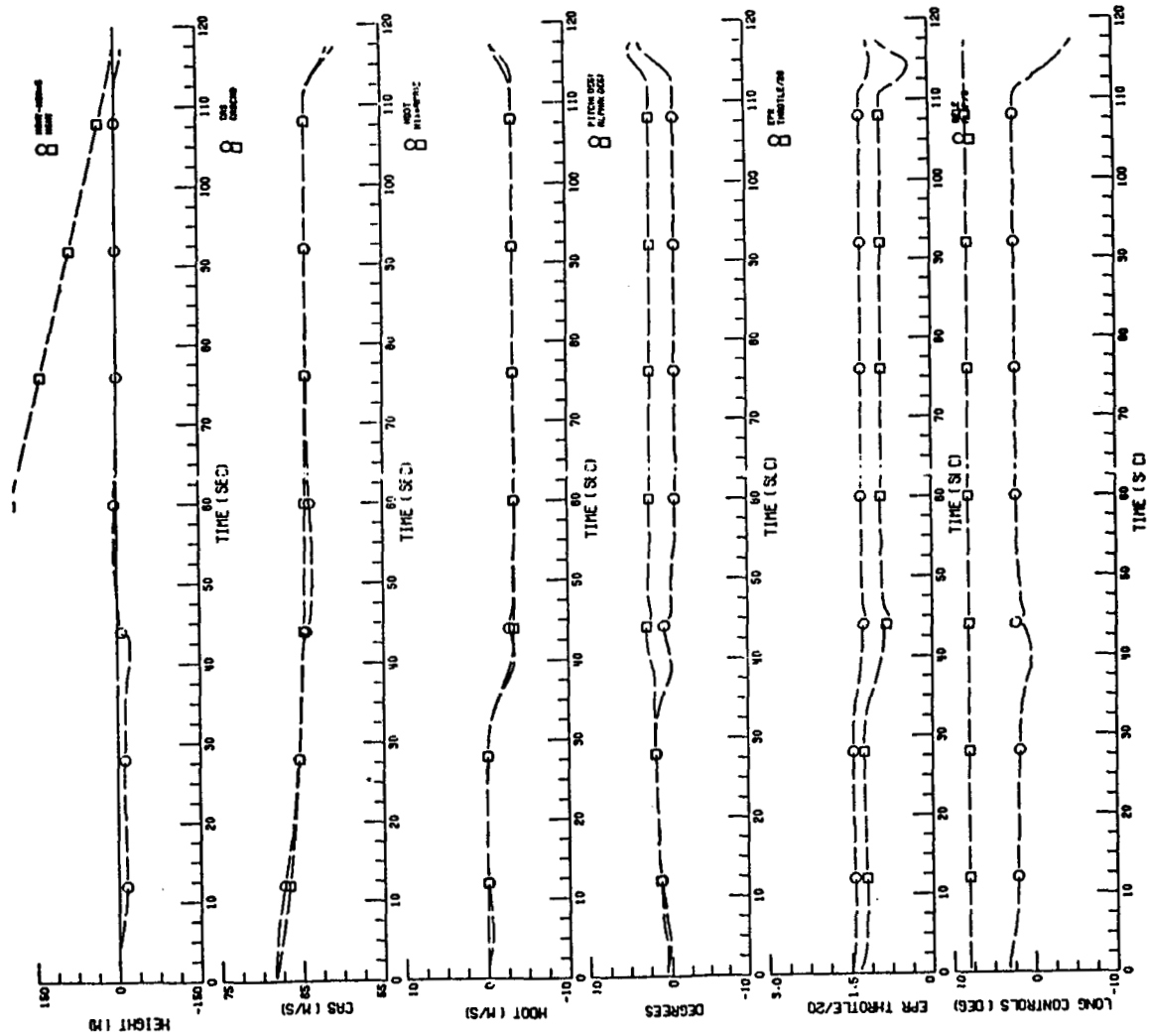

FIGURE 9a. NONLINEAR SIMULATION:

$GS = -3°$, $U_o = 125$ KTS, $\psi_I = -47°$ WT = 85,000 LBS

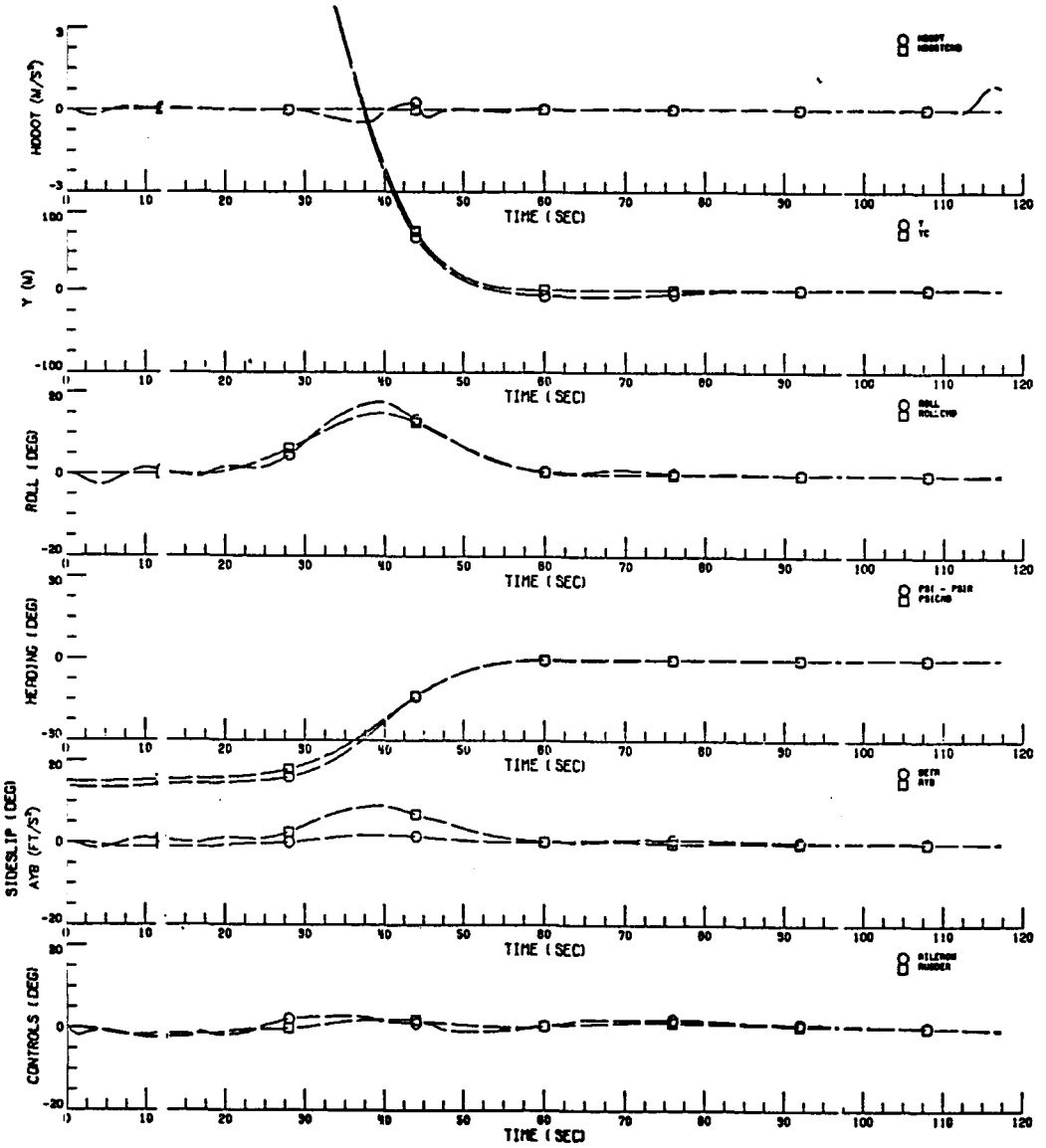

FIGURE 9b. NONLINEAR SIMULATION:

$$\mathrm{GS} = -3^{o},\ U_o = 125\,\mathrm{KTS},\ \psi_I = -47^{o}\ \mathrm{WT} = 85{,}000\,\mathrm{LBS}$$

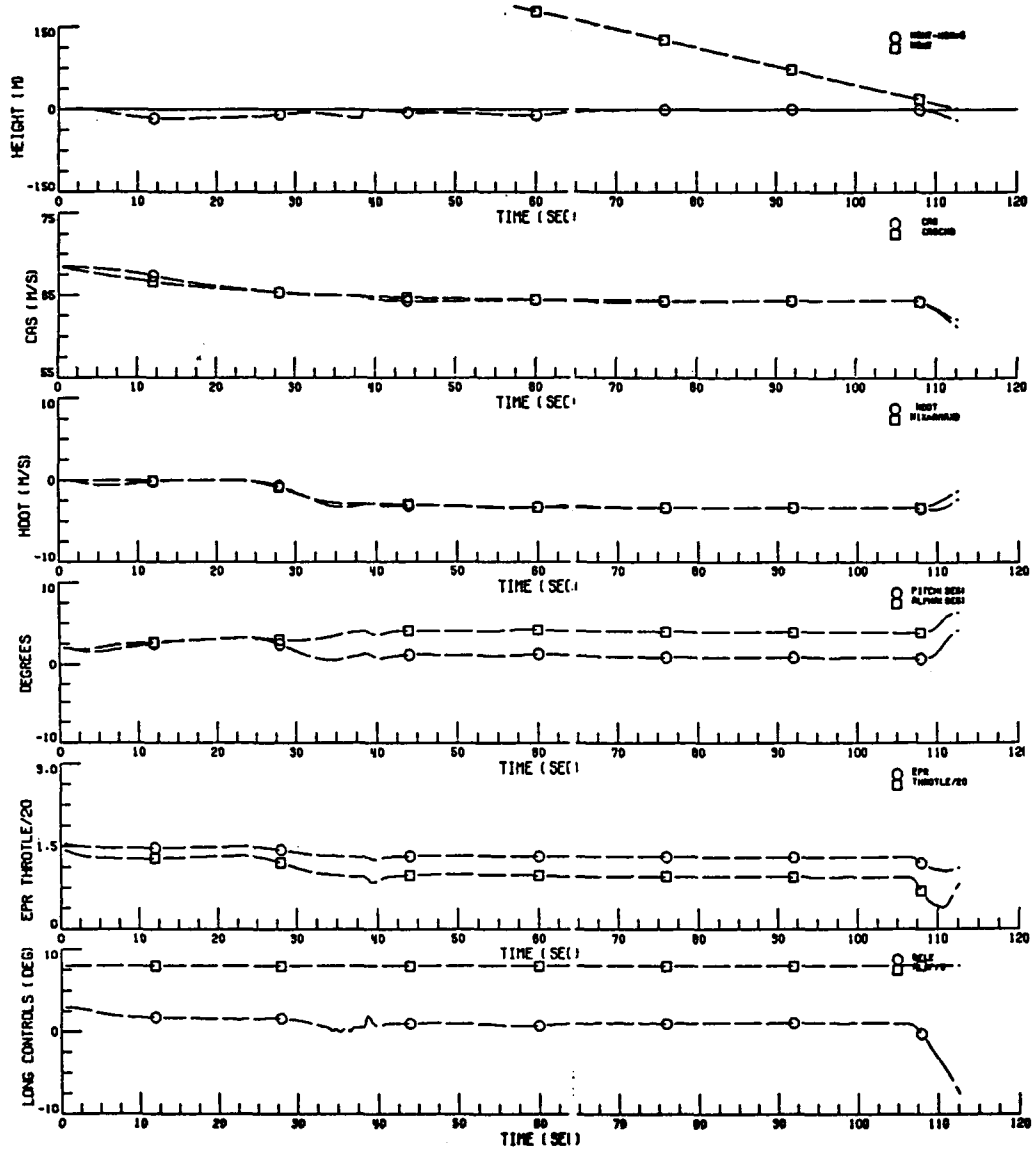

FIGURE 10a. NONLINEAR SIMULATION:

$\mathrm{GS} = -3°$, $U_o = 125\,\mathrm{KTS}$, $\psi_I = -32°$, $\mathrm{WT} = 95{,}000\,\mathrm{LBS}$, $\mathrm{C.G.} = .19$, $\mathrm{YDDMAX} = 5$

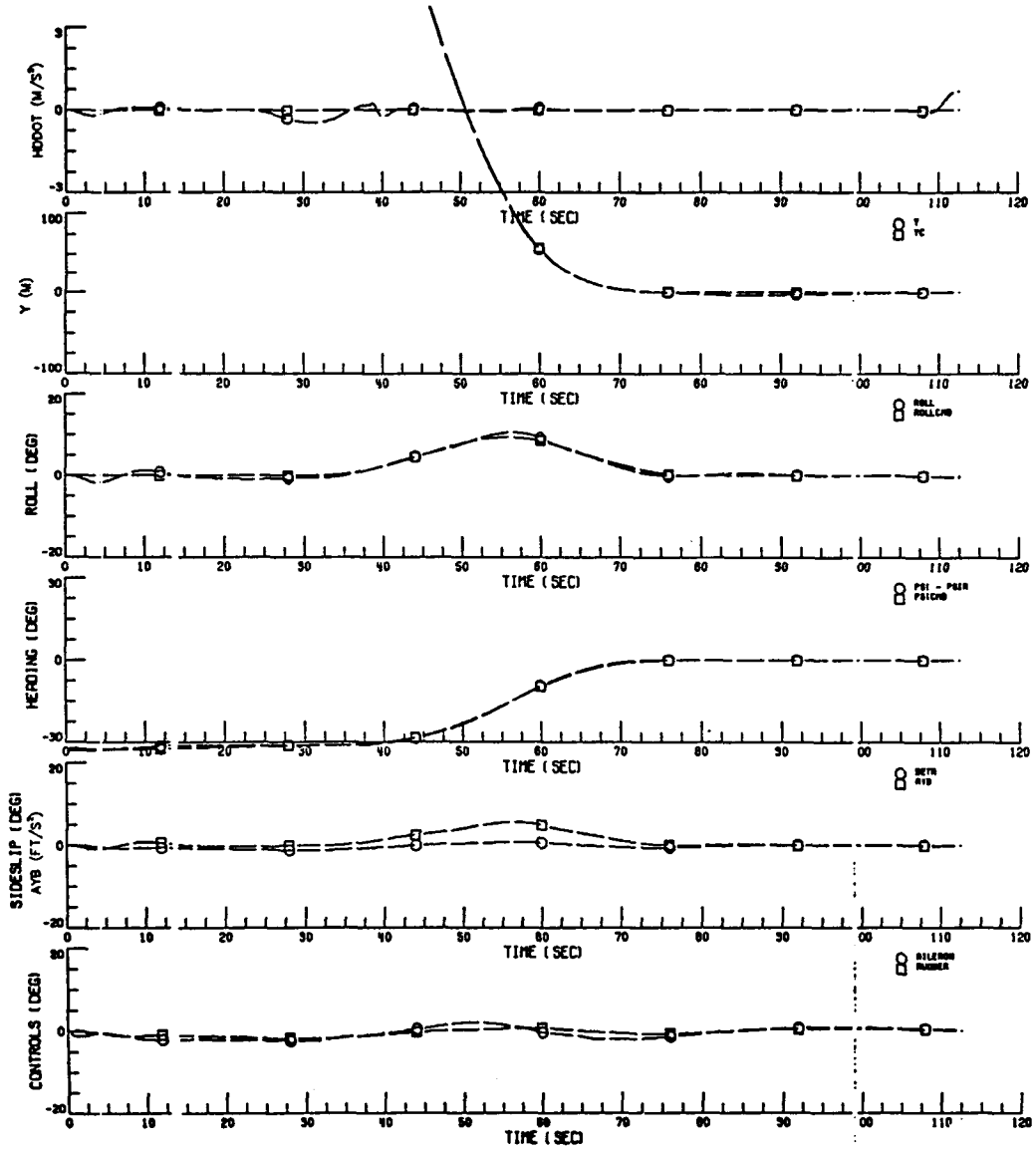

FIGURE 10b. NONLINEAR SIMULATION:

$\mathrm{GS} = -3°$, $U_o = 125\,\mathrm{KTS}$, $\psi_I = -32°$, $\mathrm{WT} = 95{,}000\,\mathrm{LBS}$, C.G. $= .19$, $\mathrm{YDDMAX} = 5$

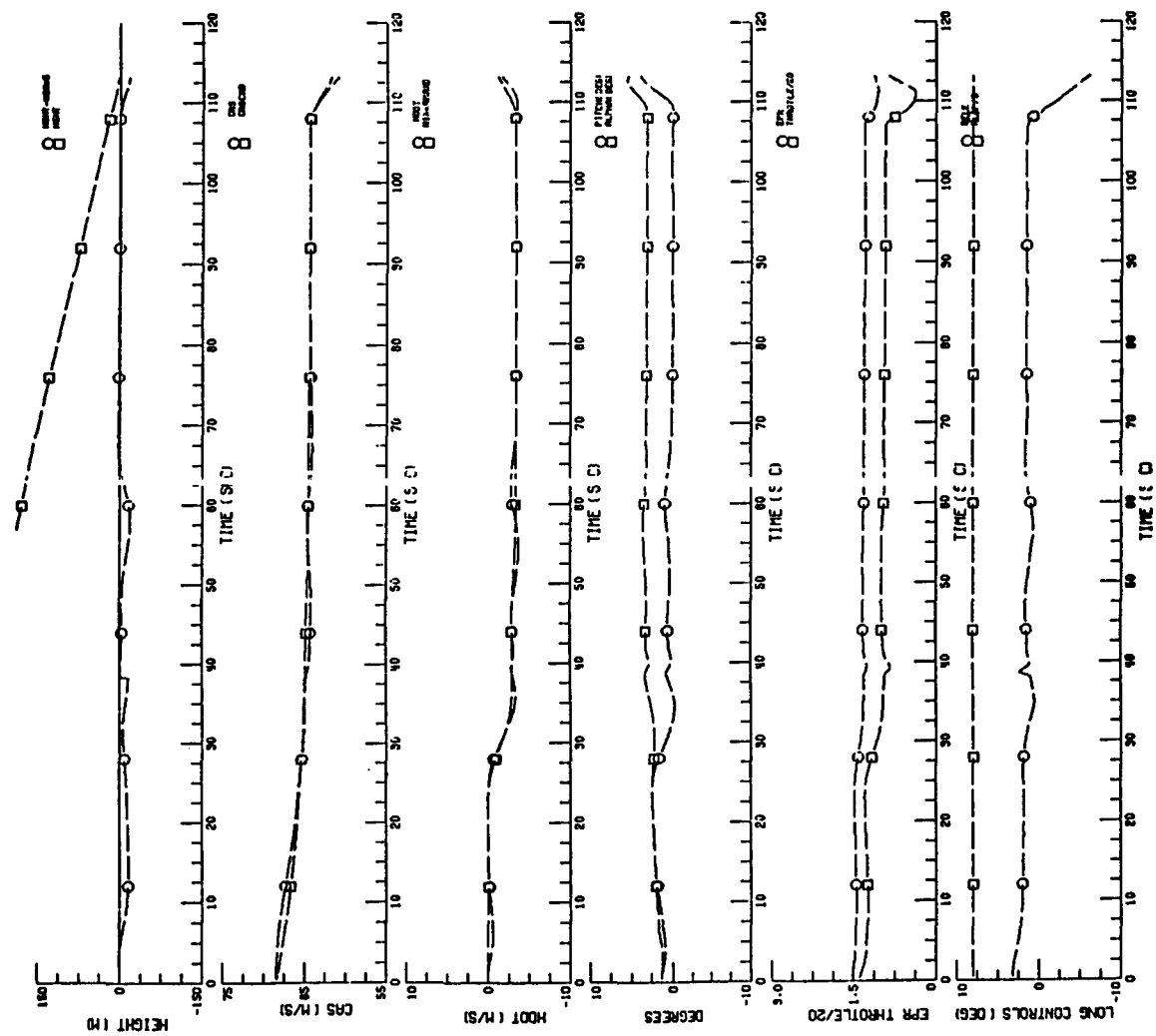

FIGURE 11a. NONLINEAR SIMULATION:

GS = −3°, U_o = 125 KTS, $\psi_I = -32°$, WT = 90,000 LBS

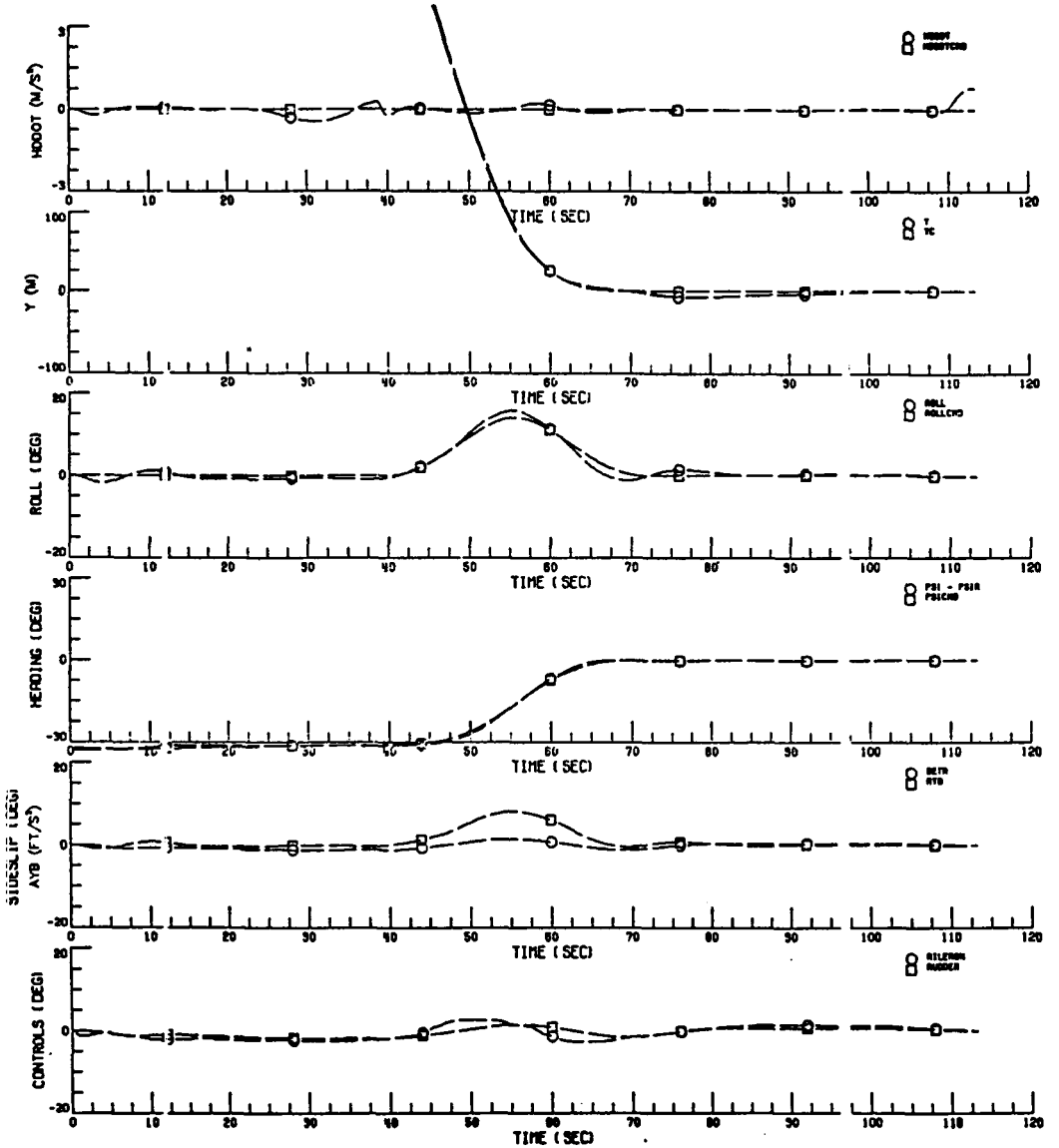

FIGURE 11b. NONLINEAR SIMULATION:

$$\mathrm{GS} = -3°,\ U_o = 125\,\mathrm{KTS},\ \psi_I = -32°,\ \mathrm{WT} = 90{,}000\,\mathrm{LBS}$$

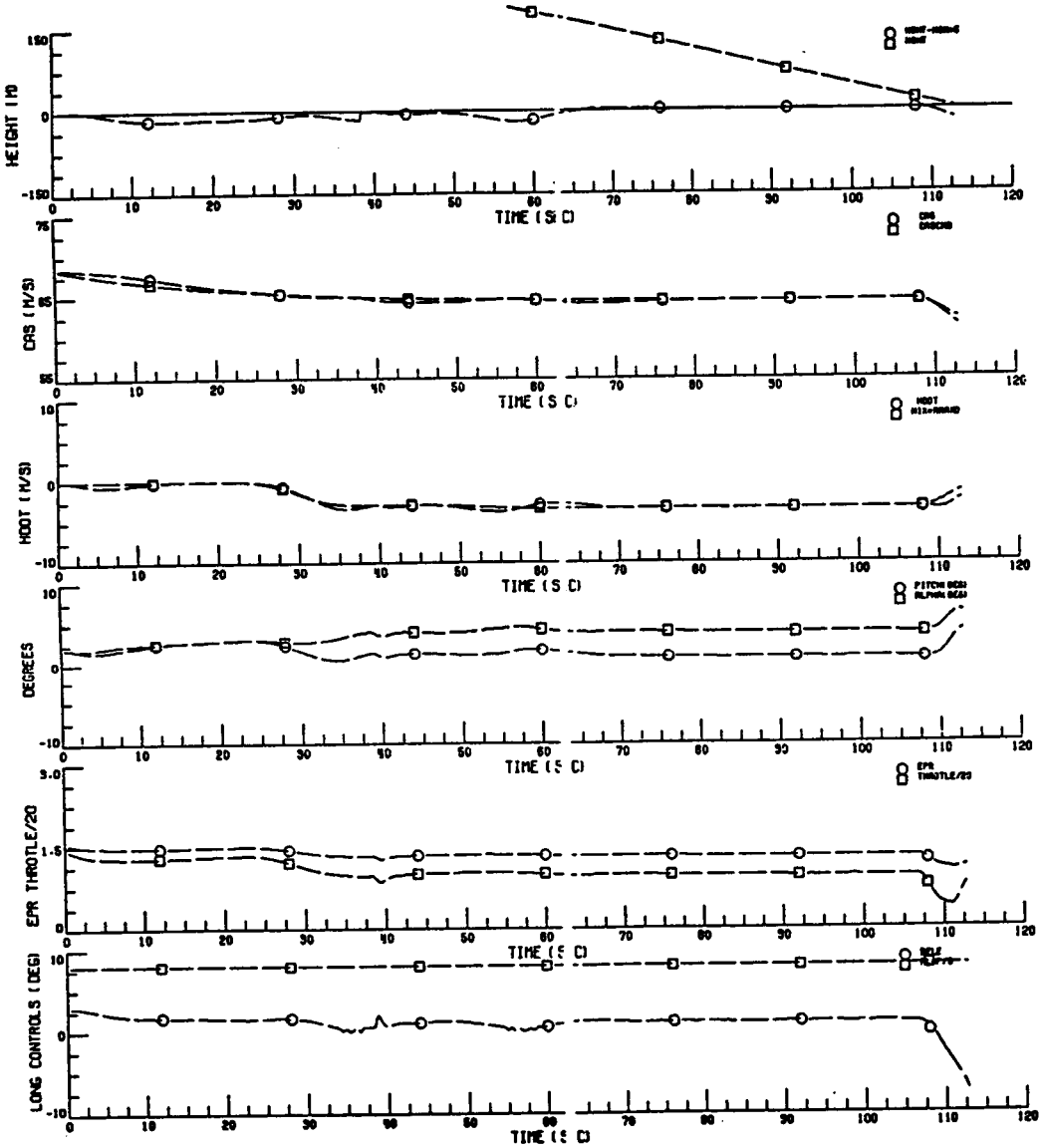

FIGURE 12a. NONLINEAR SIMULATION:

$\mathrm{GS} = -3°$, $U_o = 125\,\mathrm{KTS}$, $\psi_I = -32°$, $\mathrm{WT} = 95{,}000\,\mathrm{LBS}$, C.G. = .19

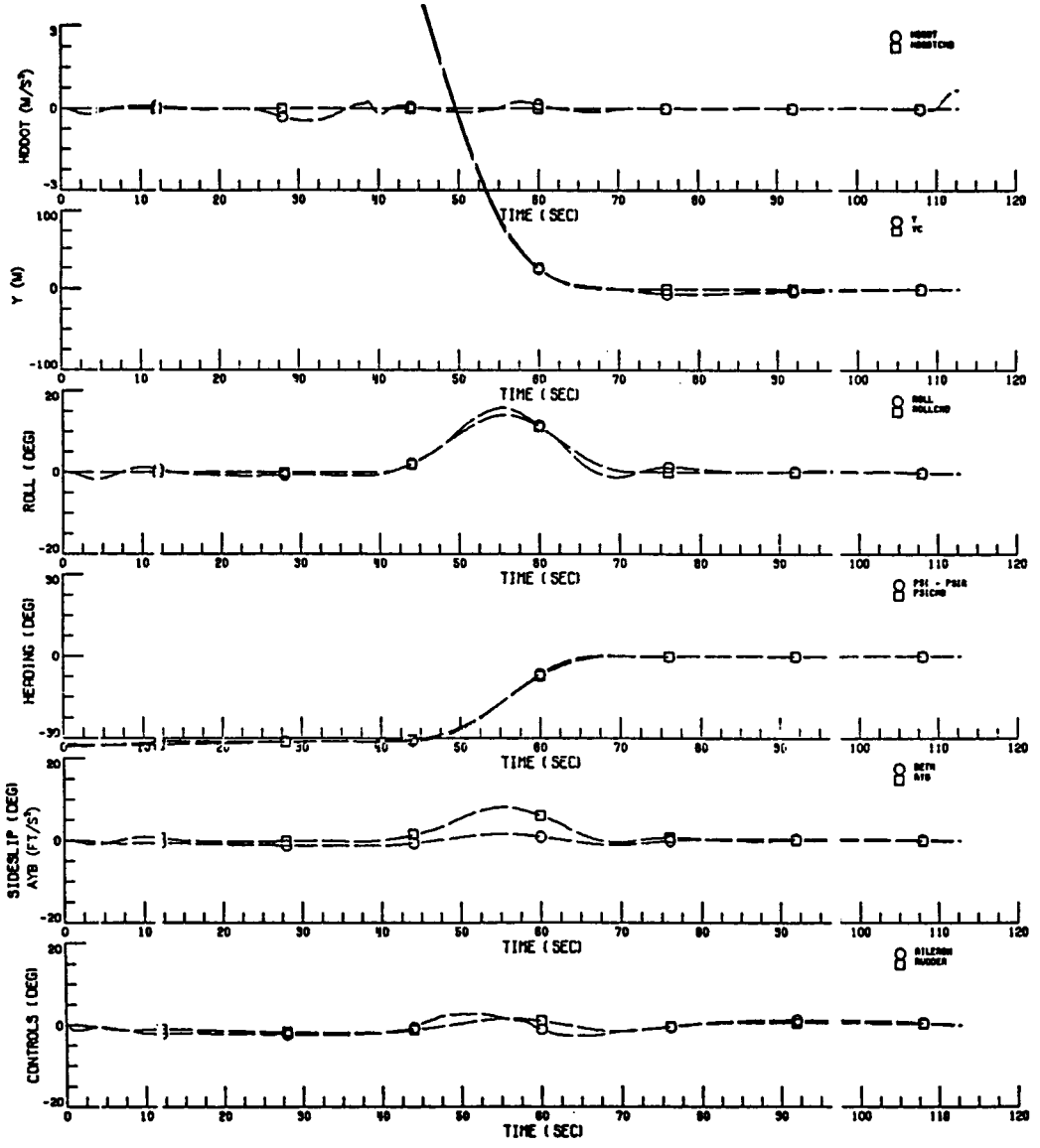

FIGURE 12b. NONLINEAR SIMULATION:

$\mathrm{GS} = -3°$, $U_o = 125\,\mathrm{KTS}$, $\psi_I = -32°$, $\mathrm{WT} = 95{,}000\,\mathrm{LBS}$, C.G. = .19

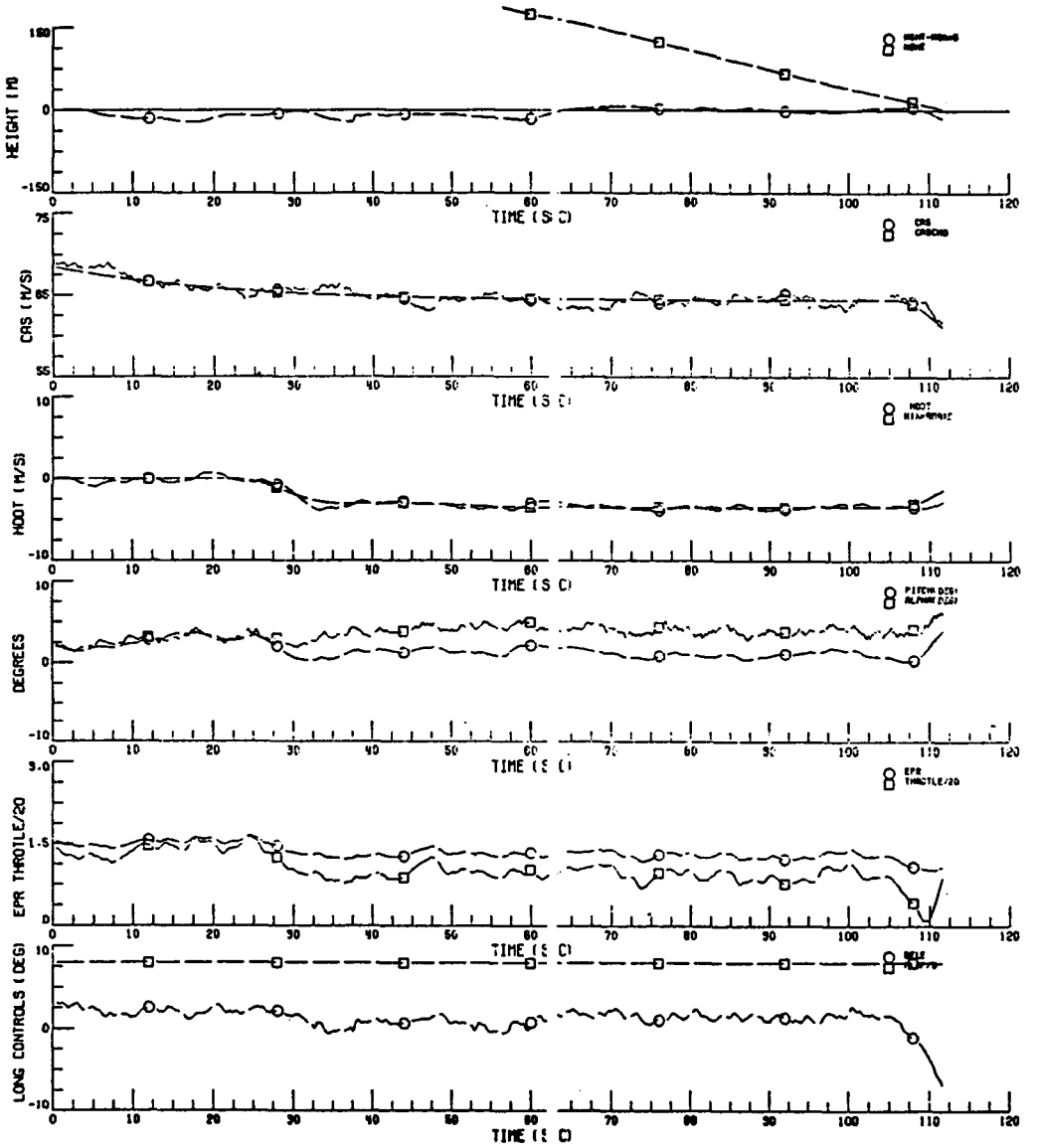

FIGURE 13a. NONLINEAR SIMULATION:

$\mathrm{GS} = -3°$, $U_o = 125\,\mathrm{KTS}$, $\psi_I = -32°$, $\mathrm{WT} = 95{,}000\,\mathrm{LBS}$, C.G. $= .19$, GUST SD $= 2\,\mathrm{FT/SEC}$.

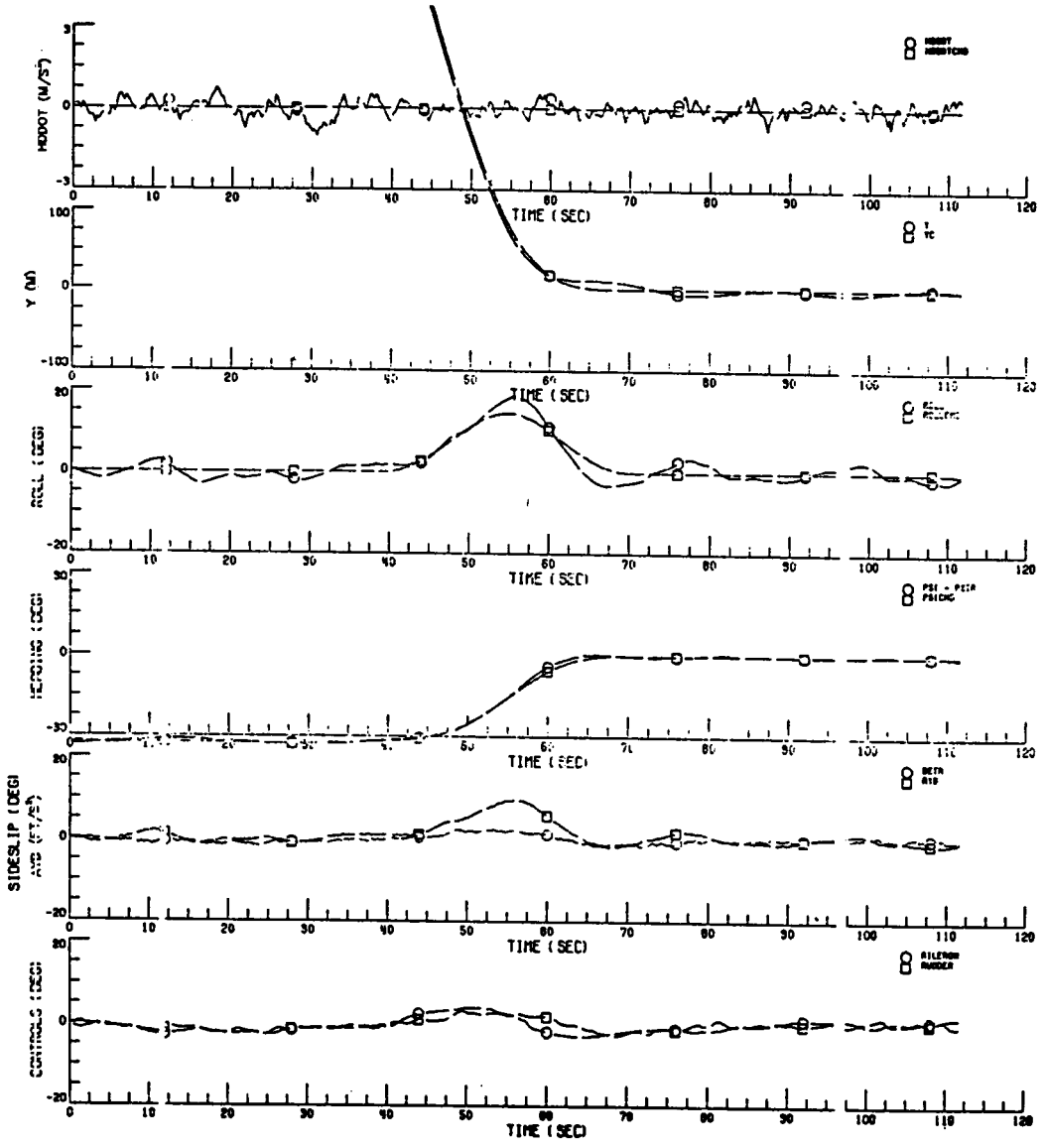

FIGURE 13b. NONLINEAR SIMULATION:

$GS = -3°$, $U_o = 125$ KTS, $\psi_I = -32°$, WT = 95,000 LBS, C.G. = .19, GUST SD = 2 FT/SEC.

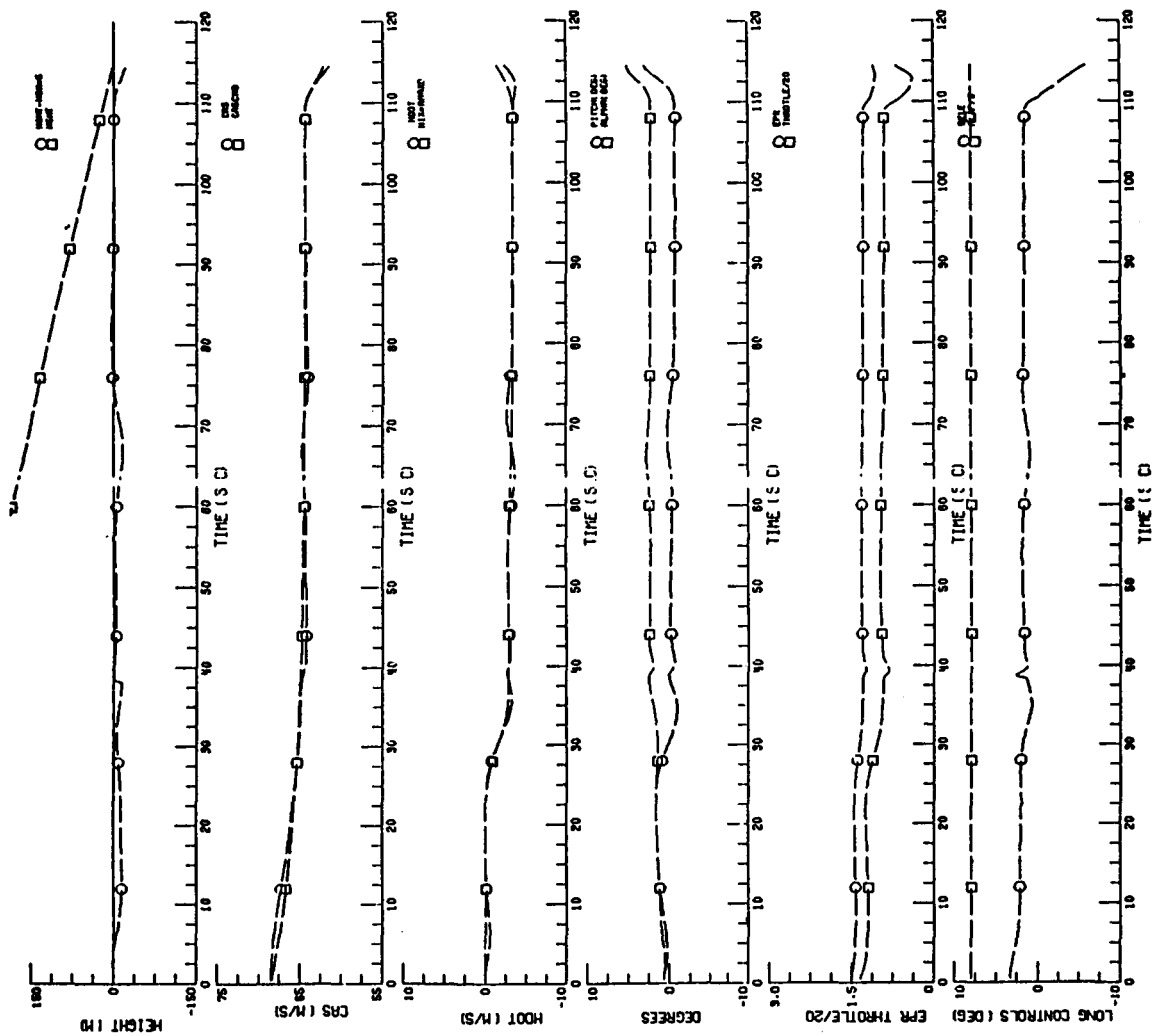

FIGURE 14a. NONLINEAR SIMULATION:

$GS = -3°$, $U_o = 125$ KTS, $\psi_I = -32°$, WS = 10 KTS, WD = 122° WT = 85,000 LBS

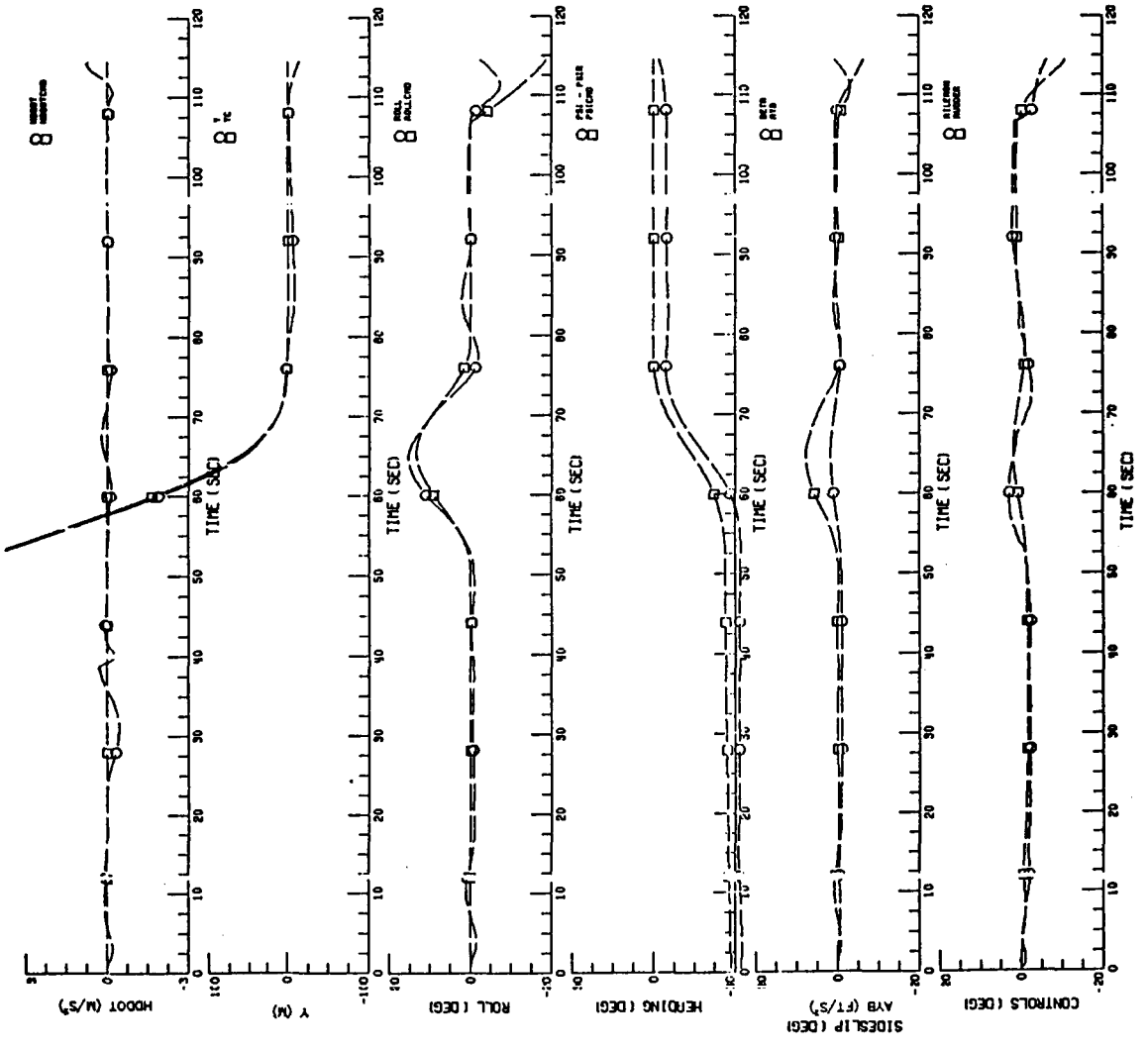

FIGURE 14b. NONLINEAR SIMULATION:

$GS = -3°$, $U_o = 125$ KTS, $\psi_I = -32°$, WS = 10 KTS, WD = 122° WT = 85,000 LBS

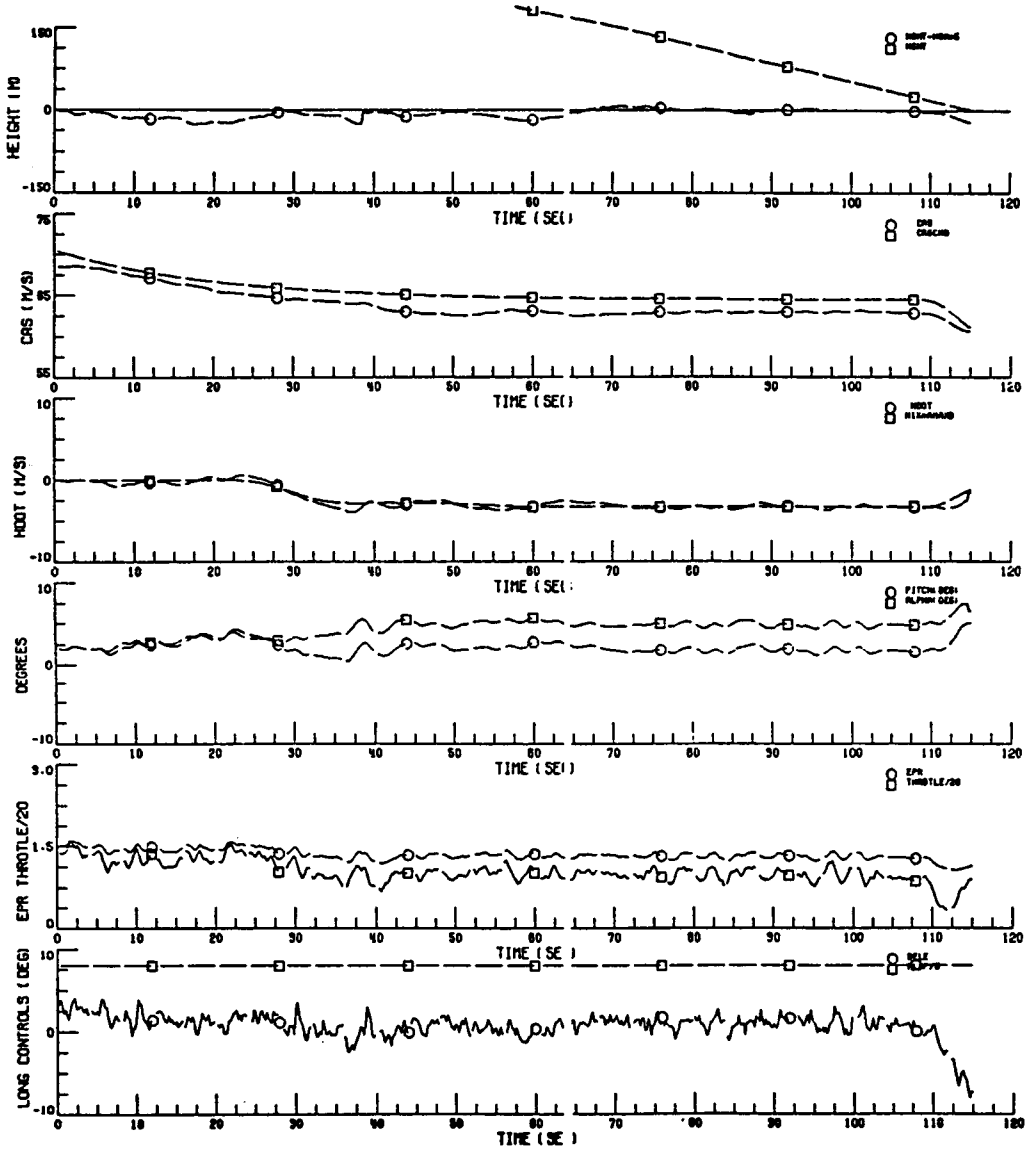

FIGURE 15a. NONLINEAR SIMULATION:

$GS = -3°$, $U_o = 125$ KTS, $\psi_I = -32°$, WT = 95,000 LBS, C.G. = .19, NOISES

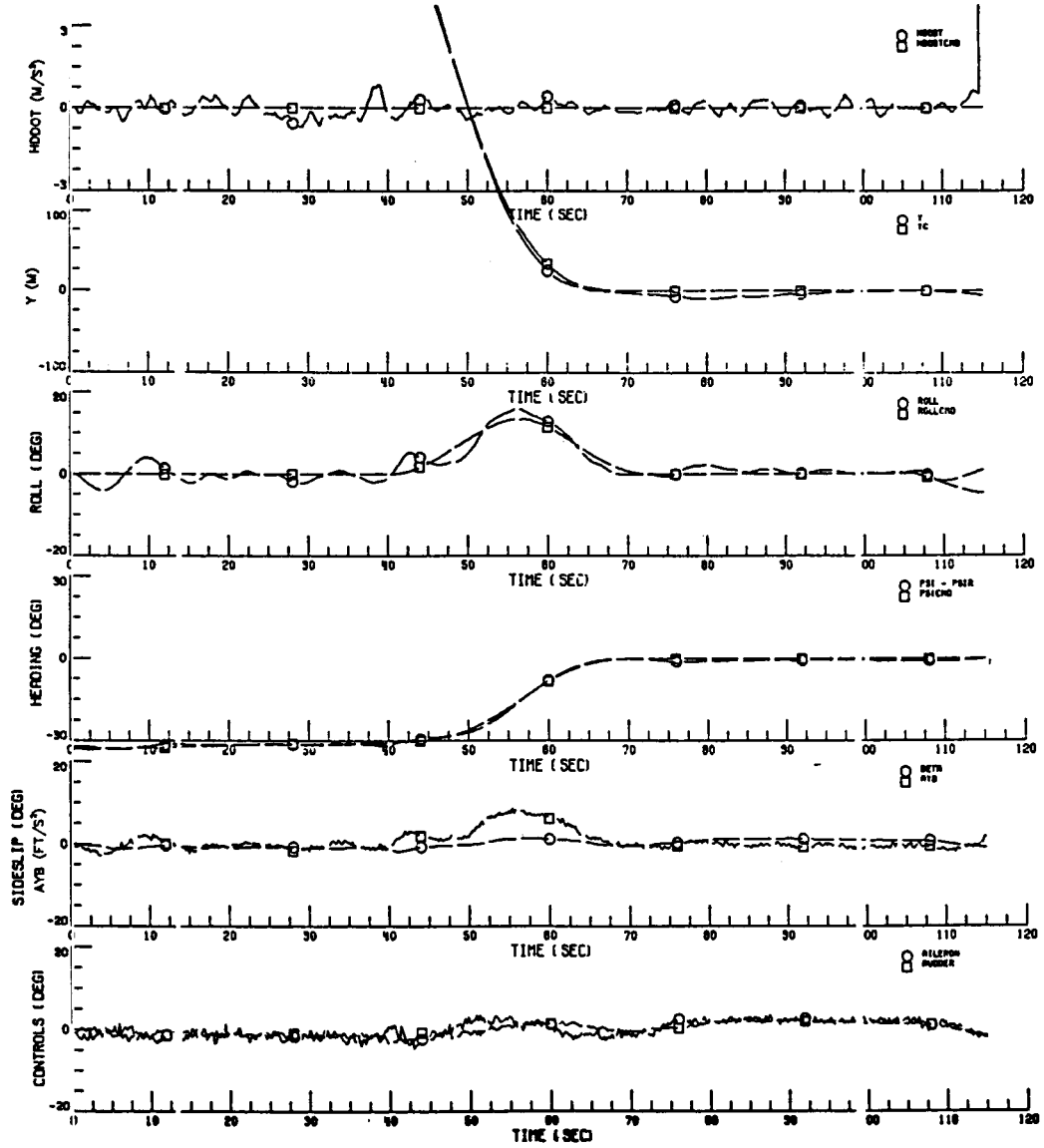

FIGURE 15b. NONLINERA SIMULATION:

$GS = -3°, U_o = 125\,KTS, \psi_I = -32°, WT = 95{,}000\,LBS$, C.G. = .19, NOISES

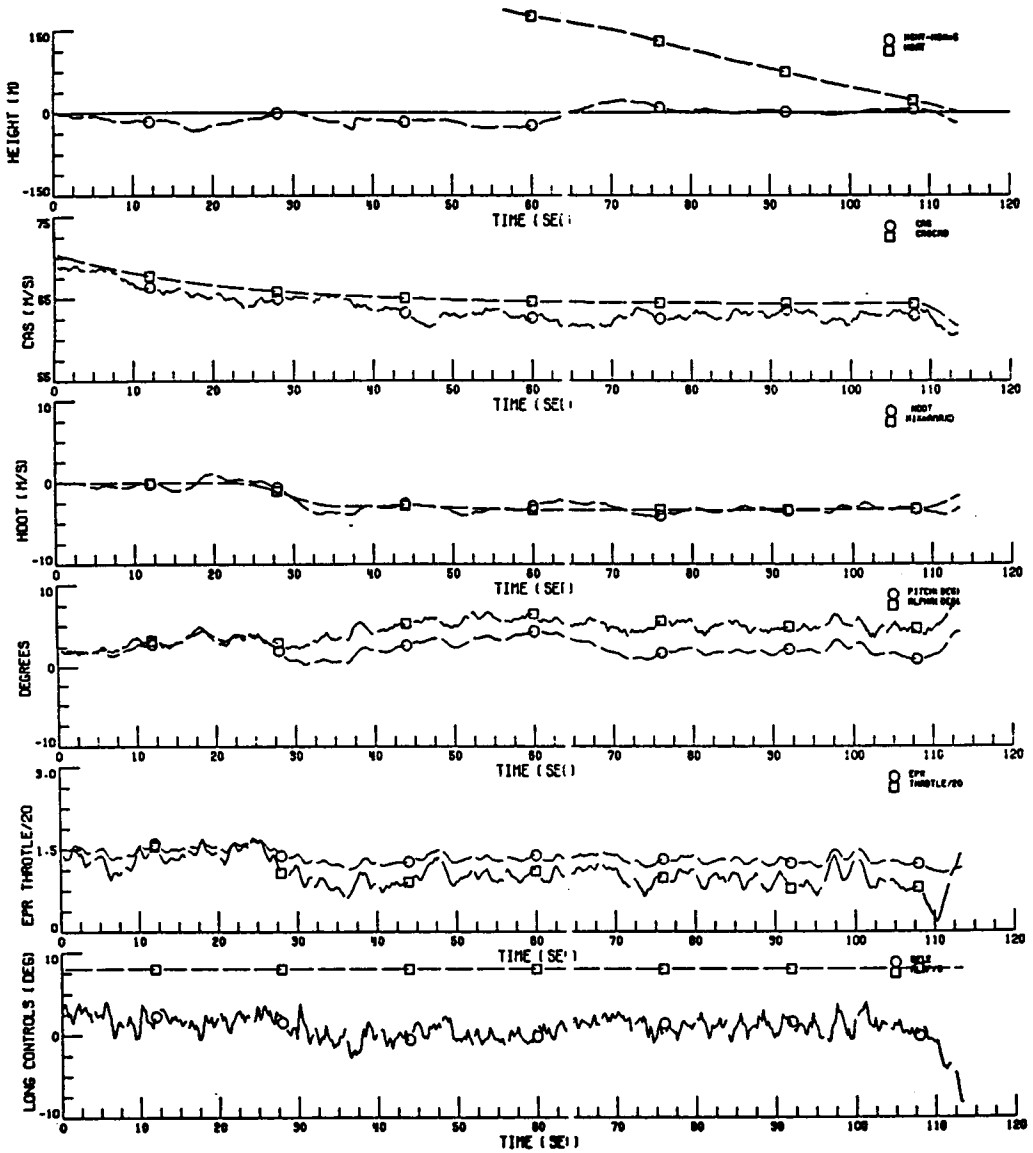

FIGURE 16a. SFF/OF DIALS SIMULATION:

$GS = -3°$, $U_o = 125$ KTS, $\psi = -32°$, WT = 95 KLBS, C.G. = .19, GUST SD = 2 FT/SEC., NOISES

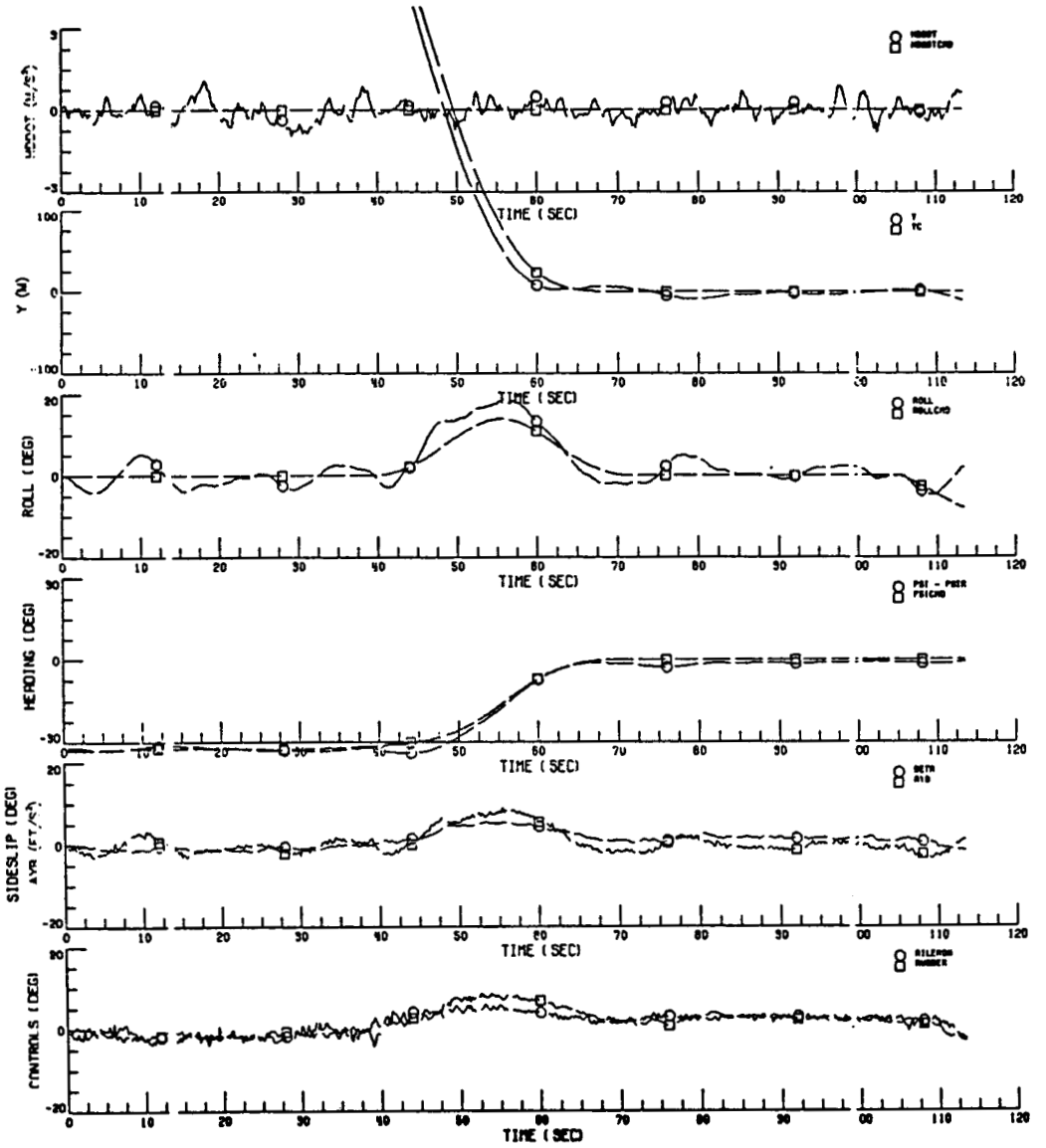

FIGURE 16b. SFF/OF DIALS SIMULATION:

$GS = -3°$, $U_o = 125$ KTS, $\psi = -32°$, WT = 95 KLBS, C.G. = .19, GUST SD = 2 FT/SEC., NOISES

Standard Bibliographic Page

1. Report No.	2. Government Accession No.	3. Recipient's Catalog No.
NASA CR-4078		

4. Title and Subtitle	5. Report Date
A Combined Stochastic Feedforward and Feedback Control Design Methodology with Application to Autoland Design	July 1987
	6. Performing Organization Code
7. Author(s)	8. Performing Organization Report No.
Nesim Halyo	*FR 687102*
9. Performing Organization Name and Address	10. Work Unit No.
Information & Control Systems, Incorporated *28 Research Drive* *Hampton, VA 23666*	11. Contract or Grant No.
	NAS1-16158
12. Sponsoring Agency Name and Address	13. Type of Report and Period Covered
National Aeronautics and Space Administration *Washington, DC 20546*	*Contractor Report*
	14. Sponsoring Agency Code
	505-66-41-04

15. Supplementary Notes

NASA Langley Technical Monitor: Richard M. Hueschen
Final Report

16. Abstract

A combined stochastic feedforward and feedback control design mehtodology is developed and a digital automatic landing system for a Boeing 737 aircraft is designed using this approach. The objective of the feedforward control law is to track the commanded trajectory, whereas the feedback control law tries to maintain the plant state near the desired trajectory in the presence of disturbances and uncertainties about the plant.

The feedforward control law design is formulated as a stochastic optimization problem and is imbedded into the stochastic output feedback problem where the plant contains unstable and uncontrollable modes. A new algorithm to compute the optimal feedforward gain is developed. A combined feedforward/feedback control law design methodology is developed. In this approach, the use of error integral feedback, dynamic compensation, control rate command structures are an integral part of the methodology. An incremental implementation is recommended. Results on the eigenvalues of the implemented versus designed control laws are presented.

The stochastic feedforward/feedback control methodology is used to design a digital automatic landing system for the ATOPS Research Vehicle, a Boeing 737-100 aircraft. The system control modes include localizer and glideslope capture and track, and flare to touchdown. Results of a detailed nonlinear simulation of the digital control laws, actuator systems, and aircraft aerodynamics are presented.

17. Key Words (Suggested by Authors(s))	18. Distribution Statement
Feedforward Control, Feedback Control, Stochastic Control, Control Law Design Methodology, Output Feedback, Digital Control, Optimal Control, Incremental Implementation, Automatic Landing, ATOPS, DIALS	*Unclassified - Unlimited* *Subject Category 63*

19. Security Classif.(of this report)	20. Security Classif.(of this page)	21. No. of Pages	22. Price
Unclassified	Unclassified	126	A07

For sale by the National Technical Information Service, Springfield, Virginia 22161

NASA-Langley, 1987